Lehrstuhl für Ernährungsphysiologie

Studies on dietary and hormonal regulation of selected nutrient transporters in mouse small intestine

Mena Katharina Eidens

Vollständiger Abdruck der von der Fakultät Wissenschaftszentrum Weihenstephan für Ernährung, Landnutzung und Umwelt der Technischen Universität München zur Erlangung des akademischen Grades eines

Doktors der Naturwissenschaften

genehmigten Dissertation.

Vorsitzender:		Univ.-Prof. Dr. M. Schemann
Prüfer der Dissertation:	1.	Univ.-Prof. Dr. H. Daniel
	2.	Univ.-Prof. Dr. M. Klingenspor

Die Dissertation wurde am 03. 04. 2014 bei der Technischen Universität München eingereicht und durch die Fakultät Wissenschaftszentrum Weihenstephan für Ernährung, Landnutzung und Umwelt am 23. 09. 2014 angenommen.

“Nur wenige wissen, wie viel man wissen muss, um zu wissen, wie wenig man weiß.”

Werner Karl Heisenberg (1901-1976)

Abstract ..... **I**

Zusammenfassung ..... **III**

1. Introduction **1**

1.1 Organization and major functions of mammalian small intestine 1

1.2 The Sodium-dependent Neutral Amino Acid Transporter B^0AT1 or the B^0 Neutral Amino Acid Transporter AT1 5

1.3 The System IMINO or the Sodium/IMINO Acid Transporter 1 (SIT1) 6

1.4 The Proton-coupled Amino Acid Transporter 1 (PAT1) 6

1.5 The Sodium-coupled Glucose Cotransporter 1 (SGLT1) 7

1.6 The facilitative Glucose Transporter Type 2 (GLUT2) 11

1.7 The Proton-coupled Peptide Transporter 1 (PEPT1) 14

1.7.1 The *SLC15A1* gene and the PEPT1 protein 14

1.7.2 PEPT1 transport mode and substrate affinity 16

1.7.3 Expression pattern of PEPT1 18

1.7.4 Regulation of PEPT1 18

2. Material and Methods **24**

2.1 Animals 24

2.2 Functional characterization of epithelial transporters 25

2.2.1 Techniques used 25

2.2.2 Preliminary studies to determine parameters of transporter activity 25

2.3 Experimental procedures intended to modify transporter activities 26

2.3.1 Effect of high-fat feeding on intestinal transporter activity 26
2.3.2 Effect of insulin on intestinal transporter function.....26
2.3.3 Luminal exposure of the small intestine to high glucose 27
2.3.4 Effect of diabetes on intestinal transporter function 28
2.4 Electrophysiological experiments using the Ussing chamber.....29
2.4.1 Electrophysiological principals.....29
2.4.2 Electrodes 30
2.4.3. Tissue preparation.....31
2.4.4 Measurements.....32
2.5 Uptake experiments using radiolabeled substrates 33
2.5.1 Tissue preparation.....33
2.5.2 Principles of uptake experiments.....34
2.5.3 Quantification 34
2.6 Intestinal RNA purification and cDNA synthesis 35
2.6.1 Quantitative real-time PCR 35
2.7 Intestinal tissue preparation 36
2.8 H & E staining 36
2.9 Tissue changes (Villus length and diameter) 37
2.10 Brush border membrane preparation 38
2.10.1 Western blot 38
2.11 Urine osmolarity.....39
2.12 Statistical analysis 39

3. Results 40

3.1 Transporter activities in jejunum – comparing wild type, *pept1*$^{-/+}$ and *pept1*$^{-/-}$ mice 40

3.1.1 Uptake studies and Ussing chamber measurements 40

3.1.2 Kinetic parameters in wt, *pept1*$^{-/-}$ and *sglt1*$^{-/-}$ mice 42

3.1.3 Segmental differences in transport of PEPT1 and SGLT1 44

3.2 Influence of diet-induced obesity on transporter function 45

3.2.1 Comparative Ussing chamber studies 45

3.3 Influence of insulin on transporter functions 47

3.3.1 *In vitro* effects of insulin 47

3.4. Effects of *in vivo* insulin treatment on transporter activities 48

3.4.1 Body weight and blood glucose 48

3.4.2. mRNA and protein concentrations of PEPT1 and SGLT1 49

3.4.3 Uptake experiments 51

3.4.4 Ussing chamber measurements 52

3.5 Effect of high luminal glucose on intestinal transporter function 53

3.5.1 Ussing chamber measurements before and after high glucose perfusion 53

3.5.2 Effect of glucose on an oral glucose bolus 56

3.6 Effect of glucose on intestinal transporters in STZ-induced type 1 diabetes 57

3.6.1 STZ-induced effects on body weight and blood glucose 57

3.6.2 Body weight 58

3.6.3 Blood glucose 58

3.6.4 Changes in tissue and organ weights in response to STZ-induced diabetes 60

3.6.5 Effects of STZ on pancreatic tissues 62

3.6.6 mRNA and protein concentrations of PEPT1 and SGLT1 62

3.6.7 Uptake experiments in everted gut rings of control and diabetic mice ... 64

3.6.8 Ussing chamber based Isc measurements in control and diabetic mice 65

4. Discussion 67

References 76

Appendix IV

Abbreviations IV

Units of measurements VIII

Diets IX

Standard chow SPF Tierhaltung IX

Standard chow open mouse facility XII

Control diet (11% energy from fat) open mouse facility XV

High-fat diet (60% energy from fat) open mouse facility XVIII

Danksagung XXI

Eidesstattliche Erklärung XXIII

Curriculum Vitae XXIV

List of Publications XXV

Tables:

Table 1 Reported SGLT1 substrate affinities (K_m) and maximal transport rates (V_{max}) 9

Table 2 SLC2-family members and their expression sites 13

Table 3 PEPT1 substrate affinities (K_m) and maximal transport rates (V_{max}) ... 17

Table 4 Composition of modified Krebs-Henseleit-Buffer in mM for Ussing chamber experiments 31

Table 5 Transporters and substrates used in Ussing chamber studies 32

Table 6 Modified KHB used for uptake experiments in everted gut rings 33

Table 7 Transporter and housekeeping genes with corresponding primer sequences 35

Table 8 Hemalum and eosin staining protocol for jejunal segments 37

Table 9 Substrate-induced short-circuit currents 42

Table 10 Isc responses before and after *in vitro* insulin treatment of tissues in Ussing chambers 48

Table 11 Body weight and blood glucose levels before and after i.p. injection of insulin 49

Table 12 Transporter-mediated Isc in insulin-treated and control mice 52

Table 13 **Open-circuit current (Ioc calculated as Isc) and measured short-circuit current (Isc) of PEPT1 and SGLT1 before and after high luminal glucose perfusion 55**

Table 14 **Tissue and organ weights of control and diabetic mice 60**

Table 15 **Substrate-induced Isc currents measured in control and diabetic mice 66**

Figures:

Figure 1 Structure and details of the gut 2

Figure 2 Transporter systems expressed in the enterocytes of the mammalian small intestine 4

Figure 3 Predicted membrane topology of the secondary structure of human SGLT1 protein 8

Figure 4 Predicted PEPT1 membrane topology 15

Figure 5 Interplay of PEPT1 (*SLC15A1*) with other solute transporters in apical and basolateral membranes of enterocytes 16

Figure 6 Schematic overview of a proposed inverse regulation of transporter proteins in the apical membrane in response to a high luminal glucose exposure 22

Figure 7 Chemical structure of Streptozotocin 28

Figure 8 Schematic illustration of an Ussing chamber 30

Figure 9 Razor blade panel with everted small intestine and 1 cm rings 34

Figure 10 [^{14}C] Gly-Sar uptake into everted gut rings in wt and *pept1*$^{-/-}$ mice ... 40

Figure 11 Representative current trace of substrate-induced Isc measured in jejunal segments of a wt and *pept1*$^{-/-}$ mouse 41

Figure 12 Kinetic parameters of PEPT1 in wt and *sglt1*$^{-/-}$ mice determined in Ussing chamber studies 43

Figure 13 Kinetic parameters of SGLT1 in wt and *pept1*$^{-/-}$ mice determined in the Ussing chamber studies 43

Figure 14 Segmental [^{14}C] Gly-Sar and [^{14}C] α-MDG uptake in wt mice 44

Figure 15 Representative current trace of electrogenic transporter activities measured in an Ussing chamber with one segment of wt mice fed a C- or HF-diet.....45

Figure 16 Transporter activities in wt mice fed a C-diet or HF-diet 46

Figure 17 Representative current traces of electrogenic transporters recorded in Ussing chambers before and after exposure of tissues to insulin 47

Figure 18 Insulin effects on blood glucose concentration 49

Figure 19 mRNA levels of PEPT1 and SGLT1 in tissues of control and insulin-treated mice 50

Figure 20 PEPT1 and SGLT1 protein tissue levels.....50

Figure 21 Transporter activities assessed in gut rings of control and insulin-treated mice 51

Figure 22 Representative current traces of Ussing chamber measurement.....52

Figure 23 Representative current traces in Ussing chambers before and after luminal perfusion 53

Figure 24 Isc responses of PEPT1, SIT1 and SGLT1 before and after 75 mM glucose perfusion 54

Figure 25 Blood glucose levels after oral glucose bolus 56

Figure 26 Substrate uptake rates after the oral glucose bolus 57

Figure 27 Body weight development over 5 days after STZ treatment 58

Figure 28 Blood glucose development over 5 days after STZ treatment 59

Figure 29 Post-injectional blood glucose measurements in STZ-treated mice 59

Figure 30 Determination of mean intestinal villus length in control and diabetic mice.....61

Figure 31 Morphology of Langerhans-islet cells of pancreatic tissue of control and diabetic mice.....62

Figure 32 Relative mRNA levels of PEPT1 and SGLT1 in intestine of control and diabetic mice 63

Figure 33 PEPT1 and SGLT1 protein levels in intestinal tissues 63

Figure 34 Transporter activities of PEPT1 and SGLT1 in control and diabetic mice.....64

Figure 35 Tissue resistance measured in control and T1-diabetic mice.....65

Figure 36 Representative current traces of Ussing chamber measurements in control and diabetic mice 66

Abstract

Transport proteins in the apical membrane of enterocytes mediate the selective uptake of ingested nutritional components into epithelial cells. Di- and tripeptides as products of gastrointestinal protein hydrolysis are transported by the proton-coupled peptide transporter 1 (PEPT1) whereas glucose absorption is mainly mediated by the sodium-dependent glucose transporter 1 (SGLT1). The proton-coupled amino acid transporter 1 (PAT1), the sodium / imino transporter 1 (SIT1) and the sodium-dependent neutral amino acid transporter (B^0AT1) are responsible for the absorption of neutral amino acids (AA) derived from protein digestion. Amongst these transporters especially PEPT1 and SGLT1 have been described as to undergo regulation by nutritional, hormonal and pathological factors with changes in expression level and in function. We here describe mouse studies that aimed to investigate the impact of such factors on the function of selected electrogenic transporters with the following questions: i) is the ablation of *pept1* compensated by an elevated uptake of AA via PAT1 and SIT1, ii) does insulin (*in vitro* & *in vivo*) regulate the expression and activity of the intestinal transporters in wild type mice and iii) does a Streptozotocin-induced diabetic state affect transporter expression and activity? To answer these questions, transporter gene expression and protein levels were quantified, whereas transporter activities were determined by electrophysiological experiments using the Ussing chamber and by everted gut rings with uptake experiments employing radiolabeled substrates.

Results showed (i) that none of the transporters (SIT1, PAT1 and SGLT1) that can be assessed by electrophysiological means displayed changes that may be taken as a compensatory adaptation to the lack of PEPT1 although heterozygous ($pept1^{-/+}$) mice revealed a decrease in AA transporter activities when compared to $pept1^{-/-}$ mice. These findings support previous studies that a PEPT1-deficiency seems – at least under normal dietary conditions – to generate no obvious phenotype. None of the experiments could confirm an effect of insulin on jejunal tissues with changes in transporter activity which suggest that insulin does not play a role in the regulation of transporter expression and function as proposed by studies in cultured cells. Induction of a diabetic state by Streptozotocin in mice caused PEPT1 mRNA and protein expression level to increase whereas transporter activity seemed reduced. SGLT1 mRNA levels were also elevated, while protein levels remained unchanged and electrogenic transporter activity was decreased.

In summary, the role of PEPT1 in overall intestinal AA absorption in mice seems less important than expected. There is also no evidence that the lack of a phenotype in animals with a deleted peptide transporter gene results in compensatory changes in electrogenic transporters that mediate the apical uptake of free amino acids or sugar. Although diabetes seems to have an impact on the investigated transporters, their functional impairments do not follow the changes in mRNA and/or protein expression suggesting that the driving forces for electrogenic transport – provided by the basolateral Na^+ / K^+ ATPase activity – may be subject to regulation in a diabetic state.

Zusammenfassung

Der Transport von Nährstoffen über die Epithelzellen des Darms wird von spezifischen, integralen Membranproteinen vermittelt. Di- und Tripeptide, welche die Hauptprodukte der gastrointestinalen Protein-Verdauung darstellen, werden vom protonenabhängigen Peptidtransporter 1 (PEPT1) in die Enterozyten aufgenommen. D-Glucose wird hauptsächlich über den natriumabhängigen Glukosetransporter 1 (SGLT1) resorbiert. Für die Aufnahme neutraler Aminosäuren (AS) dienen unter anderem der protonengekoppelte Aminosäuretransporter 1 (PAT1), der natriumabhängige IMINO-Transporter 1 (SIT1) sowie der natriumabhängige neutrale Aminosäuretransporter 1 (B^0AT1). Sie alle sind elektrogene Transportsysteme, deren Aktivität sich mittels elektrophysiologischer Techniken ermitteln lässt.

Studien an PEPT1 und SGLT1 deuteten darauf hin, dass diese Systeme durch diätetische und hormonelle Maßnahmen reguliert werden können. Die hier vorgelegten experimentellen Studien an Mäusen hatten das Ziel, im Tier und *in vitro* den Einfluss solcher Faktoren auf der Ebene der Expression und der Funktion ausgewählter Transporter zu untersuchen. Insbesondere wurde geprüft, inwieweit eine Deletion von PEPT1 zu einer gesteigerten Aufnahme von freien Aminosäuren mittels PAT1 und SIT1 führte und ob Insulin bzw. ein Insulinmangel die Expression und Aktivität der untersuchten Carrier änderte.

Auf molekularer Ebene wurden die Transporter anhand von Genexpressions- und Proteinanalysen untersucht; ihre Transportaktivität wurde mittels elektrophysiologischer Analysen in der Ussing-Kammer sowie durch Aufnahmestudien in everted gut rings unter Verwendung radioaktiver Substrate untersucht. Dabei zeigte sich, dass der Verlust von PEPT1 - der zu keinem auffälligen Phänotyp der Mäuse führt – auch keine markanten Änderungen in der Aufnahme von freien Aminosäuren herbeiführte. Allerdings waren die Transporteraktivitäten in den heterozygoten – nicht aber den homozygoten Tieren- herabgesetzt. Es konnten keine Regulationsvorgänge unter dem Einfluss von Insulin gefunden werden. Im Insulinmangel, d.h. nach Gabe von Streptozotocin zeigte sich im Darm für PEPT1 ein erhöhter mRNA- und Proteinspiegel, nicht aber eine erhöhte, sondern erniedrigte Aktivität des Transporters. Der mRNA-Spiegel von SGLT1 war unter Diabetes erhöht, die Proteinkonzentration blieb unverändert und die Aktivität war ebenfalls reduziert. Diese Diskordanz von mRNA-/Proteinspiegeln und Aktivität lässt vermuten, dass die Funktion der Na^+ / K^+ ATPase beeinflusst ist und damit keine Erhöhung der Transportleistungen elektrogener Transporter herbeigeführt werden konnte.

1. Introduction

1.1 Organization and major functions of mammalian small intestine

Since the beginning of evolution, cellular structures of organisms evolved in complexity; from protozoans (unicellular organisms) with simple cellular structures up to metazoans (multicellular organisms) with highly organized cellular structures forming tissues and organs. In all organisms, membranes separate the inter- and intracellular space from the extracellular space. Compartments built by epithelial structures, especially by polar epithelial cells, enable the controlled exchange of substances between the inner and outer milieu [1]. Changes in complexity of organisms' organization were accompanied by changes in nutrient supply. To absorb the monomers contained in complex nutritional polymers, such as proteins, lipids and carbohydrates, digestion mediated by enzyme-secreting organs such as pancreas had to evolve and the site of absorption, the intestinal tract, was evolutionarily modified to satisfy these needs.

The small intestinal tract is functionally divided in three sections: 1) the duodenum 2) the jejunum 3) the ileum. The duodenum is the first section following the stomach and is responsible for food breakdown by enzymes secreted by the pancreas (e.g. proteases, amylases and lipases) and liver (bile acids) [2]. In the jejunum, the degradation of carbohydrates into monosaccharides, of proteins into amino acids (single amino acids and oligopeptides) and of triglycerides into fatty acids is completed. The jejunum therefore is the major site of absorption that is further completed in the ileum.

The intestinal tract is characterized by enlarging folds called the Kerckig folds (Fig. 1 a, b). Attached to these folds villi further enlarge the absorptive surface area of the intestine. Villi (Fig. 1 c) are protrusions of the intestinal mucosa and consist of a layer of columnar epithelial cells, which display a polarized structure and a central core of connective tissue [2]. A further increase of the absorptive surface area is achieved by the microvilli that cover the apical membrane of epithelial cells. A layer of glycolipids, glycoproteins and mucopolysaccharides called the glycocalyx covers the brush border formed by the microvilli. The carbohydrate side chains of the glycocalyx bind water and allow enzymes secreted by the epithelial cells to adhere and to promote digestion of proteins and sugars [3]. The epithelial cells found in the small intestine possess different functions. Goblet cells (Fig. 1 c) produce and secrete mucins that dissolve in water and form the mucus layer covering and protecting the epithelial cells. Paneth cells (Fig. 1 c) at the bottom of the crypt

region serve as immune cells of the intestine and secrete for example antibacterial compounds for host defense. Endocrine cells (Fig. 1 c) are responsible for hormone secretion while the enterocytes absorb nutrients. At the bottom of the crypt region stem cells differentiate to all these kinds of epithelial cells and move along the crypt upwards. Reaching the villus mid the cells become mature and replace the once that have been sloughed off, since the lifespan of epithelial cells is only a few days [4].

Nutrients have to pass the epithelial layer to reach circulation. Two major transport routs are known: 1) the paracellular and the 2) transcellular route. Paracellular transport appears through tight junctions. Tight junctions connect the neighboring epithelial cells to each other by nearly closing the extracellular space in between. In some tissues, these connections are very tight, while in the intestine or in the proximal convolute tubule, the connection is leaky thereby allowing small molecules (e.g. water, some sugars, and alcohols) to pass [5].

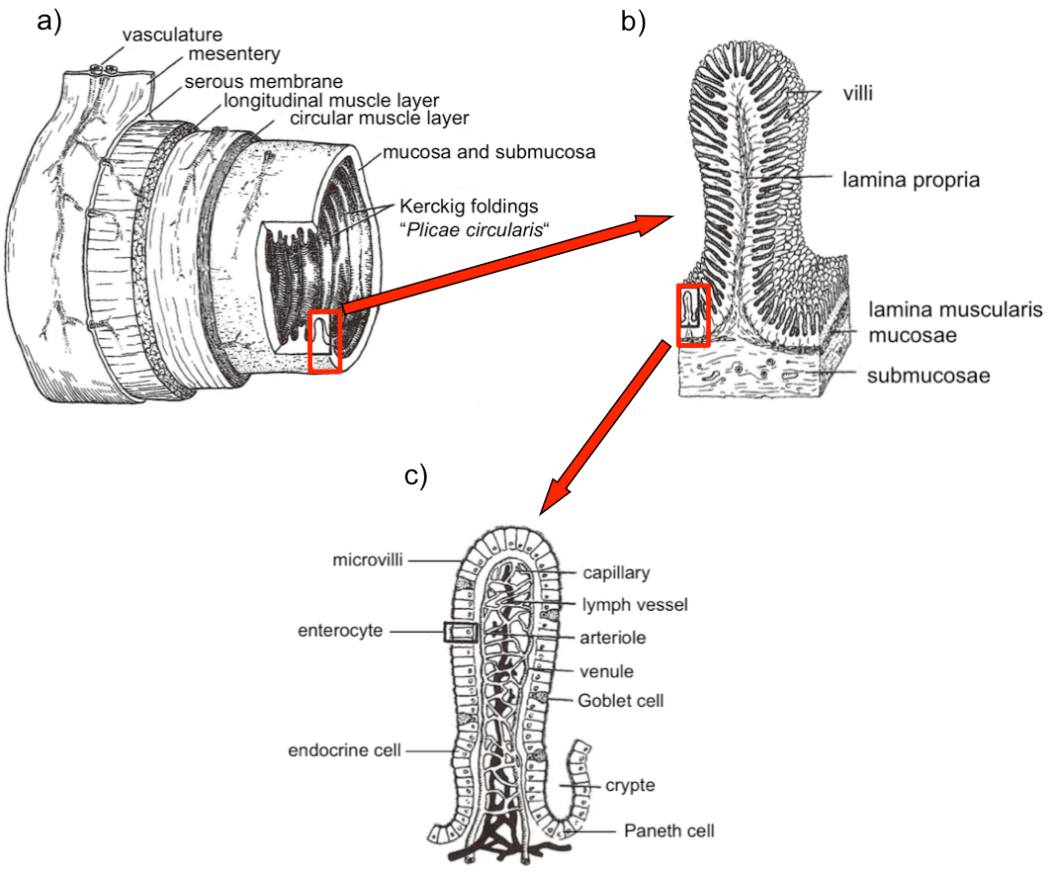

Figure 1 Structure and details of the gut

Gut architecture (a), view onto the surface area with enlarging intestinal folds (b) and villi (c) (modified according to [3]).

Transcellular transport can be passive diffusion and is thus depending on the permeability of the cell membrane for the solute. Although it was believed that permeation of lipid soluble compounds such as fatty acids, monoacylgylceroles and cholesterol occurs by passive diffusion, recent years have demonstrated that those compounds also possess specialized transport proteins. Integral membrane proteins serving as transporters can be divided into: 1) symporters, 2) antiporters and 3) uniporters. As illustrated in the Fig. 2, primary active transport (I) is energized by the hydrolysis of ATP as for example in the ABC-transporter proteins whereas secondary active transport processes are classified by coupling to sodium/potassium ATPase (Na^+ / K^+ ATPase) that provides the driving force for secondary transporter by utilizing the Na^+-gradient for uptake (e.g. NHE3, II). A tertiary active transport process may be an exchanger coupled to a secondary active transporter [6] as for example for intestinal amino acid absorption in which a Na^+-dependent transporter generates an amino acid gradient for exchange with other luminal amino acids allowing their uptake (III).

Since the jejunum is the major absorption site of nutrients that serve as building blocks for protein synthesis and energy metabolites, the pivotal role of the enterocytes is the transport of amino acids, peptides and glucose derived from the ingested food. The absorption over the apical membrane is accomplished by a variety of transporters (Fig. 2). The absorbed nutrients are secreted into systemic circulation by basolateral transporters and transport mainly follows the concentration gradient.

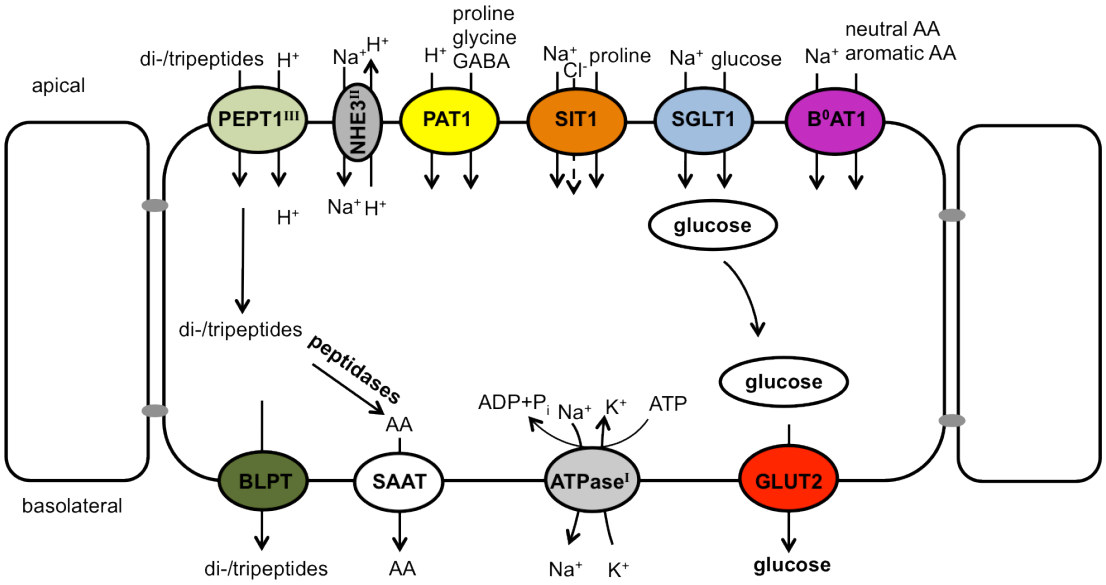

Figure 2 **Transporter systems expressed in the enterocytes of the mammalian small intestine**

Apical transporters: AA (amino acids); PEPT1 (proton-coupled peptide transporter 1, *SLC15A1*, III: tertiary active transporter); PAT1 (proton-coupled amino acid transporter 1, *SLC36A1*); SIT1 (sodium/imino-acid transporter 1, *SLC6A20*); SGLT1 (sodium/glucose cotransporter 1, *SLC5A1*); B^0AT1 (sodium-dependent neutral amino acid transporter neutral and cationic transporter, *SLC6A19*); NHE3 (sodium proton exchanger 3, *SLC9A3*, II: secondary active transporter). Basolateral transporters SAAT (single amino acid transporter); BLPT (basolateral peptide transporter); GLUT2 (facilitative glucose transporter type 2, *SLC2A2*); Na^+ / K^+ ATPase (sodium-potassium ATPase, *ATP1A1*, I: primary active transporter).

The majority of these apical transport systems, as depicted in Fig. 2, use electrochemical gradients coupled to either sodium ions (Na^+) or protons (H^+) as driving force. The Na^+-gradient is generated by the basolateral Na^+ / K^+ ATPase creating a downhill transepithelial concentration gradient for sodium across the apical membrane (Fig. 2). In case of the proton-motive force, the pH gradient is generated by the apical sodium proton exchanger NHE3 that in exchange for Na^+ in a 1:1 coupling exports protons to the lumen. The proton-gradient thus serves as a driving force for PEPT1 and PAT1.

1.2 The Sodium-dependent Neutral Amino Acid Transporter B^0AT1 or the B^0 Neutral Amino Acid Transporter AT1

Transport of neutral and aromatic amino acids across the apical membrane of intestinal and renal enterocytes is accomplished by the Na^+-depended transporter protein B^0AT1 belonging to the system B^0, also referred to as the neurotransmitter transporters (NTT's) or the neurotransmitter-sodium-symporter family [7, 8]. The transport system belongs to the solute carrier family 6 (SLC6), with the *SLC6A19* gene encoding for the transporter protein B^0AT1 [8, 9] as a secondary active transporter.

The membrane topology of this protein displays 12 transmembrane domains (TMD) with inward facing N -and C termini [10]. Most transporters of this family contain about 600 amino acids and reveal a 40% amino acid sequence identity [10]. Transport stoichiometry of the B^0AT1 transporter was identified by Böhmer *et al.* (2005), using flux and electrophysiological transport studies in *Xenopus laevis* oocytes expressing murine B^0AT1. They identified the previously described Na^+ dependency of the transport of neutral amino acids [11] with a coupling ratio of 1:1, displaying an electrogenic co-transport [12]. Substrates of the transporter are e.g. alanine and phenylalanine with a K_m of 4 mM and leucine with a K_m of 1.1 mM. While the transporter shows a rather low affinity to glycine with around 11 mM [13]. K_m values display a high heterogeneity and reflect the Na^+- dependency by a decreasing K_m with increasing Na^+ concentration [12]. It was demonstrated that the human B^0AT1 displayed the same transporter activities as the mouse orthologous with similar affinities for the substrates [8]. Mutation studies of the *SLC6A19* gene revealed SLC6A19 to be the candidate gene in the development of Hartnup disorder, an autosomal recessive disorder leading to aminoaciduria (OMIM 234500) [8] that was first described in the 1956. Up to date 21 mutations in over 20 families have been described to contribute to the disorder [13]. In rabbit ileum the B^0 class of transporters is represented by two proteins, the $B^{0,+}$ transporter that in a Na^+-dependent manner accepts large neutral amino acids and cationic amino acids and the system ASC that transports mid-sized neutral amino acids [14].

1.3 The System IMINO or the Sodium/IMINO Acid Transporter 1 (SIT1)

The intestine is the major site of proline uptake and proline metabolism is immediately linked to arginine metabolism, urea cycle and citrulline but also to creatinine or polyamine synthesis [15]. Uptake of proline and hydroxyproline in intestine occurs mainly via the sodium/imino acid transporter 1 (SIT1). The transport system belongs to the SLC6 family and the *SLC6A20* gene encodes for the transporter protein SIT1. The membrane topology of the protein displays the typical 12 transmembrane spanning domains with the inward facing N- and C-termini [16]. Investigations on the stoichiometry of SIT1 revealed many different coupling ratios depending on the transported substrate [16, 17]. Mutation, expression and functional studies of the transporter when expressed in *X. laevis* oocytes by Bröer *et al.* (2009) revealed that the substrate translocation of SIT1 is coupled to 2 Na^+ and 1 Cl^-. Two functional binding sites for Na^+ and one for Cl^- have been identified. Uptake studies showed that the Cl^- binding site is crucial for the correct folding and function of the protein [18]. The transporter protein shows a low proline affinity reflected by a K_m value of 0.2 mM [16]. Expression studies of murine XT3s1 in *X. laevis* oocytes revealed that in mice two gene homologues are expressed that share amino acid sequence identity of over 93 %. The gene encoding the transporter XT3 ($IMINO^k$) is expressed in kidney, while transcripts of XT3s1 ($IMINO^b$) were found to be expressed in lung, brain, kidney, small intestine and spleen [19, 20]. Genetic defects of the SIT1 expressed either in the kidney or the small intestine in humans causes impaired transport of hydroxyproline, proline and glycine with elevated levels in urine, defined as iminoglycinuria (OMIM 242600). Studies though indicate this genetic disorder to be rather a multiple gene based disease, that is not only caused by disturbed SIT1 function, but also by incorrect function of other transporters affecting proline absorption such as the proton amino acid transporter 1, PAT1 [21].

1.4 The Proton-coupled Amino Acid Transporter 1 (PAT1)

The transport of a variety of amino and imino acids (proline and hydroxyproline) is mediated by the proton-coupled amino acid transporter, PAT1 as a member of the SLC36 family with the *SLC36A1* gene encoding for the intestinal transporter protein [22]. The transporter was first identified in plants and yeast [23, 24] and later detected in mammals (rat, mouse, rabbit and human) [25]. The membrane topology of the protein is characterized by 11 transmembrane spanning domains with an inward facing N-terminus and an outward facing C-terminus. The transport is Na^+ and Cl^- independent but displays an H^+-coupled symport.

The stoichiometry of the co-transport of substrate to proton is 1:1. K_m values of PAT1 (1-10 mM) indicate a low affinity and high capacity transport system [26]. In epithelia PAT1 shows a Na^+-dependency, which originates likely from the function of the sodium/proton exchanger NHE3 mediating H^+ efflux via Na^+ influx. This functional cooperation has also been observed for other transporters such as PEPT1 [27].

In 2002, Boll *et al.* identified the mouse orthologous to PAT1 [21, 26] and in 2003 the PAT1 protein was identified in the human intestinal cell line Caco-2 [28]. Human PAT1 is a 476 amino acid containing membrane protein sharing about 85 % sequence identity with the rat PAT1. Tissue distribution and cellular expression of PAT1 spreads from brain, small intestine to kidney, lung and neurons [21]. A unique feature of PAT1 is that it can transport in electroneutral fashion H^+ and short-chain fatty acids such as acetate, propionate and butyrate [29].

Apart from small neutral amino acids (glycine, L-proline and L-alanine), PAT1 is also able to transport the neurotransmitter γ-aminobutyric acid (GABA) [30] and the osmolyte taurine [27]. In 2009, Anderson *et al.* [31] described two transporter systems to be responsible for intestinal absorption of taurine in humans. Under physiological conditions TauT (Cl^--dependent taurine transporter, *SLC6A6*) is responsible for the basal uptake, while under high luminal concentrations as they may occur during a meal, taurine uptake is mainly accomplished by PAT1 [31].

1.5 The Sodium-coupled Glucose Cotransporter 1 (SGLT1)

An essential feature of almost all cells (from bacteria up to highly specialized mammalian cells) is the transport of glucose and galactose across the plasma membrane. Glucose is required for many metabolic processes occurring in cells, e.g. oxidative and non-oxidative ATP production. In the intestine glucose and galactose uptake depends on the sodium/glucose cotransporter SGLT1 encoded by the *SLC5A1* gene. The *SLC5* gene family accounts for more than 298 transporter genes and expression of these transporters is found in various tissues: brain, small intestine, muscle, heart, kidney and others [32, 33]. The sodium/glucose cotransporter branch (SGLT's) include seven members (SGLT1-7) with different expression patterns [33] and the first discovered and identified cotransporter of this family was SGLT1. SGLT1 is a - species dependent - 580 to 718 (human: 664; rat: 665 and mouse: 665) amino acid containing polypeptide with a predicted molecular weight of 60 to 80 kDa. Amino acid sequence studies of rabbit, rat and human SGLT1 isoforms

expressed in *X. laevis* oocytes revealed that rat and human isoforms are functionally more similar to each other than the rabbit isoform [34]. The isoforms display different putative protein kinase C (PKC) and protein kinase A (PKA) phosphorylation sites and show different activation patterns by kinases depending on the actual amino acid sequence of the transporter protein [35, 36].

As shown in Fig. 3 the SGLT1 protein contains 14 transmembrane domains (TMD's) with N- and C- termini facing the extracellular compartment [32]. Two large loops are found at the extracellular side connecting TMDs 6-7 and TMDs 8-9 while the orientation (outward or inward direction) and existence of the third loop, connecting TMDs 13-14 is still controversially discussed [37]. The stoichometry was found to be 2 Na^+:1 glucose.

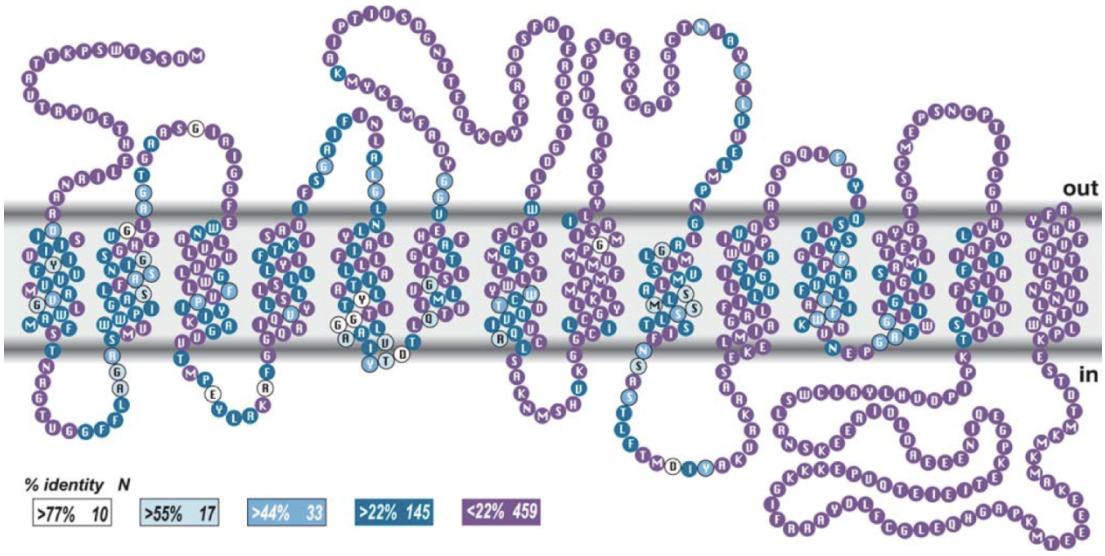

Figure 3 **Predicted membrane topology of the secondary structure of human SGLT1 protein (modified from [32])**

The model shows 14 TMD's with two large ECL's and the NH_3 and COOH termini facing the extracellular space. ECL between TMD 13 and 14 is facing the intracellular side. Color-coding reveals conservation of the amino acid residues among 19 divergent members (pro-and eukaryotes) of the sodium/substrate symporter family [37].

Crane was the first, in 1961, who described the coupled transport of Na^+ with glucose by SGLT1 (not known in nature as yet). He verified a coupled downhill Na^+ transport to uphill glucose transport across the brush-border membrane (BBM) of the small intestine [38]. The chemical Na^+ gradient needed for sugar transport is primarily maintained by the action of the basolateral Na^+ / K^+ ATPase. Transepithelial glucose transport requires the glucose transporter 2 (GLUT2) in the basolateral membrane for sugar release into circulation [39-41].

Natural substrates of SGLT1 are D-glucose and D-galactose while non-metabolizable substrates are represented by 3-O-methylglucoside and α-MDG [42].

SGLT1 is designated as a high affinity transporter [43] therefore various studies in different species, tissues and cell lines have been performed to determine apparent K_m values for the transporter (Tab.1).

Table 1 Reported SGLT1 substrate affinities (K_m) and maximal transport rates (V_{max})

BBMV: Brush-border membrane vesicles; rb SGLT1 (rabbit), rSGLT1 (rat), hSGLT1 (human); Caco-2: human epithelial colorectal adenocarcinoma cells; RIE-1: Rat Intestinal Epithelial cells; IEC: rat derived Intestinal Epithelial Cells. All data represent apparent values (n.d.: no data).

Publication	Tissue/Cell	Substrate	Concentration (mM)	K_m (mean ± SE)	V_{max} (mean ± SE)
Debnam & Levin 1974 [44]	jejunum in vivo (rat)	D-Glucose	0 – 64	22.6 ± 1.3	85.8 ± 4.8
		D-galactose	0 – 64	32.4 ± 2.3	113 ± 11.1
		α-MDG	0 – 64	31.2 ± 1.8	48.8 ± 3.9 (µm/10cm*15min)
Brot-Laroche *et al.* 1986 [45]	jejunum, BBMV (rabbit)	D-Glucose	0.1 – 350	0.4 ± 0.1	n.d.
	jejunum		0.1 – 350	0.5 ± 0.1	n.d.
	BBMV (guinea pig)	D-Glucose	10^{-6} – 10^{-3} [M]	0.4 ± 0.1	n.d.
Hirayama *et al.* 1996 [34]	*X. laevis* oocytes:				
	rbSGLT1	α-MDG	0 – 100	0.17 ± 0.01	n.d.
	rSGLT1	α-MDG	0 – 100	0.31 ± 0.02	n.d.
	hSGLT1	α-MDG	0 – 100	0.49 ± 0.03	n.d.
Cheeseman 1997 [46]	jejunum BBMV (rat)	D-Glucose	33 µM – 6.7	0.13 ± 0.01	about 400 (pmol/mg prot/sec)
Kellet & Helliwell 2000 [47]	jejunum in vivo (rat)	D-Glucose	1 – 100	26.9 ± 6.5	13.6 ± 1.5 (µmol*min^{-1}*(g of dry weight)$^{-1}$)
Mate et al. 2006 [48]	Jejunum BBMV	D-Glucose	0.01 – 100	0.14 ± 0.02	455 ± 12
	Ileum BBMV (rat)	D-Glucose	0.01 – 100	0.15 ± 0.01	200 ± 25 (pmol*mg protein^{-1}* s^{-1})
Yang *et al.* 2010 [49]	jejunum,				
	upper villus	D-Glucose	2.3 – 92	2.02 ± 0.52	390 ± 96.2
	middle villus	D-Glucose	2.3 – 92	3.7 ± 1.05	590 ± 167.7
	crypt (piglet)	D-Glucose	2.3 – 92	2.76 ± 0.5	492.4 ± 87.3 (pmol*mg protein^{-1}*s^{-1})
Zeng et al. 2011[50]	Caco-2	D-Glucose	0.5 – 50	7.5 ± 0.6	709 ± 18
	RIE-1	D-Glucose	0.5 – 50	6.7 ± 0.8	199 ± 11
	IEC-6	D-Glucose	0.5 – 50	7.6 ± 0.4	235 ± 4 (nmol/mg 1min)

The regulation of SGLT1 activity and expression was shown to depend on hormones such as insulin [51], glucagon-like peptide 2 (GLP2) from L-cells [46] and gastric inhibitory polypeptide (GIP) derived from K-cells [52]. Cholecytokinin 8 (CCK-8) secreted by I-cells [53] appeared to decrease the abundance of SGLT1 in the enterocytes of the jejunum.

Since insulin regulates glucose homeostasis, it is intriguing to assume that intestinal glucose absorption is influenced by the action of insulin. Pennington and colleagues demonstrated in 1994 that vascular as well as luminal insulin decreases the Na^+ dependent glucose uptake [51], while Banerjee and colleagues reported before (1989) that the Na^+ dependent glucose uptake is increased by the action of insulin [54]. In this respect, data are still highly controversial on whether insulin affects nutrient uptake in the gut.

In addition to hormonal regulation of SGLT1, transporter activity on an expression or functional level appears to be affected by the intracellular 617-amino-acid long protein RS1, described by Osswald *et al.* (2005). Mice lacking the *Rsc1A1* gene, respectively the RS1 protein showed increased SGLT1 activity and an accelerated development of obesity [55].

Type 1 diabetes (T1D) has been shown to have effects on SGLT1 abundance and activity. Hyperglycemia was attributed to an increased electrochemical driving force for SGLT1 mediated by increased food intake [56]. Additionally, SGLT1 appearance in enterocytes of the ileum with usually low abundance of SGLT1 and an enlargement of villus length [57, 58] was reported in diabetic rats. The renin-angiotensin system (RAS) found with its most key enzymes and peptides in the intestine is additionally described to effect SGLT1 activity in diabetes [59].

Expression studies performed in intestinal tissue of mice by Yoshikawa *et al.* (2011) indicate a wide distribution of the transporter along the small intestine. SGLT1 protein was found to be located exclusively in the BBM of enterocytes. Highest gene expression levels were observed in the proximal part of the small intestine, but compared to other glucose transporters even the distal part and the large intestine showed relatively high SGLT1 transcript levels [60]. Studies performed on villi of rabbit small intestine showed SGLT1 protein expression only in mature enterocytes and not in Paneth, Goblet and enteroendocrine cells (EEC's). No transcripts were detected in the crypt cells but expression increased about 6-fold by reaching the epithelial cells at the villus tip [61]. Apart from the intestine, SGLT1 is also expressed in the kidney – like its orthologous protein SGLT2 - which is exclusively found in the S1 and S2 segments of the renal convoluted

proximal tubules, where it is responsible for the majority of glucose reabsorption from the glomerular filtrate [62, 63].

Sugar transport studies and hormone secretion studies with ELISA-based detection of hormones have been described in GLUTag cells, a murine L cell model [64], as well as in murine K-cells [65] suggesting that SGLT1 may also be found in EE L-cells and could be involved in triggering hormone secretion.

Mutations in the human *SLC5A1* on chromosome 22 gene can lead to glucose-galactose malabsorption (GGM) with the clinical symptoms of watery diarrhea and weight loss when eating carbohydrates. The origins can be missense, frame shift, and nonsense mutations. GGM is an autosomal recessive disorder affecting mainly the trafficking of the protein to the plasma membrane [66, 67].

1.6 The facilitative Glucose Transporter Type 2 (GLUT2)

The facilitative glucose transporter GLUT2 belongs to the SLC2 family and the protein is encoded by the gene *SLC2A2*. The SLC2 protein/transporter family comprises 14 isoforms (SLCA1-14) and based on primary sequence comparison, the GLUT family can be divided in three subclasses (Tab. 2). Class I comprises GLUT1-4 and GLUT14 (splice variant of GLUT3 [68]); Class II comprises GLUT5, 7, 9 and 11 and class III includes the GLUT isoforms GLUT6, 8, 10, 12 and the proton driven myo-inositol transporter GLUT13 (HMIT) [69, 70].

Common features of the GLUT-family are 12 TMD's with N- and C-termini facing the cytoplasm. Class I-II harbor an N-linked glycosylation site in the first ECL, while class III family members exhibit that site within the 9th ECL [70]. Another common feature of the GLUT-family is the energy-independent transport of their substrates downhill the concentration gradient. These systems are also called passive carriers.

Cloning from human sample cDNA libraries in 1988 revealed prominent GLUT2 expression in liver, kidney and intestine [41]. Further analysis identified GLUT2 in insulin-producing β-cells of the Langerhans-islets in the pancreas with an apparent K_m of 17 mM for 3-*O*-methyl glucose, similar to that reported for liver GLUT2 [71, 72]. Natural occurring substrates of the glucose transporter are D-glucose (K_m ~ 17 mM), D-galactose (K_m ~ 92 mM), D-mannose (K_m ~ 125 mM) and D-fructose (K_m ~ 76 mM) [72, 73]. In 2002, Uldiy *et al.* [73] showed GLUT2 to transport also glucosamine with a much higher affinity (K_m ~ 0.8 mM) than

glucose and proposed a lack of specific substrate binding motif (QLS) in the protein of helix 7.

In the pancreatic β-cells, GLUT2 is expressed in the plasma membrane and functions together with the cytosolic localized glucose phosphorylating enzyme glucokinase as a glucose sensor for insulin secretion [74]. In the kidney and small intestine GLUT2 is expressed in the basolateral membrane of epithelial cells and participates in the release of cytosolic glucose into the bloodstream [32, 75].

The expression of GLUT2 in the basolateral membrane of epithelial cells has been studied extensively. Newer findings however question the exclusive basolateral expression. Some groups were able to show apical localization of GLUT2 in the enterocytes of the small intestine in rats [75, 77, 78]. Furthermore, a reciprocal expression pattern of GLUT2 and PEPT1 under high luminal glucose concentrations has been described [79].

Table 2 SLC2-family members and their expression sites

Modified according to [76]. Red: class I isoforms; green: class II isoforms; black: class III isoforms.

Gene	Protein	Isoform (aa)	Major site of expression
SLC2A1	GLUT1	492	Ubiquitous expression, brain
SLC2A2	GLUT2	524	Liver, islets, small intestine, kidney
SLC2A3	GLUT3	496	Brain, nerve cells
SLC2A4	GLUT4	509	Muscle, fat, heart
SLC2A5	GLUT5	501	Intestine, kidney, testis
SLC2A6	GLUT6	507	Spleen, leucocytes, brain
SLC2A7	GLUT7	524	Small intestine, colon, testis
SLC2A8	GLUT8	477	Testis, blastocysts, brain muscle adipocytes
SLC2A9	GLUT9	511/540	Liver, kidney
SLC2A10	GLUT10	541	Liver, pancreas
SLC2A11	GLUT11	496	Heart, muscle
SLC2A12	GLUT12	617	Heart, prostate, mammary gland
SLC2A14	GLUT14	497/520	Testis
SLC2A13	GLUT13 (HMIT)	618/629	Brain

To elucidate the role of GLUT2 in glucose homeostasis, different transgenic mouse models have been introduced since 1994. One of the first studies was the overexpression of a GLUT2 antisense mRNA in β-cells of transgenic mice (RIP-I/anti-GLUT2) by Valera *et al.* [80]. They showed that a significantly reduced GLUT2 protein concentration in the pancreatic β-cells led to impaired **g**lucose-**s**timulated **i**nsulin **s**ecretion (GSIS) resulting in diabetes in these animals. [80]. The next transgenic mouse model was the constitutive *glut2* knockout mouse by Guillam *et al.* in 1997 demonstrating lethality beyond the age of 3 weeks [81]. The reexpression of GLUT1 specifically in the pancreatic β-cells of the GLUT2-deficient mice rescued the animals and led to a normal first phase GSIS. On the other hand these animals showed a fasting hypoglycemia, glycosuria and a shift in pancreatic α- to β-cell ratio and an elevated glucagon to insulin ratio [82].

1.7 The Proton-coupled Peptide Transporter 1 (PEPT1)

For a long time it was believed that ingested peptides had to be hydrolyzed into single amino acids to be absorbed by the intestinal enterocytes. This was disproved by the discovery of a dipeptide carrier system in the human jejunum [83-86]. Furthermore, dipeptide uptake studies performed in intestinal brush-border membrane vesicles (BBMV) by Ganapathy & Leibach (1983, 1985) and Ganapathy *et al*. (1984) demonstrated that this was a Na^+-independent but H^+-coupled peptide transport system, which was activated by an inwardly-directed pH-gradient [87-89]. Transport studies performed in *X. laevis* oocytes expressing rabbit PEPT1 cDNA revealed that peptide transport across the membrane was independent of extracellular Na^+, K^+ and Cl^-, but driven by an electrochemical H^+-gradient and electrogenic in nature. Apart from its ability to transport over 400 dipeptides and 8000 tripeptides, the peptide transporter (PEPT1) is also capable of transporting various peptidomimetics and thereby improving the oral bioavailability of drugs such as cephalosporins, penicillins (β-lactam antibiotics), antivirals and for example pro-drugs of L-DOPA [90].

1.7.1 The *SLC15A1* gene and the PEPT1 protein

The identified intestinal peptide transporter PEPT1 belongs to the SLC15 family, which in 55 gene subfamilies has 362 functional proteins [91]. PEPT1 (*SLC15A1*) is a low affinity, high capacity transporter protein with a size of 78 kDa. An orthologous of this transporter (PEPT2) is expressed in epithelial cells of the kidney, mammary glands and other tissues with very similar characteristics and substrate specificity. Except that PEPT2 is a high affinity but low capacity transporter [92].

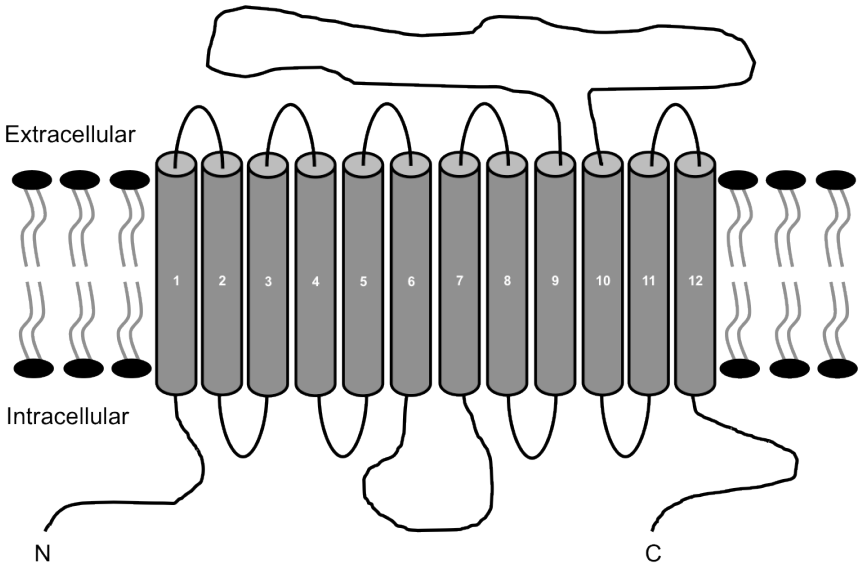

Figure 4 Predicted PEPT1 membrane topology

The model shows 12 transmembrane spanning domains (TMD's) with one large extracellular loops (ECL) between TMD 9 and TMD 10 and an intercellular facing loop between TMD 6 and TMD 7. The NH_3 and COOH termini are facing the intracellular space.

The PEPT1 protein consists of 708 amino acid residues in humans and 709 in mouse [93] and as shown in Fig. 4, 12 predicted TMD´s with a large extracellular loop between TMD 9 and TMD 10. Both amino and carboxyl termini are facing the intracellular side and there are two predicted putative protein kinase C phosphorylation sites in TMD 8-9 (Ser357) and in TMD 12 (Ser704) [93, 94]. The TMDs 1-4 and TMDs 7-9 reflect important sites concerning the affinity and binding of the substrate. Mutational studies (in *X. laevis* oocytes and HeLa cells) of the amino acid residue histidine 57 (H57), which is located in the extracellular loop between TMD1-2 and H121 that is located in the TMD 4, pronounce the importance of these residues in catalytic function of PEPT1. H57 seems to be involved in H^+ binding and H121 for the protonation of acidic peptides before the translocation by the transporter [95-98]. The aromatic tyrosine residue Y56, which flanks H57, decreases the affinity of PEPT1 for different charged dipeptides when mutated to phenylalanine [98].

Deletion analysis of the human *pept1* promoter suggested a region spanning 172 -35bp to be essential for basal *pept1* transcription activity. Though it was found that the TATA boxes were unusually far upstream the transcription start site (511-517bp), while the GC boxes (29 bp, 300 bp) are located near the transcription start site [90]. This makes the GC box a more promising promoter element [94]. The transcription factor SP1 binds to the GC-box and plays a significant role in transcriptional regulation of PEPT1. As an intestinal-specific transcription factor for the expression of the *SLC15A1* gene, Cdx2 (caudal-related

homeobox protein 2) has been identified to interact with SP1 [99] thereby regulating PEPT1 expression.

1.7.2 PEPT1 transport mode and substrate affinity

The transport of di- and tripeptides by PEPT1 is a substrate-coupled H^+-cotransport, allowing transport against the substrate concentration gradient. The accumulation of protons and the resulting acidification of the enterocyte are counteracted by the sodium-proton exchanger 3 (NHE3), found in the apical membrane of enterocytes (Fig 5). The dependency of PEPT1 activity on NHE3 has been shown by transport studies in *X. laevis* oocytes, Caco-2 cell monolayers, and intercellular pH measurements in enterocytes (*in vivo*) and oocytes [100, 101]. The extrusion of the sodium ions is accomplished by the basolateral Na^+ / K^+ ATPase (Fig 5). In addition to the apical NHE3 also the basolateral Na^+-coupled bicarbonate (HCO_3^-) symporter may influence the efficiency of PEPT1-mediated di-/and tripeptide transport [102].

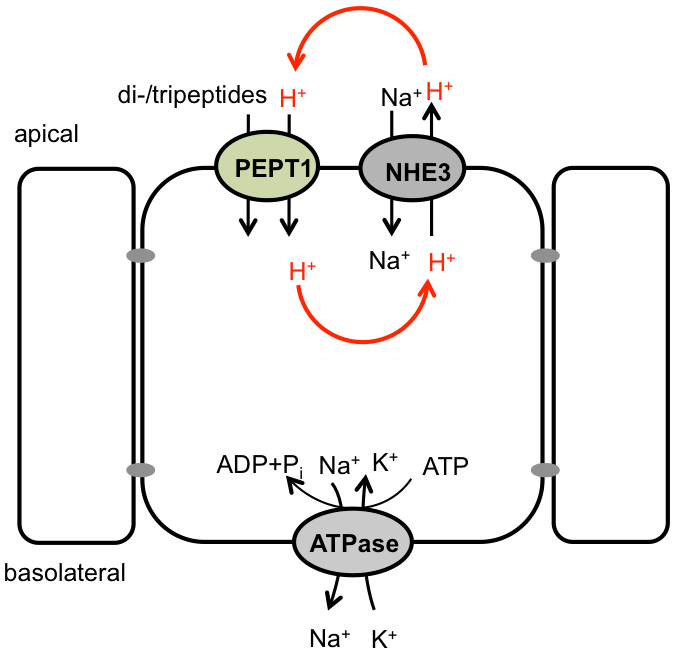

Figure 5 **Interplay of PEPT1 (*SLC15A1*) with other solute transporters in apical and basolateral membranes of enterocytes**

Acidification due to proton-coupled substrate transport by PEPT1 (light green) is counter-acted by proton extrusion via the sodium-proton exchanger NHE3 (grey). Export of sodium is accomplished by the basolateral expressed Na^+ / K^+ ATPase (sodium-potassium ATPase, grey).

The minimal requirements of a peptide to be transported by PEPT1 have been investigated by Döring *et al.* (1998) using yeast transport assay studies and *X. laevis* oocytes expressing rabbit cDNA of PEPT1 for uptake studies. These experiments showed that the minimal determinants of substrate recognition by PEPT1 requires two ionized head groups (i.e. amino-and carboxyl group), which are separated by four intermolecular spacers (CH_2) with a distance of 5 - 6.3 Å. A peptide bond is not necessarily required but only transported in the *trans*-form when present while the *cis*-form is considered to be too small to be accepted [103].

Table 3 PEPT1 substrate affinities (K_m) and maximal transport rates (V_{max})

HeLa: cervical cancer derived cell line; Caco-2: human epithelial colorectal adenocarcinoma cells; SKPT: rat renal cell line; hcDNA: human complementary DNA.

Publication	Tissue / Cell	Substrate (dipeptide)	Concentration (mM)	K_m (mean ± SEM)	V_{max} (mean ± SEM)
Adibi *et al.* 1974 [84]	human jejunum	Gly-Gly	20,50,75,100	43.3 ± 2.6	837 ± 62 (µmol/min/15cm)
Liang *et al.* 1995 [104]	HeLa hcDNA	Gly-Sar	0.05 – 5	0.29 ± 0.04	4.7 ± 0.3 (nmol/2min/ 10^6cells)
Thamotharan *et al.* 1999 [105]	rat BBMV (jejunum)	Gly-Gln	5 - 40	39.5 ± 5.11	19.9 ± 1.6 (nmol/mg protein/10s)
Thamotharan *et al.* 1999 [106]	Caco-2	Gly-Gln	0.1 – 5	1.49 ± 0.55	3.53 ± 0.61 (nmol*mg protein^{-1}*5min^{-1})
Winckler *et al.* 1999 [107]	Porcine jejunum	Gly-L-Sar	1 - 30	11.6 ± 3.32	1.67 ± 0.06 (µeq*cm^{-2}*h^{-1})
Gangopadhyay *et al.* 2002[108]	rat BBMV (jejunum)	Gly-Gln	5 - 40	15.33 ± 5.33	17.24 ± 2.75 (nmol*mg protein^{-1}*10s^{-1})
Wenzel *et al.* 2002 [109]	Caco-2	Cefexime	0.05 – 5	1.9 ± 0.2	36.2 ± 2.7 (nmol*cm^{-2} *30min^{-1})
Knütter *et al.* 2008 [110]	Caco-2	Gly-Sar	0 – 10	1.1 ± 0.1	39.4 ± 1.0 (nmol*mg protein^{-1}/10min)
	SKPT	Gly-Sar	0 – 10	0.14 ± 0.02	6.9 ± 0.3 (nmol*mg protein^{-1}/10min)
Jappar *et al.* 2010 [110]	mouse jejunum	Gly-Sar	0.01 - 200	19.8 ± 3.3	4.4 ± 0.2 (nmol/cm^2/s)
Ma *et al.* 2011 [111]	mouse jejunum	Gly-Sar	0 - 40	9.96	233 (pmol/mg/20sec)

The affinities of PEPT1 to its substrates have been determined by many groups and in many different systems [84, 104-106, 108-112]. As depicted in Tab. 3, K_m's as well as the V_{max} values display a high heterogeneity, which can on the one hand be explained by the different tissues or cells and on the other hand by the different experiments carried out.

1.7.3 Expression pattern of PEPT1

The mRNA expression pattern of PEPT1 was studied by Lu and Klaassen (2005) in 19 tissues of mice and rats (male and female). As expected, highest expression levels were found in the small intestine, especially the jejunum, which was independent of gender and species. Expression was also detected in kidney, gonads (male) and uterus (female) in rats. In mice, PEPT1 was additionally detected in the large intestine and the gonads of female animals [113].

Studies performed by Merlin *et al.* (2001, 2009) suggested an induction of PEPT1 expression in an inflammatory state (chronic ulcerative colitis and Crohn's disease) in the human colon and the induction of PEPT1 expression after inflammation in mice [114, 115]. Immunofluorescence stainings of colonic sections and mRNA expression studies (oral communication with Tilo Wünsch) additionally reveal that PEPT1 is found in the distal but not in the proximal part of the colon of healthy male C57BL/6 mice.

In 1990, first evidence of the existence of a basolateral peptide transport system was observed by Dyer *et al*., by the glycyl-L-proline transport found in rabbit basolateral membrane vesicles [116]. Further studies performed in Caco-2 cell lines by several groups enforced the existence of a basolateral peptide transport system using hydrolysis-resistant substrates such as the dipeptide Gly-Sar [117-119]. However, the nature of this protein remains a mystery and all cloning attempts failed.

1.7.4 Regulation of PEPT1

The regulation of intestinal PEPT1 protein expression and activity is influenced by various factors such as hormones, nutritional or dietary factors and by pathological states.

Insulin

So far, only a little is known about insulin receptor (IR) expression in the small intestine und literature provides conflicting data. It may be expected that IR are restricted to the basolateral side of enterocytes. However, in 1987, Weström *et al.* described high concentrations of insulin in the colostrum and in porcine milk and proposed that this insulin may affect growth of the intestine and cell proliferation during the neonatal and nursing periods [120]. The addition of oral insulin to the diet of newborn pigs indeed showed trophic effects on the intestinal cell mass and increased disaccharidase activity [121], while

inhibition of the IR's induced an inhibition of mucosal growth and expression of hydrolases in suckling and weaning rats [122]. In adult animals conflicting results were obtained on the intestinal IR expression. IR's were shown to be exclusively expressed on the vascular side of the intestinal epithelium of dogs [123], whereas in rabbit BBM of proximal colonic epithelium the expression of IR's suggest apical localization [124]. Buts *et al.* (1997) demonstrated IR expression on the endoluminal and vascular side in the rat small intestine and found it to be independent of age [125]. Human colonic adenocarcinoma cells (Caco-2) were shown to express IR's [126, 127] and those cells were used investigate possible effects of insulin on transporter function and in particular on PEPT1 which shows high expression in Caco-2 cells.

Thamotharan *et al.* (1999) demonstrated that physiological concentrations of insulin, added to the incubation medium, significantly increased PEPT1-mediated glycyl-sarcosine (Gly-Sar) transport in Caco-2 cells. This was due to an increase in maximal transporter capacity (V_{max}) of PEPT1 and postulated to result from increasing the membrane density of the transporter protein and its synthesis. Disruption of the microtubuli eliminated the effect of insulin on the peptide transporter; what is yet not defined is the mechanisms by which insulin increases the translocation of preformed PEPT1 proteins from cytoplasmic pools into the apical membrane [106]. Exposure of only the basolateral side of Caco-2 cells to insulin also increased PEPT1 activity as described by Nielsen *et al.* [128].

Leptin

Leptin is secreted as *ob* gene product mainly from adipocytes but it can also be secreted from tissues such as brain, placenta and stomach. Its pivotal role is satiety control and to regulate lipid metabolism [129-131]. Leptin receptors (*ob-R*) are expressed at both, apical and basolateral, membranes of enterocytes with adipocyte-derived leptin reaching the basolateral side and stomach-derived leptin reaching the apical membrane [131].

Studies performed in diet-induced obese (DIO) mice showed reduced dipeptide transport via PEPT1 and a down-regulation of the leptin receptor protein [131], while hyperleptinemia induced for 7 days in rats led to an increase of PEPT1 gene expression and transporter activity. In addition to the described effects of leptin on PEPT1 activity, SGLT1, PAT1 and B^0AT1 were down regulated by apical exposure to leptin in a study performed in Caco-2 cells by Ducroc *et al.* 2012 [132, 133].

Peptides and amino acids

In vitro studies performed in PEPT1 expressing Caco-2 cells [134] were carried out to determine whether expression and activity of the transporter could be influenced by its substrates. 24-hour exposure of cells to Gly-Sar increased the maximal velocity for glycylglutamine transport (Gly-Gln) and revealed a twofold increase in PEPT1 abundance. At the same time, when free glycine or sarcosine were added, no change in velocity or protein levels of PEPT1 appeared. Furthermore, it was shown that the stimulation of PEPT1 transport by its substrate was due to newly synthesized PEPT1 since stimulation was disrupted after brefeldin treatment that impairs endoplasmatic reticulum (ER) the trans-Golgi network processing [134]. The described effects were attributed to increased gene transcription and stabilization of the mRNA of PEPT1.

A feeding study performed in rats with supply for 3 days with a standardized diet supplemented with the dipeptide Gly-Phe led to an increased mRNA expression level of PEPT1 [135]. Dipeptides are thus able to stimulate PEPT1-mediated transport possibly by increasing PEPT1 membrane protein density while single amino acids fail to influence PEPT1-mediated transport [121].

Calcium-mediated regulation

The key function of cytosolic Ca^{2+} is to serve as a second messenger by regulating cellular processes such as hormone secretion, gene expression, neurotransmission and cellular proliferation [136].

Ca^{2+} is stored in intracellular pools, mainly the ER and either a receptor activation or membrane depolarization causes the raise in intracellular calcium. For example inositol-1,4,5-triphosphat (IP_3) mediates the release of Ca^{2+} from the intracellular pools with an increase in cytosolic Ca^{2+} that can further lead to activation of membrane bound voltage gated L-type Ca^{2+} channels (Ca_v 1.3) that enhance the Ca^{2+} concentration by influx from the outside. An activation of these apical Ca_v 1.3 channels can be induced by an increased entry of Na^+ ions into the cell, which in consequence via a depolarization of the membrane causes the opening of these channels [5]. Ca_v 1.3 channels were shown to reside in the apical membrane of epithelial cells of jejunum and are crucial for the control of Ca^{2+} entry into the enterocytes. Studies performed in Caco-2 cells by Wenzel *et al.* (2002) using different Ca^{2+} channel blockers, e.g. nifedipine, a specific L-type Ca^{2+} channel blocker [137], demonstrated that changes in intracellular Ca^{2+} concentration led to an upregulation in

PEPT1 mediated transport. Nifedipine treatment of cells led to an increased V_{max} of PEPT1 (K_m remained unaffected) and caused increased intracellular acidification [109].

Although SGLT1 is the prime glucose transporter in the apical membrane of enterocytes, it has been postulated – based on studies mainly in rats – that by high luminal concentrations (such as after a meal) GLUT2 may be recruited to the apical membrane and most interestingly is associated with a retrieval of PEPT1 from the apical membrane (Fig. 6). These studies were extended by Mace *et al.* (2009) demonstrating that in the small intestine of rats this may be coordinated via calcium and T1R taste receptors and thereby PEPT1 and GLUT2 function in the apical membrane of enterocytes would be regulated in a reciprocal manner [79].

The G-protein coupled receptors (GPCR's) of the family Type 1 (T1R), which can be subdivided into two groups: (a) T1R2/T1R3 heterodimers that sense sweet taste (sugar, artificial sweeteners), (b) T1R1/T1R3 heterodimers sensing umami and savory amino acids. The second taste receptor family (T2R) is responsible for mediating the bitter taste [138, 139]. Expression studies performed in various species (mouse, rat, dog and human) showed transcripts of the T1R family and T2R family along the GI tract together with transducin and α-gustducin in EECs [79, 139].

The proposed model with the reciprocal regulation of GLUT2 and PEPT1 (Fig. 6) is based on the conception that luminal high glucose levels are sensed by SGLT1 and the sweet taste receptor dimers T1R2/T1R3. SGLT1 activity would cause membrane depolarization leading to opening of apical L-type voltage gated calcium channels (Ca_v 1.3.) and calcium increase in the cells.

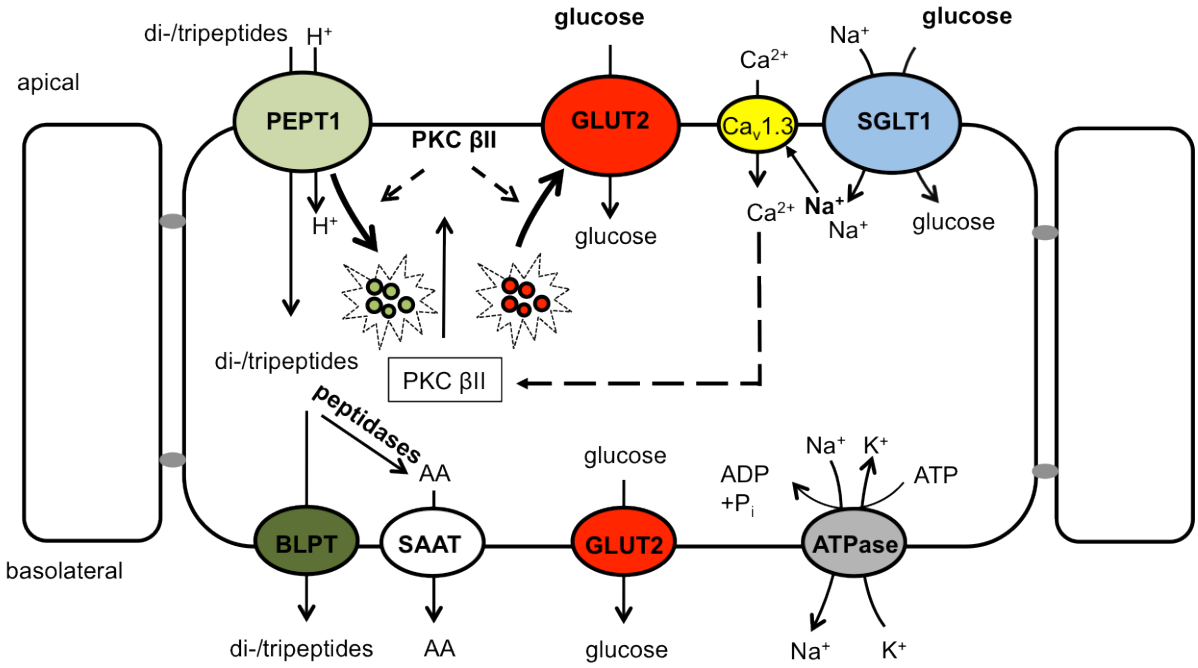

Figure 6 **Schematic overview of a proposed inverse regulation of transporter proteins in the apical membrane in response to a high luminal glucose exposure**

Reciprocal regulation under high luminal glucose concentration of PEPT1 (green) and GLUT2 (red) [79] in the apical membrane of an enterocyte, induced by the activation of Ca_v 1.3 (yellow) and Ca^{2+}-mediated (yellow dashed line) PKC βII activation. Terminal web and cytoskeletal rearrangements and PKC βII action (dashed black arrows) change expression patterns by retrieval of PEPT1 in- (black arrow) and insertion of GLUT2 (black arrow) - from intracellular preformed vesicle pools - in the apical membrane.

According to the model an increase in intracellular calcium concentration induces the translocation of cytosolic, inactive but phosphorylated protein kinase C βII (PKC βII) to the apical membrane where it becomes activated by a second signal (not depicted in Fig. 6) mediated by sweet taste receptor activation. The full activation of the pathway is achieved via diacylglycerol (DAG) promoting the removal of the N-terminal pseudosubstrate region from the active site of PKC βII. The events lead finally to terminal web and cytoskeletal rearrangements [77] that allow transporter trafficking into the apical membrane (GLUT2) from intracellular preformed vesicle pools and retrievement out of the membrane in case of PEPT1 [79].

Diabetes and Inflammatory bowel disease

Diabetes is the most progressive metabolic disease of the 21st century (WHO, 2012). Many studies have been conducted to understand the pathophysiological impact the organism.

Studies on the effect of a diabetic state on the small intestine and nutrient uptake by enterocytes started as early as the 1970´s by using isolated intestinal microvillus membranes [140]. In addition, autonomic neuropathy resulting in disturbances of gastrointestinal motility in diabetes [141] with changes in stomach emptying and a delayed stomach to caecum transit time were reported [142].

The β-cell toxic agent Streptozotocin (STZ) is frequently used to generate experimental diabetes in rodents. Gangopadhyay *et al.* in 2002 reported that PEPT1 function is altered when brush-border membrane vesicles (BBMV) from STZ diabetic rats were studied for transport. After 96 h of STZ treatment, the maximal velocity (V_{max}) of PEPT1 in BBMV was markedly increased. This was proposed to result from changes in translation as gene expression changes were not found [108]. Studies performed by Bikhazi *et al.* (2004) and Der-Bogosshian *et al.* (2010) in rats, revealed that STZ-treatment and diabetes without substitution of insulin, caused PEPT1 mRNA to increase whereas the protein level decreased. Functional studies with Gly-Sar revealed a decreased transporter activity. Although the duration of uncontrolled diabetes varied between the two studies, the results remained essentially the same [143, 144].

Besides diabetes, PEPT1 expression and activity was proposed to be altered in Crohn´s disease and ulcerative colitis [114, 115]. In addition to those reports, recent studies performed in a human colonic cell line (HT29-Cl.19A) that does not express PEPT1 under basal conditions, showed induction of expression of PEPT1 upon exposure to enteropathogenic *Escherichia coli* possibly via the transcription factor Cdx2 [115]. In addition to Cdx2, intact lipid rafts seem to be as well important role in PEPT1 activation [115].

2. Material and Methods

2.1 Animals

Wild type C57/BL6J and C57/BL6N mice were either breed in the open mouse facility (Liese-Beckmannstr.4, 85350 Freising/Weihenstephan, Kellerraum K20), or in the SPF (Specific Pathogen Free) facility (SPF-Tierhaltung Biowissenschaften, Gregor-Mendel-Strasse 2, 85350 Freising/Weihenstephan). The *pept1*$^{-/-}$ mice were obtained from Deltagen (San Mateo, USA) and breed in house, in the open and SPF facilities. The *sglt1*$^{-/-}$ mice were kindly provided by Prof. Koepsell (Lehrstuhl für Anatomie, Würzburg, Germany) and further breed under SPF conditions.

Mouse husbandry

All mice were kept under a 12h dark-light cycle at 24°C room temperature. Animals had free access to water and were kept on a standard laboratory chow (SPF- facility: V1534-3 sniff, Germany; open facility: V-1534-0, sniff, Germany) *ad libitum* or a modified glucose deficient diet (sniff, Germany). The homozygous C57BL/6 wild-type mice (*pept1*$^{+/+}$) were mated, as well as the homozygous PEPT1-deficient (*pept1*$^{-/-}$) mice, to obtain entirely homozygous offspring. All animals were treated according to the German guidelines for animal care as approved by the states ethics committee (reference number: 55.2.1-54-2532-22-11 and reference number: 55.2.1-54-2532-39-10).

For the conducted studies animals were anesthetized by inhalation of Isoflurane (Baxter, Germany), and immediately killed by cervical dislocation. The small intestine was carefully and quickly removed after dissection and stored in ice cold modified Krebs-Henseleit Buffer (mKHB, for composition see Tab. 4).

2.2 Functional characterization of epithelial transporters

2.2.1 Techniques used

Functional characterization of transporters was performed by electrophysiological measurements using Ussing chambers and by quantifying uptake using radiolabeled substrates in everted gut ring preparations.

Ussing chamber

Jejunal segments of homozygous wild type (C57/BL6J), *pept1*$^{-/-}$ and the heterozygous *pept1*$^{+/-}$ mice, as well as *sglt1*$^{-/-}$ mice were used to determine changes in selected transporters by electrophysiological measurements as described below (2.4) in detail.

Uptake of radiolabeled substrates

Everted gut rings of the small intestine of wild type (C57/BL6J), and *pept1*$^{-/-}$ mice were prepared as described below (2.5) and uptake of radiolabeled substrate was determined. In the following, these experiments will be referred to as “uptake experiments”.

2.2.2 Preliminary studies to determine parameters of transporter activity

Kinetic studies

To study PEPT1, SGLT1, B^0AT1 and SIT1 substrate affinities [120] and maximal transporter velocities (I_{max}), transport studies were conducted in the Ussing chamber. Jejunal segments of wild type (C57/BL6J), *pept1*$^{-/-}$ and *sglt1*$^{-/-}$ mice were used to determine major kinetic parameters. In these experiments, the basolateral and apical solutions both contained 75 mM glucose and were constantly recirculated. Every 2 min, substrate was added to the apical solution from a stock with increasing concentrations (1, 5, 10, 20, 35, 50, 75 mM). By carefully pipetting the individual volumes into the apical reservoir, the starting volume of 5 ml was maintained and any pressure differences were prevented.

Segmental uptakes

To determine PEPT1 and SGLT1 highest regional activity in the small intestine, the complete small intestine of wild-type mice (C57/BL6J) was everted and segments were prepared with

three consecutive rings incubated together for 2 min with the respective radiolabeled PEPT1 or SGLT1 substrate.

2.3 Experimental procedures intended to modify transporter activities

2.3.1 Effect of high-fat feeding on intestinal transporter activity

By 6 weeks of age wild type mice (C57/BL6J, SPF-facility) received a high-fat (HF) diet containing 60 % of energy from fat (E15741-34, sniff, Germany) for twelve weeks. The control mice of same age, received a corresponding control (C) diet containing 11 % energy from fat (E15000-04, sniff, Germany). Electrophysiological analysis of the transporters (PEPT1, PAT1, SIT1 and SGLT1) was conducted in the Ussing chambers.

2.3.2 Effect of insulin on intestinal transporter function

In vitro

In wild type (C57BL/6J) mice, substrate-induced short-circuit currents (Isc's) of PEPT1, SIT1 PAT1, EAAC1 and SGLT1 were measured in the Ussing chambers before and after a 30 min exposure to insulin (100 nM, Sigma Aldrich, USA) added to the basolateral compartment.

In vivo

Twelve week old male, wild type (C57/BL6N) mice were treated with a single intraperitoneal (i.p.) insulin injection (0.1 U/kg body weight, Sigma-Aldrich, Missouri, USA) in HEPES buffer (pH 8.2), or received a vehicle of same amount (HEPES buffer, pH 8.2) (n = 10 per group). Blood glucose concentration was measured 30 min following the i.p. injection and for this blood was drawn from the tail tip and determined by using a glucose monitoring device (FreeStyle® Freedom Lite, Abbott, Germany). Transporter activities of PEPT1, SIT1 B^0AT1 and SGLT1 in jejunal segments were analyzed by electrophysiological and uptake experiments. RNA and protein amounts were determined by following the protocols described in 2.6 and 2.10.

2.3.3 Luminal exposure of the small intestine to high glucose

In vitro

In wild type (C57BL/6J) mice substrate-induced short-circuit currents (Isc's) of PEPT1, SIT1 and SGLT1 were measured in the Ussing chamber before and after a luminal exposure for 30 min to a high glucose (75 mM) containing modified Krebs-Henseleit Buffer (mKHB, for composition see Tab.4). Control measurements were conducted in wild type (C57BL/6J) mice with mKHB containing 75 mM glucose to exclude possible osmotic effects. Experiments following the same protocol were conducted at open-circuit voltage, given as a calculated Ioc to assess if changes in membrane potential by short-circuiting had any effect on the observed glucose induced changes of transporter activities.

***In vivo* oral glucose bolus**

Uptake experiments to investigate PEPT1, GLUT2 and SGLT1 transporter activity in jejunal everted gut rings, were conducted in twelve weeks old wild-type mice (C57/BL6J) that were fasted for 6h and subsequently received an intragastric gavage of 20 % glucose (glucose / kg body weight in 250 µl tap water). Control mice received a vehicle (tap water). Glucose concentration at defined time points (30, 60 and 90 min) after the intragastric bolus was measured from blood collected from the tail tip by using a glucose monitoring device (FreeStyle® Freedom Lite, Abbott, Germany).

2.3.4 Effect of diabetes on intestinal transporter function

Streptozotocin treatment

Streptozotocin (STZ) (Fig.7) is known to cause cell-death of insulin producing β-cell of Langerhans-islets leading to a type 1 diabetes (T1D).

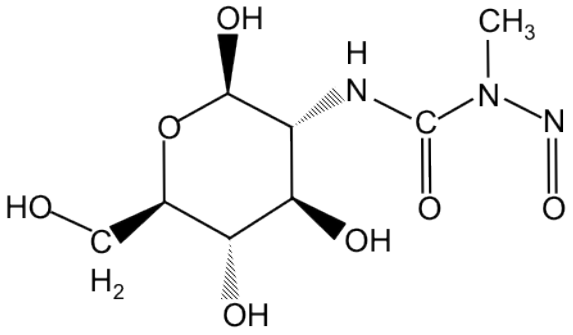

Figure 7 Chemical structure of Streptozotocin

A cytotoxic methylnitrosourea moiety (N-methyl-N-nitrosourea) linked to the carbon 2 of the glucose (2-deoxyglucose) molecule. The hydrophilic β-cell selective toxin is used to induce experimental T1D in animals**.**

Twelve week old, male wild-type (C57/BL6N) mice were separated into two groups (n = 10 per group). The diabetes group received a single high-dose i.p. injection (180 mg/kg body weight) of Streptozotocin (STZ, Sigma-Aldrich, Missouri, USA), dissolved in 0.1 M citrate buffer (pH 4.5). The control group received the same amount of 0.1 M citrate buffer (pH 4.5), as a vehicle. Before injection, each mouse (unfasted) was weighted and blood glucose was determined by collecting blood from the tail tip (FreeStyle® Freedom Lite, Abbott, Germany). Body weight and blood glucose were monitored for the subsequent 5 days post STZ-injection to document and ensure a proper health status and to observe the development of hyperglycemia in the STZ-treated group.

Lengths and diameter of jejunal villi were measured and evaluated under the light microscope (Leica, Wetzlar, Germany). Histological sections and stainings of the pancreas were produced and evaluated. Organ weights and the length of the intestine were measured.

Activity of transport systems of jejunal tissue segments was profiled using radiotracer substrates (for PEPT1 and SGLT1) or electrophysiology (PEPT1, B^0AT1, SIT1 and SGLT1). Furthermore, tissue samples were used for RNA quantification (PEPT1, SGLT1,

Glyceraldehyde-3-phosphate dehydrogenase (GAPDH) and Villin) and protein isolation (PEPT1, SGLT1 and Villin).

2.4 Electrophysiological experiments using the Ussing chamber

In 1950, the Danish biologist Hans H. Ussing and his colleague Zerahn established a method to determine sodium/chloride transport and the resulting current across the frog skin, the Ussing chamber. In order to quantify the amount of transported substrate only by active transport systems (electrogenic transporters), Ussing clamped the spontaneous transepithelial potential (V_t), which might drive diffusion processes, to zero [122] by short-circuiting the epithelia. The recorded short circuit current [110] allowed quantification of substrates actively transported over the epithelia. Therefore, Ussing chambers offer studies on transport processes of drugs, nutrients, and ions.

2.4.1 Electrophysiological principals

To obtain the electrophysiological data by Ussing chamber measurements a piece of epithelial tissue is mounted vertically between the two chamber halves (Fig. 8). Two sets of electrodes are connected to the chambers. Voltage sensing electrodes, placed close to the tissue, are connected by agar bridges (3 %) to the chamber and measure the transepithelial potential (V_t) difference. Current electrodes, placed at the outer end of the chamber, conduct current of an external current source to the mounted tissue. Both electrode pairs are connected to the clamp device that injects current to keep the V_t at zero (short circuit current) thus allowing measuring the sum of active electrogenic transport processes across the epithelium.

Change in the tissue potential difference (ΔV_t) by the application of a defined amount of current impulse (ΔI) allows the calculation of transepithelial resistance (TER; R_t) by Ohm's law: $R = U / I$ (R: resistance; U: voltage; I: current), which is an indirect measure of tissue integrity.

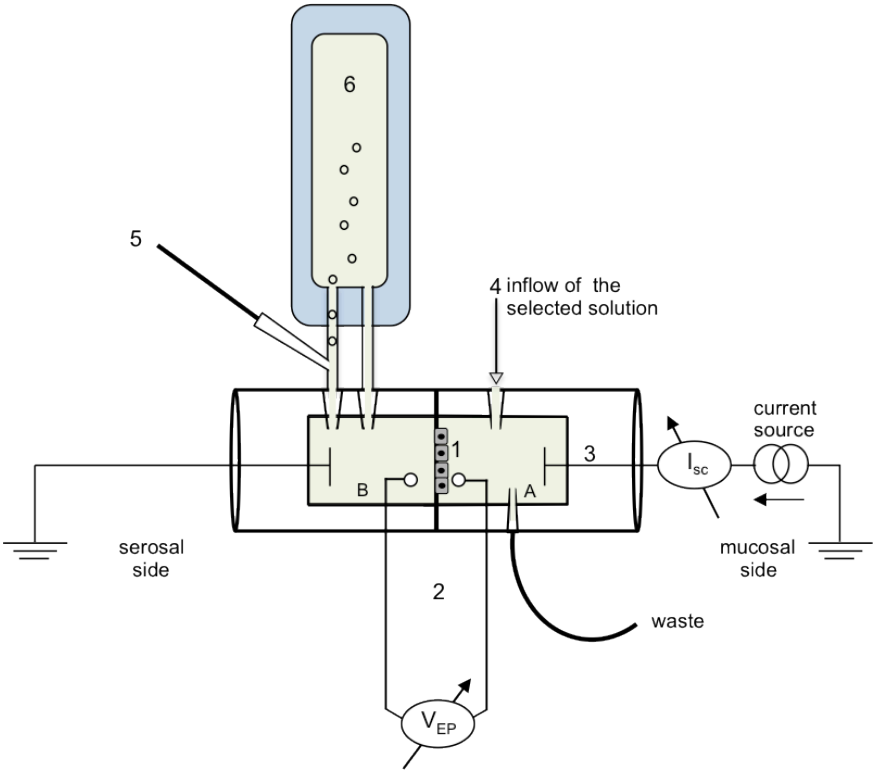

Figure 8 Schematic illustration of an Ussing chamber

The mounted epithelia (1) is vertically separating the chamber halves in the mucosal (A) and the serosal side (B). Tissue close potential electrodes (2) connected by KCl agar bridges and the current (Ag/AgCl) electrodes, which are placed at the outer chamber, used (3) for defined current entry. Inflow for selected substrates (4). Entrance for carbogen gassing (5) on the serosal side and mixture of the glass lift reservoir-containing buffer (6). Luminal (A): one-pass perfusion, serosal (B): recirculation.

Recording and analysis of all experiments was performed by a computer-based program (Aquire and Analyze 2.3 181, Physiological Instruments, USA).

2.4.2 Electrodes

Two voltage-sensing electrodes (DRIREF-5SH, World Precision Instruments, Inc., Florida, USA) were connected to each of the Ussing chamber sides. The 3 % agar-bridges were prepared by heating 3 g of agar in 100 ml of 3 M KCl. The liquid agar was filled by a syringe into the electrodes and PE tubes and were stored at 4 °C in 3 M KCl and reused until bacterial growth was detected. The current electrodes consisted of an Ag / AgCl wire, which was fixed in an electrode and was ready for measurement. The voltage-sensing and the current electrodes were linked to a converter that was connected to the multichannel voltage-current-clamp (VCC MC6, Physiological Instruments, Inc., California, USA). Before

each experiment, the voltage-sensing electrodes were set on 0 mV. Additionally, the resistance of the " empty " chambers was measured and corrected.

2.4.3. Tissue preparation

All procedures have been carried out in ice-cold modified KHB (mKHB, for composition see Tab. 4). The freshly, removed jejunum was cut into four 1.5 cm long pieces. After cutting along the mesenteric border, the tissue samples were carefully stretched and fixed with insect pins (Minutien: 0.15 x 12 mm, Bioform, Nürnberg, Germany) on a parafilm piece (Brand/Merz & Co., Germany). The parafilm was placed on a Sylgard® plate, and the tissue pieces were showing up with the serosal side (blood side) for preparation. After fixation, each tissue was prepared by seromuscular stripping of the *Tunica serosa* and the underlying *Tunica muscularis*, with the *Stratum longitudinale* and *Stratum circulare* by using fine forceps (FST, Fine Science Tools, Heidelberg, Germany).

Table 4 **Composition of modified Krebs-Henseleit-Buffer in mM for Ussing chamber experiments**

Chemicals	+ Mannitol pH 7.4 serosal	+ Mannitol pH 6.4 apical	+ Substrate pH 6.4 apical
NaH_2PO4	1.2	1.2	1.2
NaCl	97	117	117
Cholinchlorid	20	-	-
$NaHCO_3$	22	2	2
KCl	4.7	4,7	4.7
$MgCl_2$	1.2	1.2	1.2
$CaCl_2$	1.2	1.2	1.2
MES	-	20	20
Mannitol	20	20	-
Substrates	-	-	20

To mount the tissue in the chamber, the left part of the chamber, which was equipped with fine preparation needles, was carefully pressed on the stripped tissue and lifted. The underlying parafilm was helping not to loose and finally to gently pull down the tissue until it was lying straight on the chamber half. Before the chamber halves were put together, the edges of the tissues were trimmed. The other chamber half was prepared with a silicon ring to avoid edge damage of the tissues while the chamber halves were put together. The mounted tissue had an exposed surface area of 0.287 cm^2.

2.4.4 Measurements

Short-circuit measurements

After mounting of the tissues, the four chambers were installed into their fixtures. Serosal mKHB (pH 7.4, 37 °C) and mucosal mKHB (pH 6.4, 37 °C) were filled into the chambers simultaneously, to avoid strong stretching of the tissue by differential pressure.

The tissues were clamped to a potential of 0mV and equilibration started for 20 min, while the mucosal sides of the tissues were one-pass perfused (constantly) with mKHB at pH 6.4, at 37 °C. The selected substrates were applied at a temperature of 37 °C to the mucosal side of the tissues over a selecting valve for 2 min, followed by a washout period for 7 minutes. The resulting substrate-induced transport current [110] was calculated as the peak current in the presence of substrate (Tab. 5) minus the baseline current. The resulting Isc was defined as the degree of electrogenic transport over epithelia and was given as μA cm^{-2}.

Table 5 Transporters and substrates used in Ussing chamber studies

Transporter	Substrates
PEPT1	Glycyl-Sarcosine (Gly-Sar)
PAT1	Glycine
SIT1	L- Proline
EAAC1	L-Glutamat
B^0AT1	L-Leucine
SGLT1	D-Glucose

Open-circuit (OC) voltage

In some experiments, measurements were performed in the OC mode. Active transport of ions from apical to serosal side was measured without the application of external current by the current electrodes. The resulting transepithelial voltage [Ut] was calculated into short-circuit currents by the computer program A & A 2.3. (Physiological Instruments, USA).

2.5 Uptake experiments using radiolabeled substrates

2.5.1 Tissue preparation

Freshly removed small intestine was moisturized with ice-cold mKHB (for composition see Tab. 6), carefully turned insight out by fixing one side to a metal rod (Ø 2 mm) and pulling the intestine down over the rod.

Table 6 Modified KHB (in mM) used for uptake experiments in everted gut rings

After 1 h of carbogen gassing the pH of both solutions were adjusted.

Chemicals	Transporter tested	
	PEPT1 at pH 6.4	**SGLT1 at pH 7.4**
NaCl	119	119
KCl	4.7	4.7
$CaCl_2$	2.5	2.5
$MgSO_4$	1.2	1.2
KH_2PO_4	1.2	1.2
$NaHCO_3$	12.5	25
MES	22.5	-
HEPES	-	10

As soon as the intestine was everted, it was placed on an ice cooled acrylic glass plate (Fig. 9). The proximal 8 rings were used to investigate PEPT1 mediated [^{14}C] Gly-Sar (GE Healthcare, Germany) uptake at pH 6.4, followed by the consecutive 8 rings, which were used to study [^{14}C] α-MDG (Hartmann, Germany) uptake at pH 7.4.

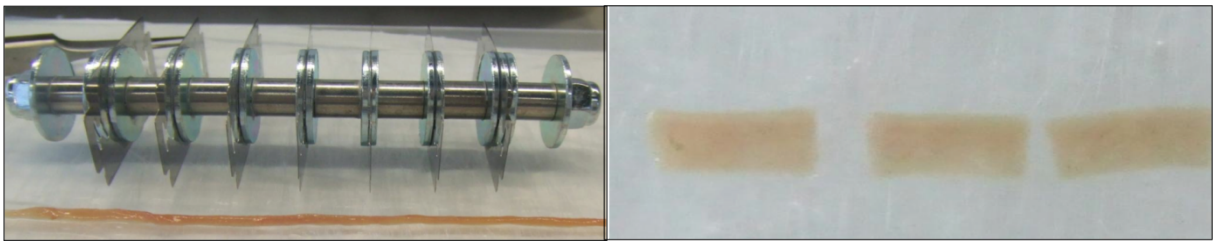

Figure 9 Razor blade panel with everted small intestine (left) and 1 cm rings (right)

Starting at the ligament of Treitz, reflecting the junction of duodenum to jejunum, 16 cm of intestine were cut into single rings of 1 cm length (reflecting the proximal length of the jejunum). Cutting was performed by a rod with 7 razor blades, which were exactly aligned in a distance of 1 cm from center to center on a threaded rod (left).

For testing whether GLUT2 can be found in the apical membrane, [^{3}H]-labeled 2-deoxy-D-glucose (Hartmann, Germany) was used (at pH 6.4) with only duodenal tissue samples. To reduce variability due to the experimental settings and the regional distribution of transporter activity, the order of rings was strictly attended.

2.5.2 Principles of uptake experiments

Everted gut rings were incubated in 9 well plates (Becton Dickson Labware, Germany) on a constant shaking device (Heidolph-Titrimar 100, Germany) at 37 °C. A radiolabeled solution (the measuring solution) containing 10 µM [^{14}C] labeled Gly-Sar and 1 mM non-labeled Gly-Sar (1 : 100) was prepared and used to measure PEPT1 activity. An “ inhibition ” solution was prepared, by a concentration of non-labeled Gly-Sar of 100 mM (ratio labeled/unlabeled, 1 : 10000) to assess only uptake into tissues with full inhibition of the transporter. For SGLT1, a substrate solution containing 1 µM of ^{14}C-labeled α-MDG and inhibitor-solution, containing a 10000-fold excess of unlabeled substrate was employed. ^{3}H labeled 2-d-D-glucose (0.19 µM) was used for GLUT2 with non-labeled substrate excess of 1 : 10000 for inhibition. All incubations were performed for 2 min and the rings were quickly removed and placed in 3 ml of ice-cold mKHB and washed 3 times with ice-cold buffer. The rings were carefully dried and separately placed in scintillation vials for drying over night at 50 °C.

2.5.3 Quantification

After overnight drying, tissues were solubilized in 200 µl Biosol® (National Diagnostics, USA) for two hours on a shaking device (Heidolph-Titrimar 100, Germany) at 37 °C. After dissolving of the rings, 10 % v/w hydrogen peroxide (H_2O_2) was added for discoloration and

incubated for 1 hour. The clear solution in every vial was then spiked with 3 ml of Bioscint® (National Diagnostics, USA) and placed in racks in the β-TriCarb™ 2810TR Scintillation Analyzer (PerkinElmer, USA). Transporter activity was determined as the difference between test and inhibition sample.

2.6 Intestinal RNA purification and cDNA synthesis

Small intestinal mucosa was scraped off and stored at -80 °C for RNA purification and mRNA quantification. Briefly, samples were kept on ice and 1 ml of TRIZOL® (Invitrogen, Karlsruhe, Germany) was added and followed by homogenizing using an Ultraturrax (Polytron Pt1600E, Kinematic AG, Switzerland). Chloroform (Roth, Germany) was added to each sample and centrifuged with 13.000 rpm (Eppendorf, Hamburg, Germany) for 30 min at 4 °C. The clear phase was taken and 1 % volume of 96 % EtOH was added. For further RNA purification, the Rneasy Mini Kit (Quiagen, Hilden, Germany) procedures were followed. RNA concentrations were measured by NanoDrop (NanoDrop, 1000, PeqLab) and the required amount of 5 µg RNA for reverse cDNA transcription was calculated and performed by using the Transcriptor High Fidelity cDNA Synthesis Kit (Roche, Germany).

2.6.1 Quantitative real-time PCR

For quantitative real-time PCR 62.5 ng / µl cDNA were used per reaction and performed using a Light Cycler (Roche, Germany). The FastStart SYBR Green Kit (Roche, Germany) was used for quantification of the PCR products by using the product specific primers (Tab. 7).

Table 7 Transporter and housekeeping genes with corresponding primer sequences

Protein	Gene	Forward primer	Reverse primer
PEPT1	Slc15a1	TGATCCGAAGGGCGAG	GGCGAATATCACGCAG
SGLT1	Slc5a1	TACCGTTGGAGGCTTC	AGATACTCCGGCATCG
GAPDH	GAPDH	ATCCCAGAGCTGAACG	GAAGTCGCAGGAGACA
Villin	Villin	CTCTCGGACGGAGAAACAAG	GAACACATCCTCCTCCTCCTCCA

Cycle parameters were annealing at 62 °C for 10 s, elongation at 72 °C for 10 s and melting at 95 °C for 10 s. Melting curve analysis controlled the specificity of PCR products. The

geometric mean of crossing points (CP) of the two housekeeping genes GAPDH and Villin was calculated and the Bestkeeper Index was used as CP of the reference gene to calculate and normalize the mean values of the transporter expression of the samples.

2.7 Intestinal tissue preparation

Freshly collected tissue was immediately transferred into a 4 % formalin solution (Roth, Germany) and stored for 10-12 h on a shaking device. Until preparation, the tissue and organ samples were stored in 70 % EtOH at 4 °C. Tissues were then dehydrated in ascending concentrations of ethanol and xylene at 40 °C (70 % and 80 % 30 min, 2 x 95 % 45 min, 3 x 100 % 45 min and 2 x 100 % xylene 45 min). The embedding followed in paraffin (Paraplast embedding media, Sigma Aldrich, Germany). Samples were cut in 7 µm slices and fixed on Superfrost Plus microslides (Menzel GmbH, Germany) and dried over night at 37 °C. Further preparation of the samples was performed by incubation steps for 2 x 5 min in 100 % Xylol for dewaxing and for dehydration in decreasing concentration of ethanol (2 x 100 %, 96 % and 80 %). Slides were subsequently, three times washed under running water and cooked in citrate-buffer (0.1 M citric acid, 0.1 tri-sodiumcitrate-dihydrate, pH 6.0) for 20 min at 95 °C.

2.8 H & E staining

Tissue samples were cut in 7 µM slices after paraffin embedding. Hemalum and Eosin (H & E) staining was used to visualize cellular nuclei in dark violet and the eosinophilic structures of the cytosol in pink shades. The selected slices were rehydrated by the following incubation steps (Tab. 8) and carried out at room temperature.

Table 8 Hemalum and eosin (H & E) staining protocol for jejunal segments

Agent	Time
100 % Xylol	3 min
100 % Xylol	3 min
100 % Ethanol	2 min
96 % Ethanol	2 min
80 % Ethanol	1 min
deionized water	1 min
Meyer's Hemalum	4 min
Tap water 2 min	2 min
96 % Ethanol	0.5 min
Eosin	2 min
70 % Ethanol	1 min
96 % Ethanol	1 min
100 % Ethanol	1 min
100 % Ethanol	1.5 min
100 % Xylol	1.5 min

Slides were covered by a drop of mounting medium (DAKO fluorescent mounting medium S3023, Dako, California, USA) and covered with a cover slip. Drying was allowed under the hood for one day until the mounting medium was dried out completely and slides were examined under the light microscope (Leica, Wetzlar, Germany).

2.9 Tissue changes (Villus length and diameter)

Villus length and diameter were quantified in control and diabetic mice using paraffin embedded jejunal sections, which were treated as described above (2.7). The length was measured from the bottom villus, at the starting region of the crypts up to the top of the villus. Diameters were determined in the upper third of the villus part. Three animals per group were compared (N = 17 villi) using a light microscopy with a 10 x magnification (Leica Microsystems, Wetzlar, Germany).

2.10 Brush border membrane (BBM) preparation

Segments of the small intestine were quickly everted by use of a metal rod and the mucosa was scraped off by a glass slide and immediately frozen (-80 °C). Scrapings were defrosted on ice and homogenized by Ultraturrax (Polytron, Pt1600E, Kinematic AG, Switzerland) for 30 sec in ice-cold M300 buffer (300 mM glucose, 20 mM HEPES, pH 7.4 adjusted with Tris). Quickly 1 % protease inhibitor (Protease Inhibitor Tablets, Roche, Germany) was added to the M300 buffer and again homogenized for 2 x 10 seconds. For BBM preparation the $MgCl_2$ EGTA precipitation was used. 1 M of $MgCl_2$ and 0.416 M of EGTA was added to the homogenate containing M300 anti-protease buffer and centrifuged for 5 min at 4 °C at 3600 rcf (Beckmann, Germany). The pellet was discarded and the supernatant was incubated for 15 min with 20 mM of $MgCl_2$ on a mixing device on ice followed by a centrifugation step for 15 min at 4 °C at 2400 rcf. The obtained supernatant was transferred in a new tube and again centrifuged by 32400 rcf at 4 °C for 30 min (Ultraspeed-Vacuum Centrifuge). The pellet was resuspended in M300 buffer containing 1 % anti-protease using by a 23 G needle and frozen in liquid nitrogen and stored at -80 °C.

2.10.1 Western blot

A BioRad protein assay (Bradford) was used to determine protein concentration. 12 µg protein were separated by SDS-10 % PAGE followed by a transfer to a nitrocellulose membrane in a full tank blotter (Bio-Rad Laboratories GmbH, München, Germany). After blocking with blocking buffer (PBST: 1x PBS, 0.1 % Tween20, 1 % skim milk powder) 3 x times for 20 min, the primary antibodies (rabbit anti-mouse PEPT1 (1 : 5000), rabbit anti-mouseSGLT1 (1 : 5000) Pineda Antikörper Service, Germany) and goat anti-mouse Villin (1 : 1500) Santa Cruz Biosciences, Inc., USA) were added and incubated over night at 4 °C in PBS-T additionally, containing 1 % BSA. After washing, the secondary antibodies for PEPT1 and SGLT1 (donkey anti-rabbit (1 : 12000), IRDye 680, Licor Biosciences GmbH, Germany) and for Villin (donkey anti-goat (1 : 12000), IRDye 800, Licor Biosciences GmbH, Germany) were added. After incubation at room temperature (2 h) and 3 x times washing with PBS, fluorescence was detected by Odyssey Infrared Imaging System (LI-COR, Germany). For quantification of band intensities the Odyssey V3.0 Image software was used.

2.11 Urine osmolarity

Urine from STZ-treated T1D mice and control mice was collected each day to measure osmilarity and samples were immediately frozen at -20 °C. To detect changes in osmolarity, 50 µl of urine of each mouse were used and analyzed by a Micro-Osmometer Type OM 806 (Vogel, Gießen, Germany).

2.12 Statistical analysis

Using GraphPad Prism 4.01 statistical analysis was performed. Unless not quoted differently an unpaired Student's t-test, Mann-Whitney test or a two-way ANOVA and Bonferroni test was used to quantify statistical significance. Data are presented as mean ± SEM.

3. Results

3.1 Transporter activities in jejunum – comparing wild type, *pept1*$^{-/+}$ and *pept1*$^{-/-}$ mice

In patients suffering of Hartnup syndrome and cystinuria it was shown that the peptide transporter delivers the critical amino acids that cannot be absorbed by the malfunction of the amino acid transporter [145]. It was therefore reasonable to assume that in *pept1*$^{-/-}$ mice some compensation of the loss of peptide transporter by amino acid transporters might occur. This was expecting since the animals lacking PEPT1 did not display any distinct phenotypic changes. To demonstrate loss of PEPT1 uptake experiments were conducted with radiolabeled Gly-Sar as a substrate. In order to evaluate a possible compensation by other transporter systems we performed also other functional, mainly electrophysiological measurements in the Ussing chamber.

3.1.1 Uptake studies and Ussing chamber measurements

Uptake of Gly-Sar into jejunal tissues of wild type and PEPT1-deficient mice (Fig. 10) demonstrates that dipeptide uptake is essentially missing in animals lacking the transporter.

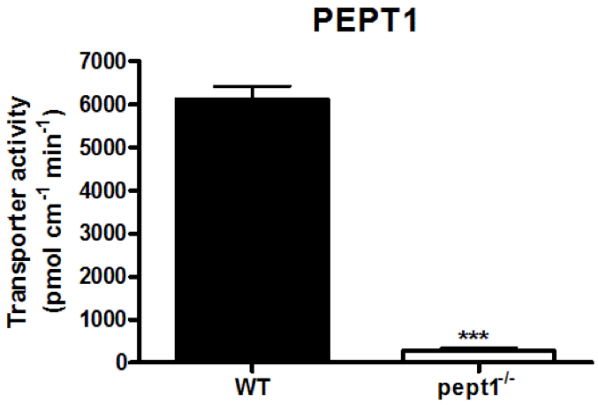

Figure 10 [^{14}C] Gly-Sar uptake into everted gut rings in wt and *pept1*$^{-/-}$ mice

Everted gut rings were prepared from proximal jejunum of wt (n = 3) and *pept1*$^{-/-}$ (n = 3) mice and incubated in 1 mM of [^{14}C] radiolabeled Gly-Sar for 2 minutes. Statistical analysis was performed by unpaired student t-test. Data are presented as mean ± SEM (*** $p < 0.001$).

Functional transport studies in the Ussing chamber were carried out in wt, *pept1*$^{-/-}$ and the heterozygous *pept1*$^{+/-}$ mice. Transport currents were recorded for PEPT1 with Gly-Sar, for PAT1 with glycine, for SIT1 with L-proline and for SGLT1 with D-glucose as substrates. All substrates were added at 20 mM concentration. Jejunal segments of the different genotypes were short-circuited and substrate-induced changes were recorded as Isc in the Ussing chamber.

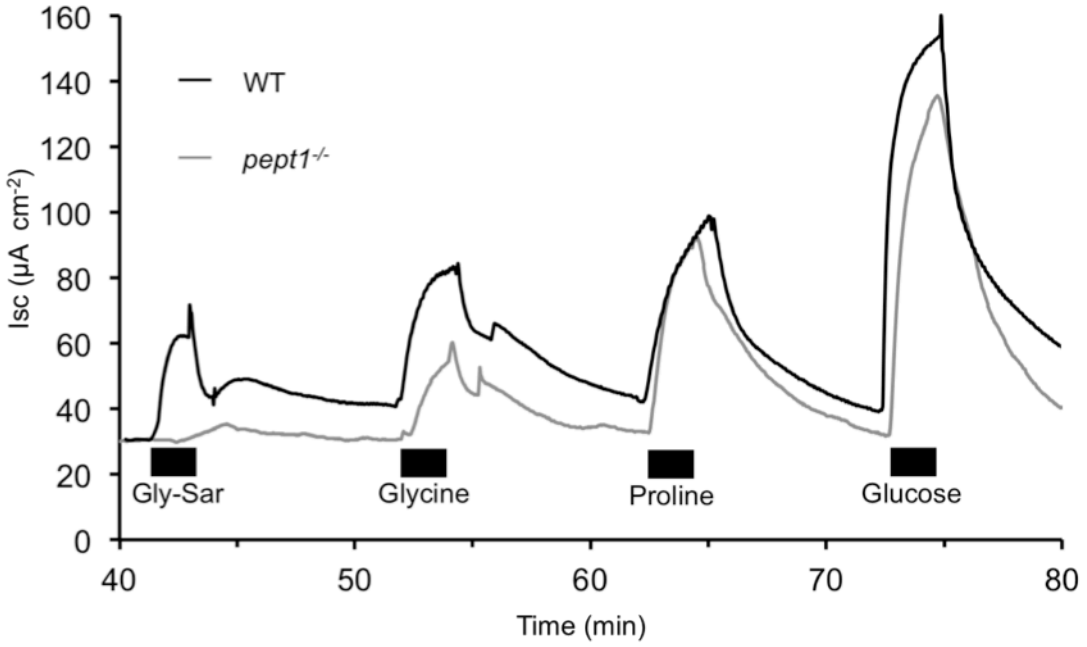

Figure 11 Representative current trace of substrate-induced Isc measured in jejunal segments of a wt and *pept1*$^{-/-}$ mouse

Measurements in one jejunal segment of a wt (black line) and *pept1*$^{-/-}$ (grey line) mouse were performed in Ussing chamber. Each substrate (20 mM) was applied for 2 min (black bar) followed by a washout period of 7 minutes.

PEPT1-mediated Gly-Sar transport was absent in *pept1*$^{-/-}$ mice ($p < 0.001$) when compared to the wild type mice (Fig. 11, Tab. 9). In contrast, neither glycine transport by PAT1, L-proline transport by SIT1 nor glucose transport by SGLT1 was significantly altered in the *pept1*$^{-/-}$ mice, compared to wt mice (Tab. 9).

Table 9 Substrate-induced short-circuit currents

Absolute values of substrate-induced short-circuit currents (Isc, µA cm^{-2}) measured in wt (n = 8), *pept1* $^{+/-}$ (n = 5) and *pept1* $^{-/-}$ (n = 8) mice. Data presented as mean ± SEM, wt vs. *pept1*$^{-/-}$ (* $p < 0.05$; *** $p < 0.001$) and *pept1*$^{-/+}$ vs. *pept1*$^{-/-}$ (§§§ $p < 0.001$; § $p < 0.05$).

Substrates	Mouse genotype		
	wt	*pept1* $^{+/-}$	*pept1* $^{-/-}$
Gly-Sar	29 ± 10	19 ± 5 §§§	0 ± 7 ***
Glycine	30 ± 10	23 ± 6§	34 ± 10
L-Proline	41 ± 12	39 ± 8§	53 ± 19
D-Glucose	93 ± 26	84 ± 23§	111 ± 31

Although, heterozygous mice when compared to the *pept1*$^{-/-}$ mice revealed significant changes in all transporter activities (Tab. 9) this can be attributed to a rather low variability in currents, in homozygous animals compared to wild type these differences – except for PEPT1 – were not found.

3.1.2 Kinetic parameters in wt, *pept1*$^{-/-}$ and *sglt1*$^{-/-}$ mice

Data on substrate affinities and maximal transport rates for PEPT1 and SGLT1 (for reference see table 1 & 3) mostly come from cell culture studies (with or without heterologous expression of the transporter) or from tissues of rats and mice.

We carried out transport studies in Ussing chambers to determine apparent substrate affinities and maximal transport rates (expressed as I_{max} current) of the PEPT1 protein in wt and in *sglt1*$^{-/-}$ mice and for SGLT1 in wt and *pept1*$^{-/-}$ mice (Fig. 14, 15). Apparent K_m and I_{max} were determined by a non-linear regression fit based on the Michaelis-Menten equation ($Y = V_{max} * X / (K_m + X)$) of the different genotypes.

The Michaelis-Menten plot in Fig. 12 (black line) revealed an apparent K_m value of 21.3 ± 2.2 mM and a I_{max} of 66.0 ± 2.6 µA cm^{-2} respectively, for PEPT1 mediated Gly-Sar transport in wt mice. The affinity of the transporter in the *sglt1*$^{-/-}$ mice to Gly-Sar showed a K_m of 22.24 ± 1.4 mM and a maximal velocity of I_{max} of 51.64 ± 1.31 µA cm^{-2} (Fig. 12, grey line), thus not different between the two different genotypes.

Affinity studies for SGLT1 in wt mice determined an apparent K_m of 13.6 ± 0.5 mM and an I_{max} of 95.7 ± 1.1 µA cm^{-2} (Fig. 13, black line), while in the *pept1*$^{-/-}$ mice the affinity [120] of SGLT1 to its substrate glucose was elevated up to 24.6 ± 1.0 mM.

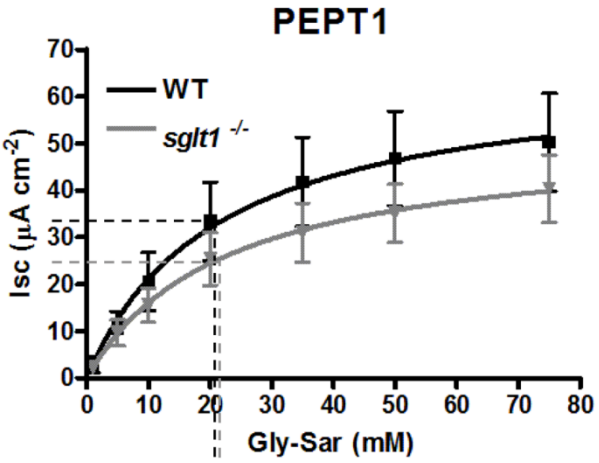

Figure 12 **Kinetic parameters of PEPT1 in wt and *sglt1*$^{-/-}$ mice determined in Ussing chamber studies**

Transport currents induced by apical Gly-Sar (1, 5, 10, 20, 35, 50 and 75 mM) were recorded at a constant osmolarity and K_m and I_{max} were determined (wt: black line, n = 4; *sglt1*$^{-/-}$: grey line, n = 4). Data were fitted by non-linear regression analysis to the Michaelis-Menten equation to determine K_m and I_{max} (mean ± SEM) using GraphPad Prism 4.0™.

The maximal velocity of the glucose transporter in the knockout mouse (*pept1*$^{-/-}$) remained unaffected (I_{max}: 104.7 ± 1.7 µA cm^{-2}) (Fig. 13, grey line).

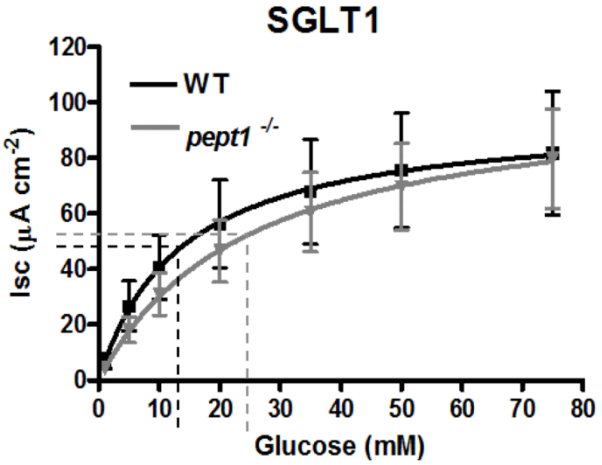

Figure 13 **Kinetic parameters of SGLT1 in wt and *pept1*$^{-/-}$ mice determined in the Ussing chamber studies**

Transport currents induced by apical D-glucose (1, 5, 10, 20, 35, 50 and 75 mM) were recorded at constant osmolarity and K_m and I_{max} were determined (wt: black line, n = 4; *pept1*$^{-/-}$: grey line, n = 4). Data were fitted by non-linear regression analysis to the Michaelis-Menten equation to determine K_m and I_{max} (mean ± SEM) using GraphPad Prism 4.0™.

Substrate affinities and maximal transport rates of the other electrogenic transporters SIT1 and B^0AT1 in wt mice revealed for SIT1 with glycine a K_m value of 28.9 ± 1.9 mM and a I_{max} of 51.8 ± 4.3 µA cm^{-2}, while B^0AT1 revealed a K_m value of 9.5 ± 0.7 mM and a I_{max} value of 67.8 ± 1.3 µA cm^{-2} (data not shown).

3.1.3 Segmental differences in transport of PEPT1 and SGLT1

Tracer uptake studies using 1 mM Gly-Sar and 1 mM α-MDG as specific substrates for PEPT1 and SGLT1 respectively, were performed to determine segmental activities of the transporters along the small intestine of mice for further uptake experiments.

As shown in Fig. 14, the highest transporter activity for both, PEPT1 (a) and SGLT1 (b) was detected in the proximal part of the small intestine (ring 6-15) with decreasing activity towards the distal small intestine.

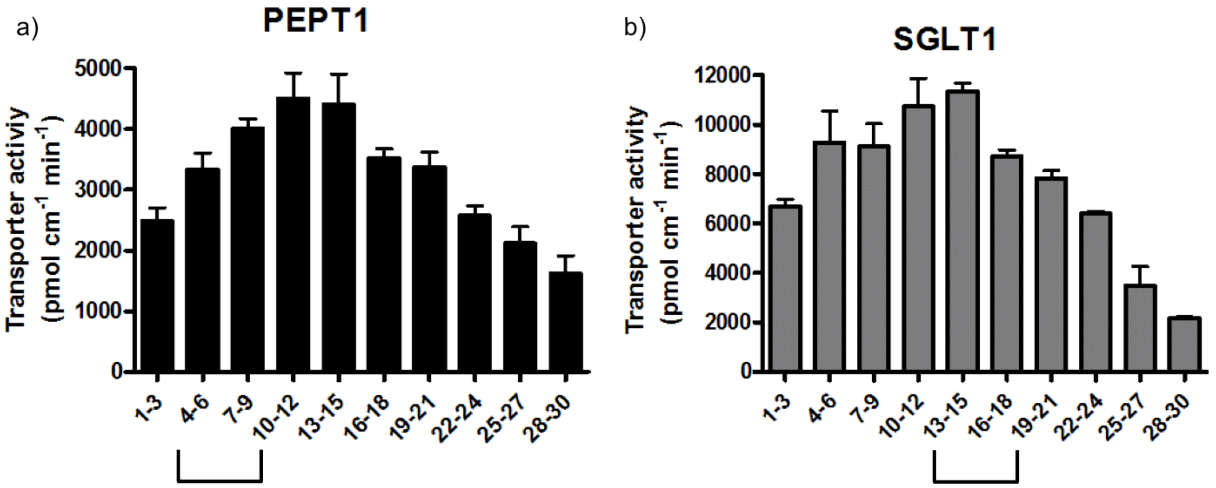

Figure 14 Segmental [^{14}C] Gly-Sar and [^{14}C] α-MDG uptake in wt mice

PEPT1 (n = 6) and SGLT1 (n = 3) activity was determined by uptake experiments of the transporter specific substrate throughout the whole length of the small intestine. Represented by the numbering on the X-axis, 3 rings each were incubated together (mean ± SEM).

For further uptake studies we decided to use rings 4-11 (indicated by the black lines, Fig. 14 a) for PEPT1 and rings 12-19 (indicated by the black lines, Fig. 14 b) for SGLT1. It became obvious, that uptake by SGLT1 was almost twice as high when compared to Gly-Sar uptake mediated by PEPT1.

3.2 Influence of diet-induced obesity on transporter function

Diet-induced obesity (DIO) in mice was described to affect PEPT1-mediated transport in the small intestine via a down-regulation of transporter mRNA and protein levels [131]. Furthermore, Caco-2 cells expressing PEPT1, SGLT1, PAT1 and B^0AT1 and exposed apically to leptin (leptin levels are increased on obese states) showed a reduced transporter activity for all proteins [132, 133]. However transport currents of the respective proteins have so far never been determined. Thus, effects of HF feeding (60% energy from fat) on activities of PEPT1, PAT1, SIT1 and SGLT1 were compared to those in mice fed a control diet (C-diet, 11% energy from fat).

3.2.1 Comparative Ussing chamber studies

Four segments of stripped jejunum of each mouse were used for Ussing chamber measurements. The following transporter specific substrates (each 20 mM) were used to quantify transporter activity (measured as short-circuit current, Isc), in the Ussing chamber: Gly-Sar (PEPT1), Glycine (PAT1), L-proline (SIT1) and D-glucose (SGLT1).

As shown in Fig. 15, Ussing chamber measurements revealed a significant decrease in transporter activity in the mice that received the HF-diet.

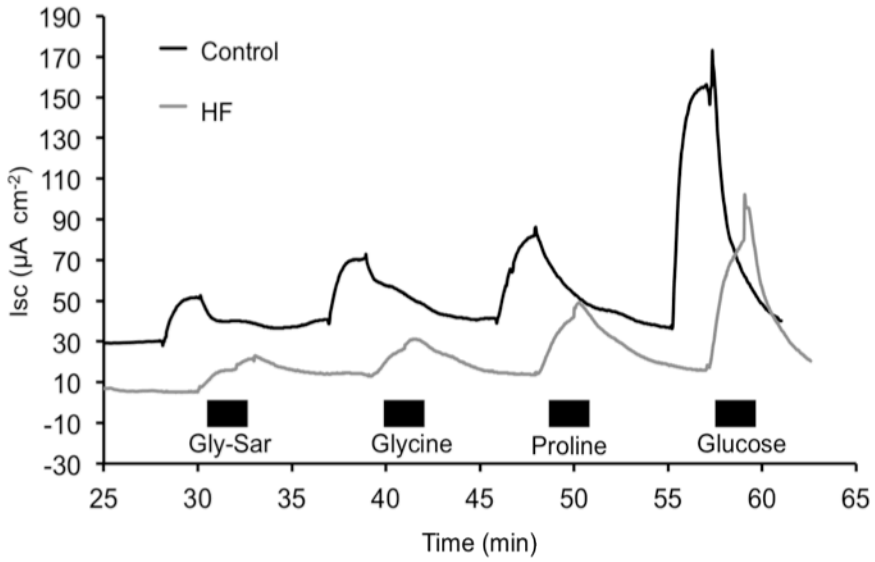

Figure 15 Representative current trace of electrogenic transporter activities measured in an Ussing chamber with one segment of wt mice fed a C- or HF-diet

After equilibration, transporter specific substrates (black bars) were applied for 2 min at a concentration of 20 mM and each application was followed by a 7 min washout period. Grey line: HF-diet mouse (60%), black line: C-diet mouse (9%).

PEPT1 mediated Gly-Sar current displayed a basal activity in C-diet fed mice of 27.6 ± 5.78 µA cm^{-2} (Fig. 16 a), while in the HF mice showed a significant decrease of PEPT1 activity to 4.2 ± 0.58 µA cm^{-2} ($p < 0.01$).

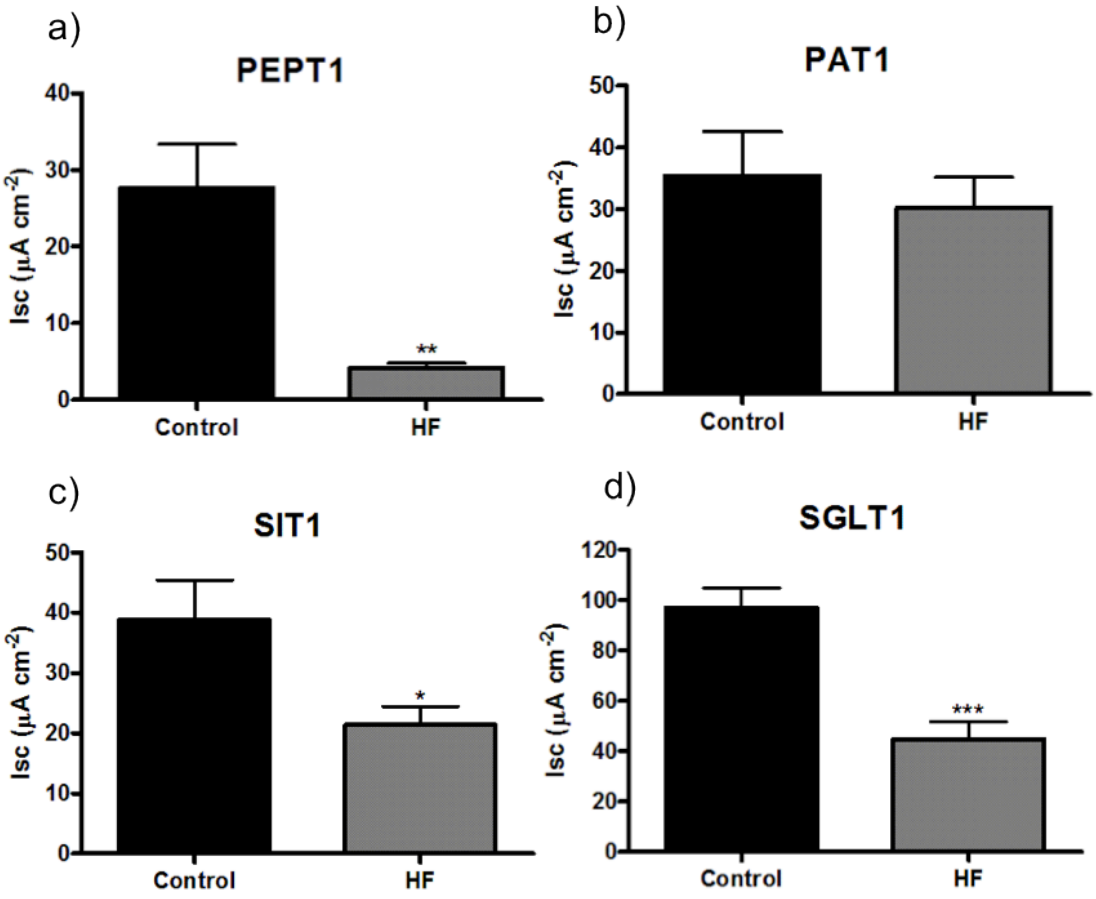

Figure 16 Transporter activities in wt mice fed a C-diet or HF-diet

Transporter activities of (a) PEPT1 (Gly-Sar), (b) PAT1 (Glycine), (c) SIT1 (L-proline) and (d) SGLT1 (D-glucose) were measured in wt mice receiving either a C-diet (n = 5) or HF-diet (n = 5). Values of the substrate induced Isc by the selected electrogenic transporters were compared (mean ± SEM) (* $p < 0.05$, ** $p < 0.01$, *** $p < 0.001$).

The PAT1-mediated Isc by 20 mM glycine remained essentially unaffected by the HF-diet (Fig. 16 b) whereas the IMINO-transport system SIT1 (Fig. 16 c) displayed a basal activity of 38.8 ± 6.2 µA cm^{-2} in wt mice fed the C-diet and significantly lower levels in the HF group reduced to 21.4 ± 3 µA cm^{-2} ($p < 0.05$). Glucose-induced SGLT1-mediated Isc in wt mice on C-diet accounted to 96.8 ± 8.2 µA cm^{-2} (Fig. 16 d) and was reduced to 45.0 ± 7.2 µA cm^{-2} in the HF fed group ($p < 0.001$).

3.3 Influence of insulin on transporter functions

Insulin was shown in Caco-2 cells to increase PEPT1 transporter activity after a short-term (30 min) basolateral exposure to cells [106, 146] at physiological concentrations of 5 nM. *In situ,* SGLT1 transporter activity was shown to be maximally reduced by the action of insulin at a concentration of 100 nM [51]. We first assessed whether jejunal segments of wt mice mounted in the Ussing chamber change current responses to a short term (30 min) basolateral insulin (100 nM) exposure.

3.3.1 *In vitro* effects of insulin

Jejunal segments of wt (C57BL/6J) mice were freshly prepared and mounted into the Ussing chambers. One half of the segments of each mouse were used for the insulin incubation experiment and one half was used as a control. Transporter activities (PEPT1, SIT1, PAT1, EAAC1 and SGLT1) were measured before and after 30 min of basolateral insulin exposure (Fig. 17).

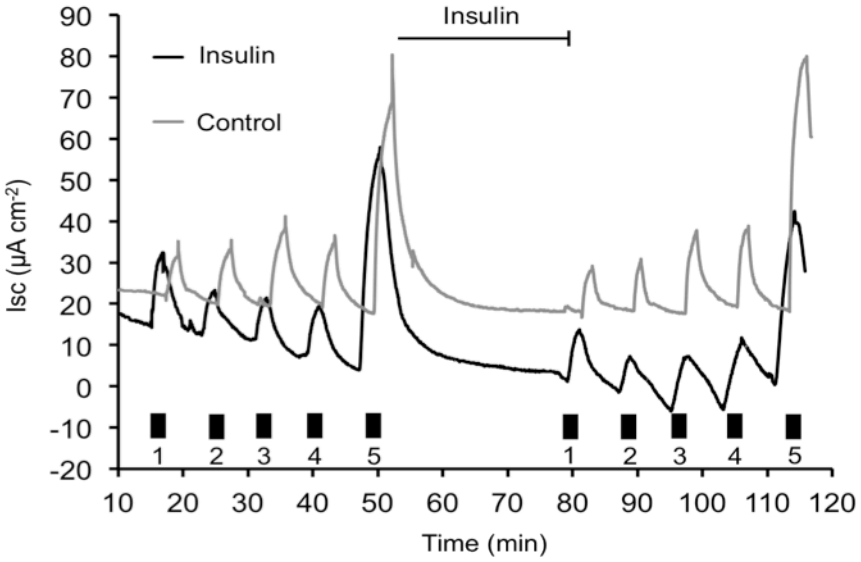

Figure 17 Representative current traces of electrogenic transporters recorded in Ussing chambers before and after exposure of tissues to insulin

First, basal transporter activities of PEPT1 (1: Gly-Sar), PAT1 (2: Glycine), SIT1 (3: L-proline), EAAC1 (4: L-glutamate) and SGLT1 (5: D-glucose) were measured after the 2 min application of the transporter specific substrates (indicated by the black boxes) each followed by a 7 min washout period. 100nM insulin was added to the basolateral side (indicated by the black arrow) and after 30 min all substrates were applied again to determine transporter current responses.

In essence, none of the transporters showed any significant changes in transport currents in response to insulin exposure of tissues as shown in Tab. 10.

Table 10 Isc (µA cm^{-2}) responses before (basal) and after *in vitro* insulin treatment of tissues in Ussing chambers

Data are presented as mean ± SEM.

	PEPT1	PAT1	EAAC1	SIT1	SGLT1
Basal activity	29 ± 7 (n = 10)	24 ± 6 (n = 5)	31 ± 18 (n = 2)	37 ± 8 (n = 8)	85 ± 8 (n = 9)
After insulin incubation	20 ± 2 (n = 8)	16 ± 3 (n = 5)	29 ± 10 (n = 2)	30 ± 5 (n = 6)	105 ± 11 (n = 8)
After time control	26 ± 10 (n = 5)	14 ± 3 (n = 5)	29 ± 10 (n = 2)	49 ± 22 (n = 4)	116 ± 19 (n = 5)

Other experiments with prolonged (60 min) expose times of insulin of the same concentration did also not reveal changes in any of the electrogenic transporters (data not shown).

3.4. Effects of *in vivo* insulin treatment on transporter activities

Previous studies suggested that insulin affects the peptide transporter in the intestine. This was studied *in vivo* in non-diabetic male rats, treated with an i.p. injection (1U / kg bw) twice daily, for one month [144]. In these experiments, insulin did not affect blood glucose concentrations but decreased PEPT1 mRNA concentration without alterations in PEPT1 protein levels or transport activity. Our study was intended to show short-term (acute) effects of insulin and thus wt mice were treated with insulin and after 30 min PEPT1 and SGLT1 activities were analyzed.

3.4.1 Body weight and blood glucose

C57BL/6J wt mice (12 weeks) were separated in two groups (each n = 10) with one group of animals receiving a single i.p. injection of 0.1 U / kg bw human insulin in HEPES 2-[4-(2-hydroxyethyl)-1-piperazineethanesulfonic acid] (pH 8.4) and the control group was HEPES injected, as a vehicle. Blood glucose concentration was measured before and 30 min after the injection.

Table 11 Body weight and blood glucose levels before and after i.p. injection of insulin

Data are presented as mean ± SEM (*** $p < 0.001$) (n = 10 each group).

Treatment	Body weight (g)	Basal blood glucose (mg / dl)	After injection (mg / dl)
0.1 U/kg bw insulin	30 ± 1	126 ± 5	130 ± 9
0.1U / kg bw control	29 ± 1	126 ± 8	183 ± 7 ***

As shown in Tab. 11, all mice started out with a similar basal blood glucose concentration (n = 20). The i.p. administration per se (HEPES) increased blood glucose levels, most likely as a consequence of a stress-mediated release of glucose from liver glycogen that was markedly reduced as shown in Fig. 18 by insulin administration ($p < 0.001$).

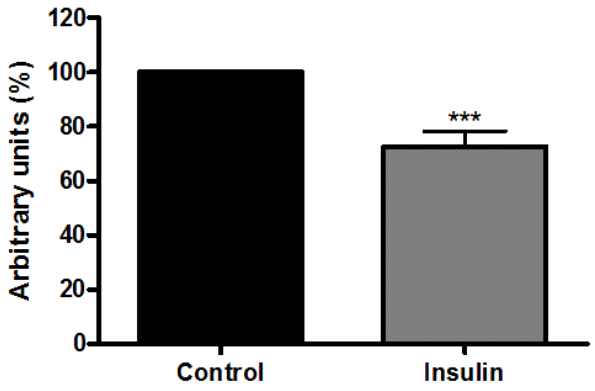

Figure 18 Insulin effects on blood glucose concentration

Blood glucose concentration before and after 0.1 U kg^{-1} bw i.p. injection of insulin (30 min). Data are normalized to the HEPES injected controls and presented as mean ± SEM (*** $p < 0.001$).

3.4.2. mRNA and protein concentrations of PEPT1 and SGLT1

mRNA and protein levels were determined in samples of freshly scraped mucosa of the small intestine of the insulin treated mice, as well as of the controls. Determinations of transporter mRNA amounts were carried out by Light Cycler measurements. Villin (actin-binding protein) and GAPDH (glyceraldehyde-3-phosphate dehydrogenase) were chosen and used as housekeeping genes and transporter mRNA was normalized to the chosen reference genes.

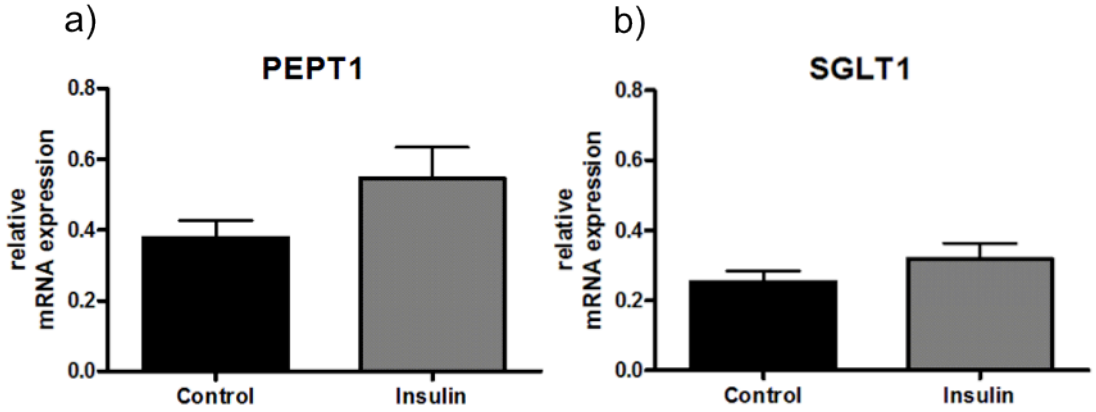

Figure 19 mRNA levels of PEPT1 and SGLT1 in tissues of control and insulin-treated mice

PEPT1 mRNA (a) and (b) SGLT1 mRNA content of isolated mucosal tissue. Villin and GAPDH were used as housekeeping genes and used as references for normalization of transporters mRNA amount. Data are presented as mean ± SEM (control mice: n = 5, black bar) (insulin treated mice: n = 5, grey bar).

The mRNA concentration of PEPT1 measured by qRT-PCR (Control: 0.38 ± 0.05) revealed no significant changes when compared (Insulin: 0.55 ± 0.09) (Fig. 19 a).

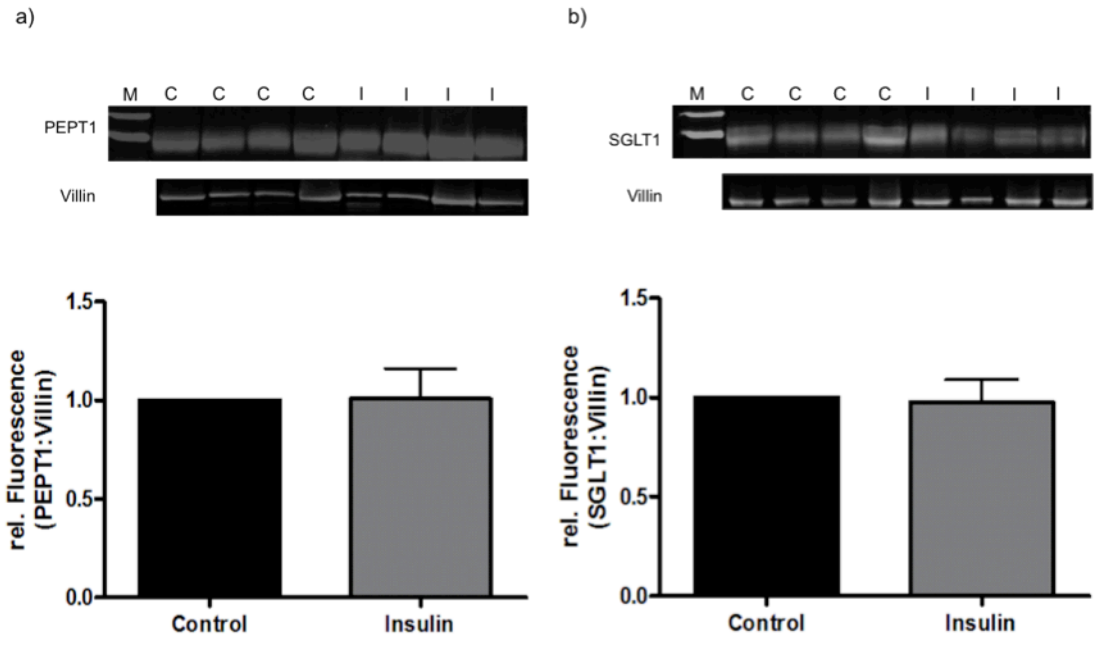

Figure 20 PEPT1 and SGLT1 protein tissue levels

Western blot analysis was performed using (a) mPEPT1 antibody in control mice (black bar, n = 4) and insulin-treated mice (grey bar, n = 4), with a related ~90kDa protein band and (b) mSGLT1 antibody in control (black bar, n =4) and insulin treated mice (grey bar, n = 4). Villin (~43 kDa) was used as reference protein for analysis. Statistical analysis was performed by Mann-Whitney-test and data are presented as mean ± SEM.

For SGLT1 also no differences in mRNA levels were found (Fig. 19 b). Western blot analysis of PEPT1 and SGLT1 protein levels in control mice and insulin-treated mice revealed also no significant changes in PEPT1 (Fig. 20, a) or SGLT1 (Fig. 20, b) levels in the two groups.

3.4.3 Uptake experiments

To determine PEPT1 and SGLT1 activity in control and insulin-treated mice, everted gut rings of the proximal small intestine were used for uptake of radiolabeled substrates.

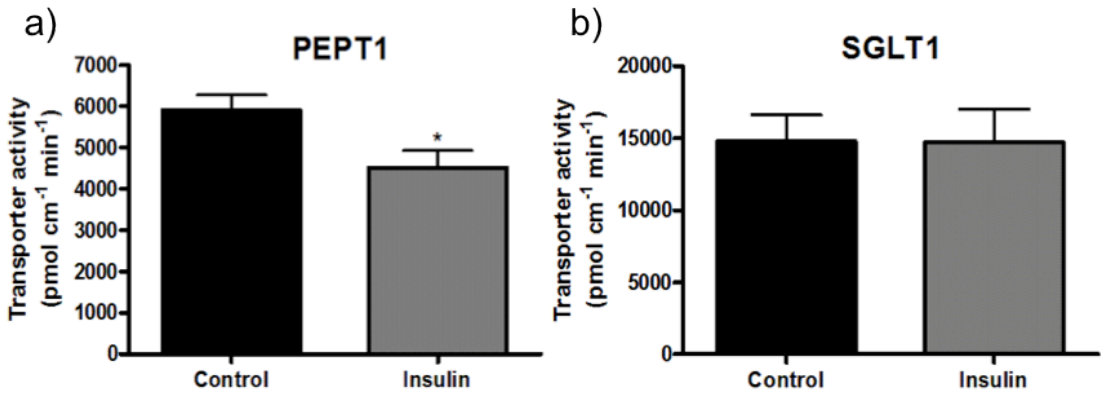

Figure 21 Transporter activities assessed in gut rings of control and insulin-treated mice

PEPT1 activity determined by [^{14}C] Gly-Sar (a) and SGLT1 activity by [^{14}C] α-MDG (b) uptake for 2 min in control (black bar; n = 5) and insulin-injected mice (grey bar; n = 5; mean ± SEM) (* $p < 0.05$).

PEPT1 activity (Fig. 21 a) was significantly decreased in the insulin-injected mice (4513 ± 414 pmol cm^{-1} min^{-1}; $p < 0.05$) when compared to control animals (5904 ± 366 pmol cm^{-1} min^{-1}).

Whereas SGLT1 transporter activity (Fig. 21 b) was not altered by insulin administration (C.: 14780 ± 1853 pmol cm^{-1} min^{-1}, insulin: 14513 ± 2280 pmol cm^{-1} min^{-1}).

3.4.4 Ussing chamber measurements

A representative current trace obtained in Ussing-chambers is depicted in Fig. 24 for a jejunal segment of either an insulin -treated, or control mouse.

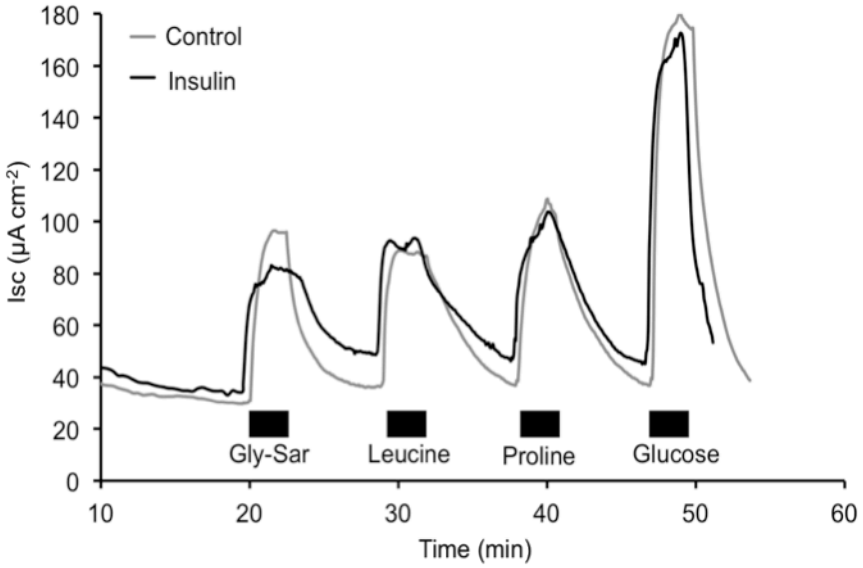

Figure 22 Representative current traces of Ussing chamber measurement.

Substrate (black bars) induced Isc by the selected transporters (PEPT1 (Gly-Sar), B^0AT1 (L-leucine), SIT1 (L-proline), SGLT1 (glucose)) were recorded for the insulin injected mice (grey line) and control mice (black line).

Mean values for the Isc in tissues of animals treated with insulin or HEPES are summarized in Tab.12.

Table 12 Transporter-mediated Isc (µA cm^{-2}) in insulin treated and control mice

Data are presented as mean ± SEM.

Treatment	PEPT1	B^0AT1	SIT1	SGLT1
HEPES	30.4 ± 3.9	34.8 ± 2.1	35.3 ± 4.7	78.5 ± 10.7
Insulin	29.5 ± 3.7	34.4 ± 2.2	36.0 ± 3.4	71 ± 7.7

Taken together, insulin administration *in vivo* led to a decrease in blood glucose levels 30 min after injection but failed to affect the intestinal transporters assessed by changes in mRNA and protein levels or function.

3.5 Effect of high luminal glucose on intestinal transporter function

Previous studies in rats with *in situ* perfusion of the small intestine suggested that high luminal glucose levels (75 mM) as they may occur after a meal lead to a significant decrease in apical PEPT1 protein and increase apical GLUT2 by recruiting this protein from vesicles into the brush border membrane [79]. To mimic this condition, we performed prolonged luminal perfusions (30 min) of jejunal segments with 75 mM glucose and assessed transporter activity of PEPT1 and SGLT1 in Ussing chambers. Since GLUT2 is not an electrogenic transporter, we additionally investigated GLUT2 activity under high glucose conditions by an oral glucose tolerance test (OGGT).

3.5.1 Ussing chamber measurements before and after high glucose perfusion

To assess the response to high luminal glucose conditions (75 mM), jejunal segments of wt mice were constantly perfused for 30 min with mKHB containing 75 mM of glucose or 75 mM mannitol, serving as osmotic control (Fig. 23). The short circuit currents induced by Gly-Sar (PEPT1), L-proline (SIT1) and D-glucose (SGLT1) before and after the perfusion were recorded and compared.

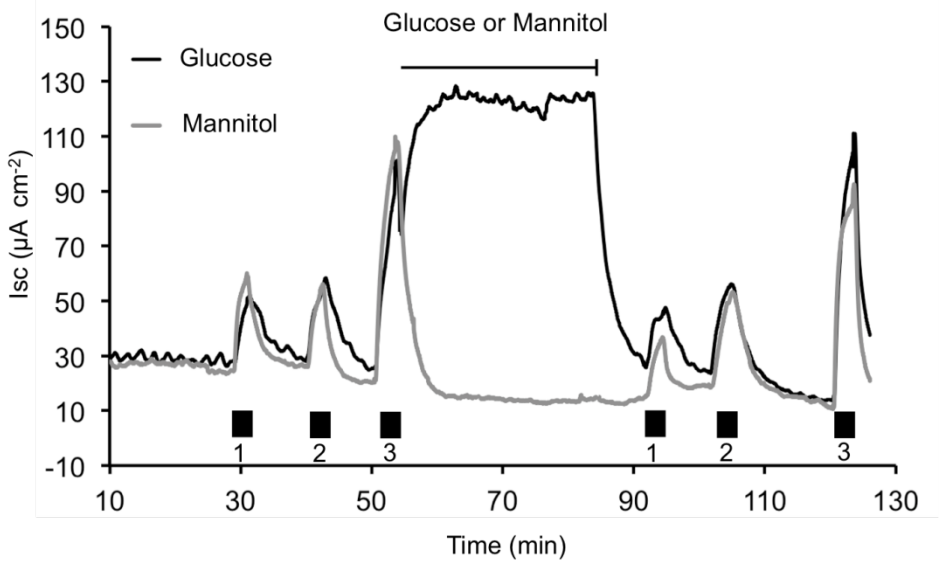

Figure 23 Representative current traces in Ussing chambers before and after luminal perfusion

Substrate (black bars, 1: Gly-Sar, 2: L-proline, 3: glucose) induced short-circuit currents were measured before and after 75 mM glucose (black line) or 75 mM mannitol serving as control (grey line). Substrates were again applied in the same order (black bars).

As shown in Figure 24 a, the initially measured Gly-Sar-induced PEPT1-mediated Isc (23.8 ± 3.7 µA cm^{-2}) revealed a significant decline to 14.3 ± 2.5 µA cm^{-2} after the high glucose perfusion. The control recording did not reveal any alterations of PEPT1 activity before (23.1 ± 3.2 µA cm^{-2}) and after mannitol perfusion (22.1 ± 4.1 µA cm^{-2}).

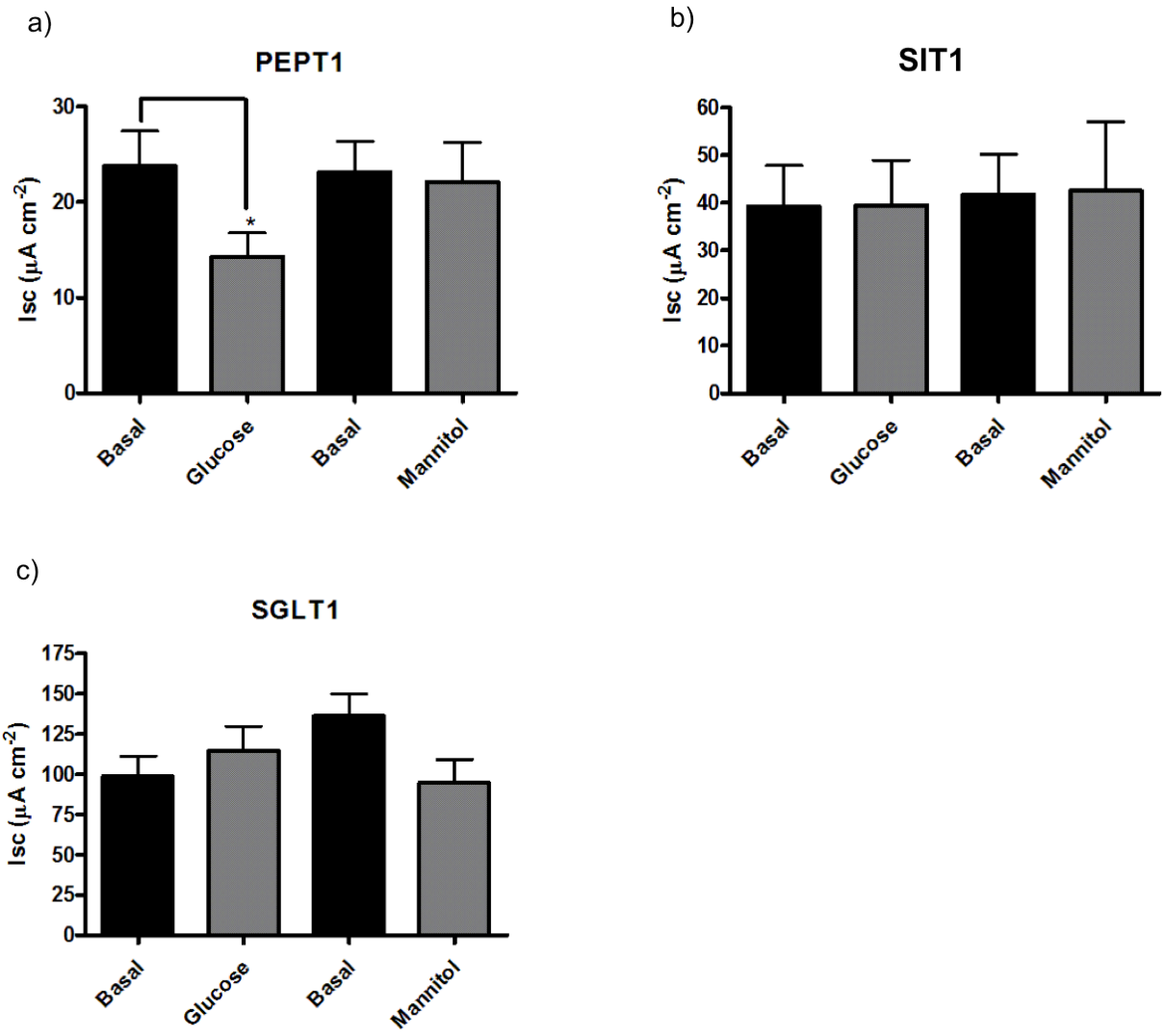

Figure 24 **Isc responses of PEPT1, SIT1 and SGLT1 before and after 75 mM glucose perfusion**

Basal transporter activities (black bars) of PEPT1 (n = 10), SGLT1 (n = 11) and SIT1 (n= 5) before the glucose or glucose (PEPT1, n = 7; SGLT1, n = 9; SIT1, n = 4) perfusion were recorded. Following the 30 min incubation of either 75 mM glucose or 75 mM mannitol, the transporter activities were determined again (grey bars). Data are presented as mean ± SEM (* $p < 0.05$).

The SGLT1-mediated Isc levels (Fig. 24 b) were not significantly altered by the high glucose perfusion (114.5 ± 15.3 µA cm^{-2}) when compared to the initially measured Isc (98.7 ± 12.4 µA cm^{-2}). Control measurements revealed also no changes in the glucose induced Isc before

(136.1 ± 13.9 µA cm^{-2}) and after (94.8 ± 14.5 µA cm^{-2}) mannitol perfusion. SIT1-mediated L-proline currents (39.2 ± 8.6 µA cm^{-2}) remained unaffected, as shown in Figure 24 c, by glucose perfusion (39.4± 9.5 µA cm^{-2}) and control values before (41.8 ± 8.4 µA cm^{-2}) and after (42.5 ± 14.6 µA cm^{-2}) mannitol perfusion did not change.

Additional measurements in the open-circuit voltage mode [V_{oc}] of jejunal segments were performed in wt mice under high luminal glucose (75 mM). Activity of PEPT1 was significantly reduced by the high luminal glucose perfusion, as shown by short-circuit and open-circuit measurements (Tab. 13). Measurements of SGLT1 activity before and after high luminal glucose revealed no changes either in the open-circuit mode or in the short-circuit mode.

Table 13 Open-circuit current (Ioc calculated as Isc) and measured short-circuit current (Isc) of PEPT1 and SGLT1 before and after high luminal glucose perfusion

Data are presented as µA cm^{-2} and expressed as mean ± SEM.

	PEPT1	SGLT1
Ioc calculated to Isc		
Basal	59.1 ± 7.8	138.0 ± 12.8
After 75 mM glucose	35.6 ± 5.9 *	114.5 ± 15.3
Measured Isc		
Basal	23.8 ± 3.7	98.7 ± 12.4
After 75 mM glucose	14.3 ± 2.5 *	114.5 ± 15.3

Control measurements did not indicate any significant effects of glucose perfusion in the open-circuit mode (data not shown).

3.5.2 Effect of glucose on an oral glucose bolus

Blood glucose

After an oral glucose bolus (20 % in 200 µl), blood was drawn by tail punctuation and blood glucose levels were measured at defined time points (basal, 15, 30, 90 min).

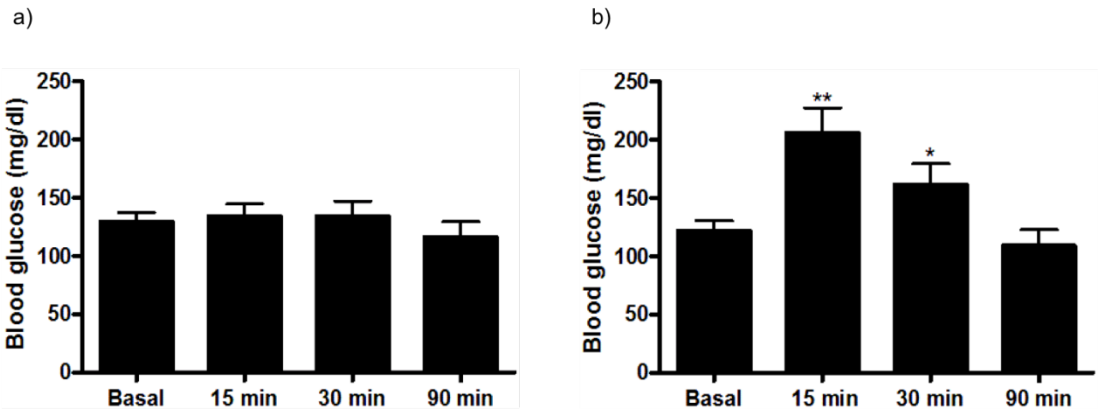

Figure 25 Blood glucose levels after oral glucose bolus

Blood glucose was determined by tail puncture for each time point (basal, n = 9; 15 min, n = 7; 30 min, n = 4 and 90 min, n = 3) after glucose (a) or (b) tap water gavage (n = 5 per time point). Data are presented as mean ± SEM (* $p < 0.05$; ** $p < 0.01$).

Blood glucose significantly increase from 122 ± 8 mg / dl to 206 ± 21 mg / dl ($p < 0.01$) at 15 min and returned to 109 ± 14 mg / dl 90 min after the gavage (Fig. 25 a). The gavage itself – by administration of water - did not change blood glucose levels (basal: 126 ± 10 mg / dl; 15 min: 139 ± 13 mg / dl; 30 min: 132 ± 19 mg / dl and 90 min: 116 ± 13 mg/ dl, Fig. 25 b).

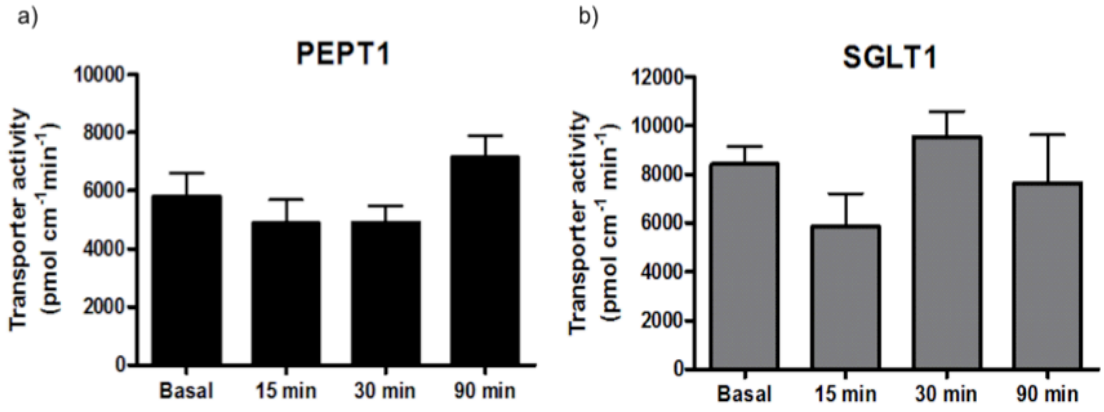

Figure 26 Substrate uptake rates after the oral glucose bolus

Transporter activity of (a) PEPT1 by [^{14}C] Gly-Sar and (b) SGLT1 by [^{14}C] α-MDG was determined at basal state (n = 9) and after 15 min (n = 7), 30 min (n = 4) and 90 min (n = 2). Data are presented as mean ± SEM.

Transporter activity of PEPT1 and SGLT1 determined in mice that received a glucose bolus displayed no significant changes in [^{14}C] Gly-Sar (Fig. 26 a) or [^{14}C] α-MDG (Fig. 26 b) uptake at any time point

Uptake studies for GLUT2 in these mice failed to detect any GLUT2 activity in the everted gut rings with the [^{3}H] 2-deoxy-D-glucose as a GLUT2-substate (data not shown).

3.6 Effect of glucose on intestinal transporters in STZ-induced type 1 diabetes

STZ-induced diabetes in rats was shown to dramatically increase blood glucose and to additionally modulate PEPT1 and SGLT1 expression and function [144, 147, 148]. We therefore tested in analogy whether STZ treatment in mice alters blood glucose, body weight and organ / tissue and transporter function. STZ-treatment was performed by a single high-dose i.p. injection of STZ or a vehicle (citrate buffer). Intestinal expression of PEPT1 and SGLT1 was determined on mRNA and protein levels. Functional studies were performed by uptake and in Ussing chambers experiments.

3.6.1 STZ-induced effects on body weight and blood glucose

Twelve weeks old male wt (C57BL/6N) mice received a single high-dose i.p. injection of STZ (180mg / kg bw) in 0.1mol/L citrate-buffer (pH 4.5; n = 10). The control group (n = 10) received citrate buffer as a vehicle. Body weight and blood glucose levels were determined before injection and for the consecutive five days after STZ-injection.

3.6.2 Body weight

Body weight of the STZ-treated mice over five days post-injection (p.i.) showed a significant decrease. While the body weight in the control group did not change over 5 days p.i. (28 ± 1.2 g), the STZ-treated mice showed a significant loss of bodyweight over time (23.2 ± 0.9 g; $p < 0.001$) accounting to around 20 % (Fig. 27).

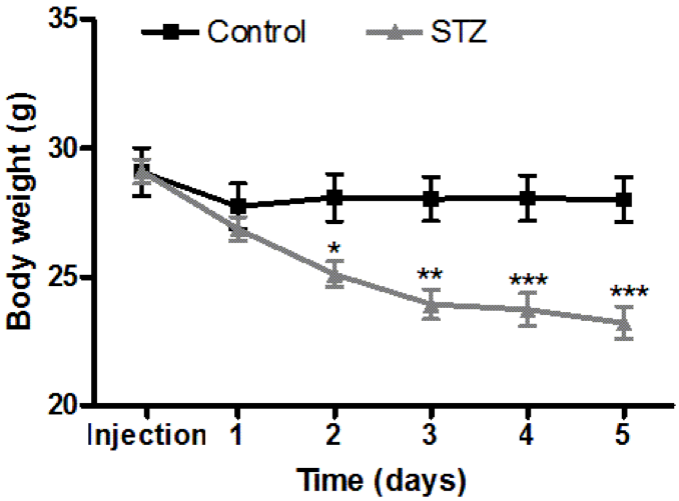

Figure 27 Body weight development over 5 days after STZ treatment

The control group (black line, n = 10) received a vehicle (0.1 M citrate buffer) injection and the STZ-treated mice (grey line, n = 10) received 180mg / kg bw Streptozotocin. Body weight was monitored over five consecutive days post injection. Statistical analysis was performed by 2-way ANOVA (* $p < 0.05$, ** $p < 0.01$, *** $p < 0.001$).

3.6.3 Blood glucose

Blood glucose measurements were performed by tail punctuation and measured before the i.p. injections and continuously every day at 9:15 for the next five days. Whereas basal blood glucose concentration of the control group (Figure 28 a) varied between 110 and 125 mg / dl glucose in STZ-treated mice (Figure 28 b), glucose concentrations here, significantly decrease just one day post-injection from 109.2 ± 4.8 mg / dl to 65.2 ± 13.4 mg / dl, ($p < 0.001$). On the second day after the injection, blood glucose concentration increased to 143.9 ± 31.4 mg / dl and significantly increased further to reach 283.6 ± 41.4 mg / dl ($p < 0.001$) at day three, 368 ± 26.6 mg / dl ($p < 0.001$) at day four and 428.9 ± 20.5 mg / dl on day five ($p < 0.001$).

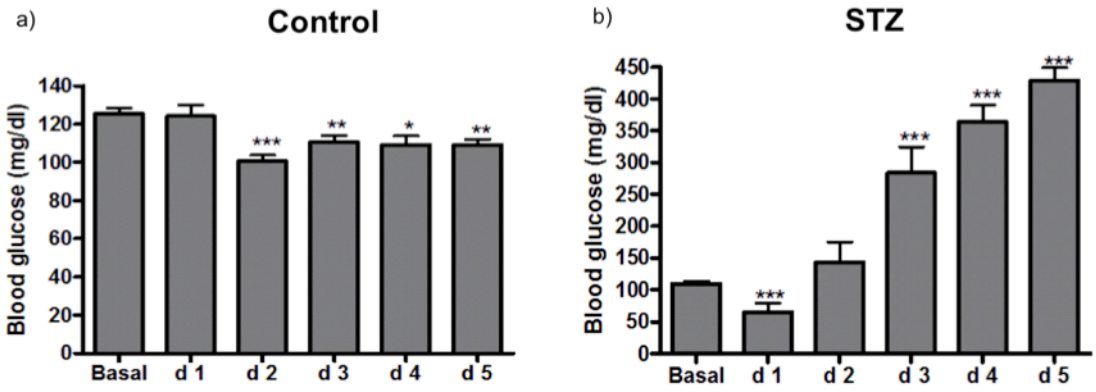

Figure 28 Blood glucose development over 5 days after STZ treatment

Blood glucose was determined before injection (basal) and measured every day continuously (day 1 – day 5) until day five post injection of either (a) the control (n = 10) or (b) the STZ treated mice (n = 10). Data are presented as mean ± SEM (* $p < 0.05$, ** $p < 0.01$, *** $p < 0.001$).

To determine the onset of the initial hypoglycemia, blood glucose concentration of the STZ-treated mice was measured over nine hours post injection (Fig. 29). Blood glucose revealed a significant increase from basal state, measured at 9:15 in the morning, from (104 ± 4.3 mg / dl) up to 181.2 ± 5.2 mg / dl ($p < 0.001$) three hours post STZ injection.

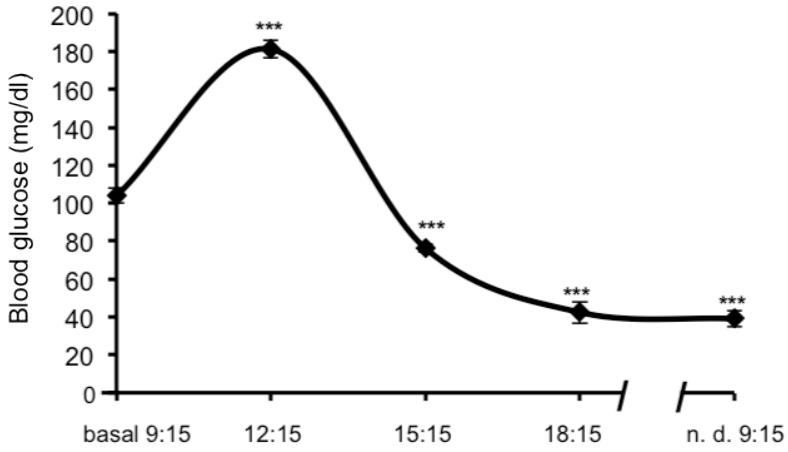

Figure 29 Post-injectional blood glucose measurements in STZ-treated mice

After basal blood glucose determination at 9:15, repeated measurements followed 3 h, 6 h, 9 h and 24hours post injection of STZ (n = 5). Data are presented as mean ± SEM (*** $p < 0.001$).

Measurements at 15:15 revealed a significant decline in blood glucose to 76.2 ± 2 mg / dl ($p < 0.001$), 42.4 ± 5.7 mg / dl ($p < 0.001$) at 18:15 and further declined on the next day at 9:15 to 39.0 ± 4.1 mg / dl ($p < 0.001$, Fig. 29).

3.6.4 Changes in tissue and organ weights in response to STZ-induced diabetes

All tissues and organs were immediately dissected from the sacrificed mice at the last day of the experiment. As shown in Table 14 organ weights of pancreas, liver and kidney did not change 5 days post injection in the STZ-induced T1D mice compared to the control mice. However, muscle displayed significantly reduced organ weights in STZ-treated mice (C: 0.151 ± 0.016 g, STZ: 0.126 ± 0.004 g). Epididymal fat tissue declined from 0.29 ± 0.02 g (control animals) to 0.06 ± 0.01 g ($p < 0.001$) in diabetic mice (Tab. 14).

Table 14 Tissue and organ weights of control and diabetic mice

Data are presented in gram (g) and presented as mean ± SEM (** $p < 0.01$; *** $p < 0.001$).

Tissue/ Organ weights	Control	Diabetic
Pancreas	0.26 ± 0.02	0.21 ± 0.02
Liver	0.30 ± 0.02	0.26 ± 0.02
Kidney	0.16 ± 0.05	0.16 ± 0.01
Thigh muscle	0.15 ± 0.02	0.13 ± 0.00**
Epididymal fat	0.29 ± 0.02	0.06 ± 0.01***

The length of the small intestine, caecum and colon of the control group (n = 5) and the STZ-treated group (n = 5) was also determined (data not shown). The length of the small intestine in the control group (33.4 ± 0.68 cm) did not differ when compared to the diabetic group (34.8 ± 0.86 cm) and no changes in caecum between the two groups (C: 2.9 ± 0.19, STZ: 2.8 ± 0.2 cm) nor in colon length (5.5 ± 0.27 versus 6.3 ± 0.37 cm) was found.

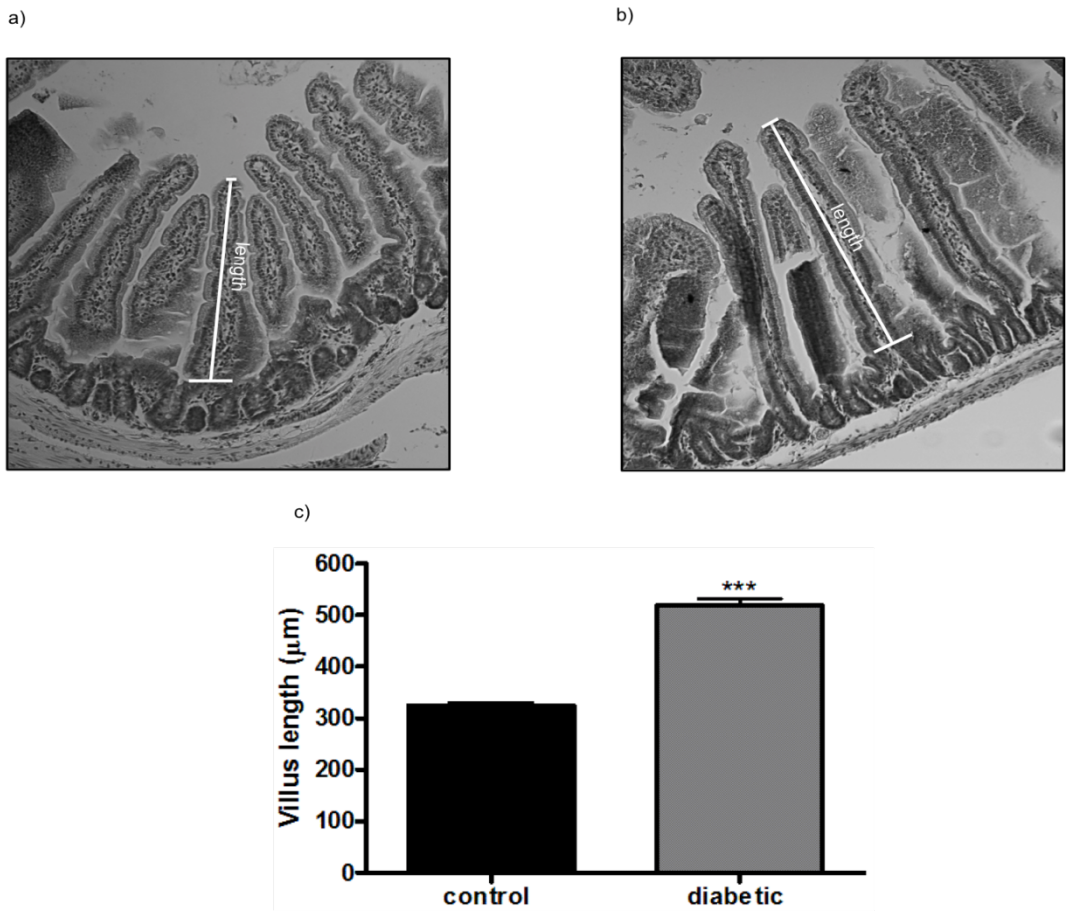

Figure 30 Determination of mean intestinal villus length in control and diabetic mice

Determination of mean villus length in control (a, n = 3, N = 17 per mouse) and STZ-treated mice (b, n = 3, N = 17 per mouse) based on light microscopy (10 x magnification) measurements. Data are presented as mean ± SEM (*** $p < 0.001$).

Mean villus length in diabetic animals increased significantly from 324 ± 7.1 µm (controls) to 519 ± 12.7 µm as shown in Figure 30 c. Mean villus diameter did not change (data not shown).

3.6.5 Effects of STZ on pancreatic tissues

Histological sections of pancreatic tissue of the control and diabetic mice were obtained (Fig. 31) and visualized by hematoxylin and eosin (H & E) staining to identify the abnormalities in the Langerhans islets as induced by STZ.

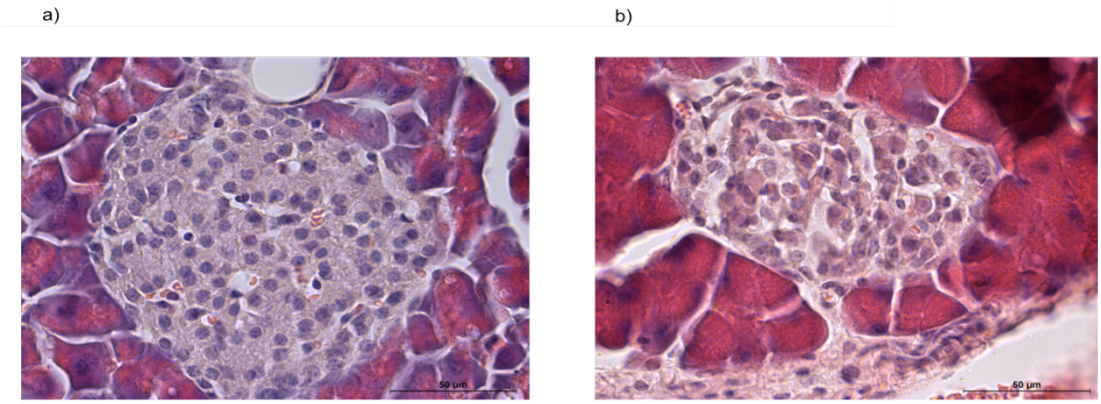

Figure 31 Morphology of Langerhans-islet cells of pancreatic tissue of control and diabetic mice

Langerhans-islet cells in (a) control mice and (b) after diabetic mice (H & E staining, 10 x field).

Morphological changes in Langerhans-islets with cellular atrophy, accompanied by beginning vacuolization and infiltration of lymphocytes were detected in the STZ-treated animals (Fig. 31).

3.6.6 mRNA and protein concentrations of PEPT1 and SGLT1

Freshly scraped intestinal mucosa from both, the control group and the STZ-treated group were used for RNA isolation. Light Cycler measurements were performed to determine PEPT1 and SGLT1 mRNA levels (Fig. 32).

PEPT1 mRNA levels were significantly higher in tissues of STZ-treated mice (Fig. 32 a) with a mean increase of around 52 % ($p < 0.05$) in case of PEPT1 and 53 % ($p < 0.05$) in the case of SGLT1 (Fig. 32 b).

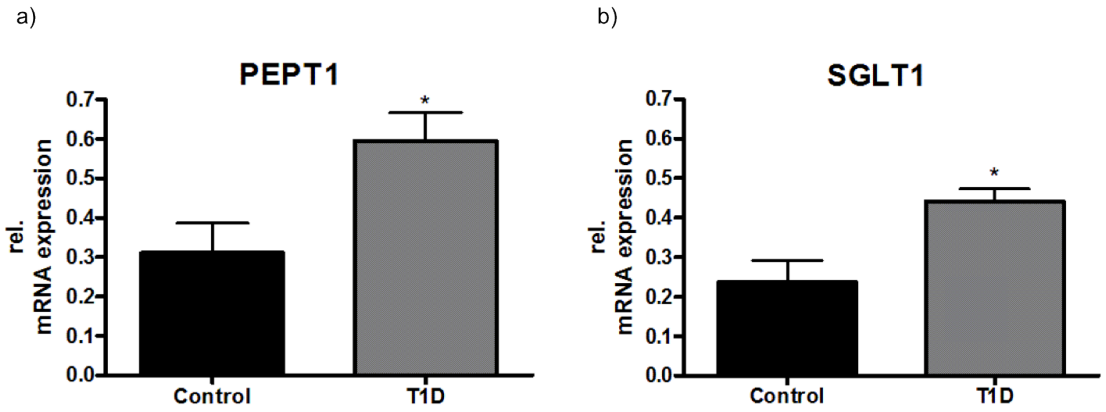

Figure 32 Relative mRNA levels of PEPT1 and SGLT1 in intestine of control and diabetic mice

PEPT1 and (b) SGLT1 mRNA measured in small intestinal samples (a) of control (black bar) and diabetic mice (grey bar, each group n = 5). Villin and GAPDH were used as housekeeping genes and used as references for normalization. Data are presented as mean ± SEM (* p < 0.05).

PEPT1 and SGLT1 protein levels were determined (Fig. 33) in fresh mucosal scrapings from the control group and the STZ-treated group by western blot analysis with 20 µg of protein applied for each sample. Villin was used as reference protein.

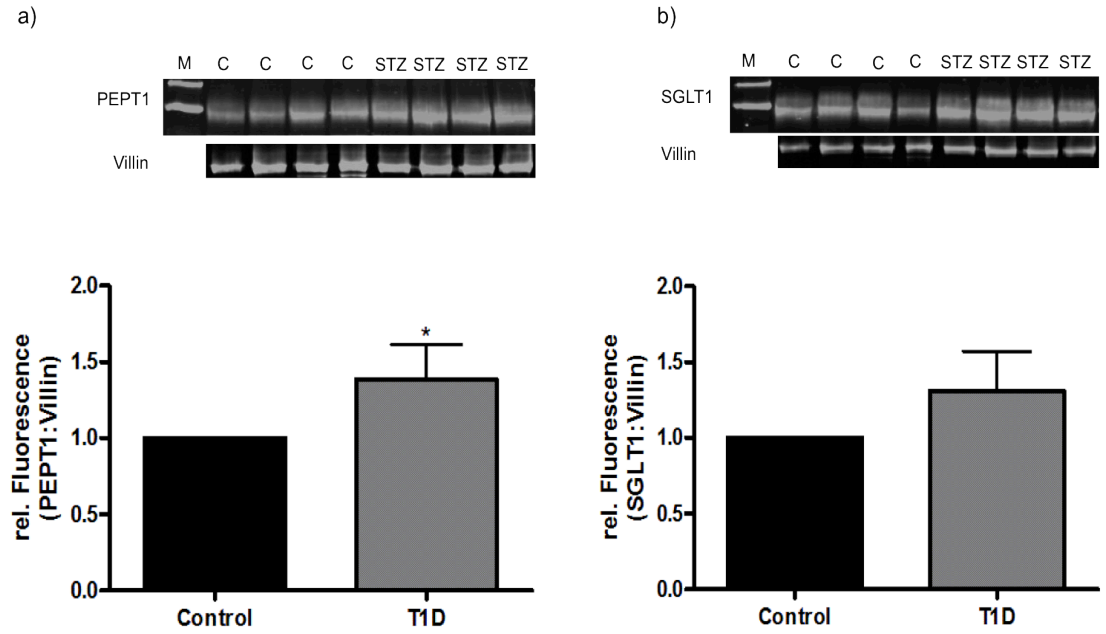

Figure 33 PEPT1 and SGLT1 protein levels in intestinal tissues

Western blots analysis was performed using (a) mPEPT1 antibody in control mice (black bar, n=4) and diabetic mice (grey bar, n = 4), with a related ~ 90 - kDa protein band and (b) with an mSGLT1 antibody in control (black bar, n = 4) and diabetic mice (grey bar, n = 4). Villin (~ 43 kDa, green) was used as reference protein for analysis. Statistics was performed by Mann-Whitney-test (mean ± SEM) (* p < 0.05).

Whereas the protein concentration of PEPT1 was significantly increased in the STZ-treated mice ($p < 0.05$) when compared to control mice (Fig. 33), SGLT1 protein changes failed to reach significance in the diabetic mice.

3.6.7 Uptake experiments in everted gut rings of control and diabetic mice

Everted gut rings and radiolabeled substrates were used, to determine PEPT1 and SGLT1 transporter activity in control and diabetic mice.

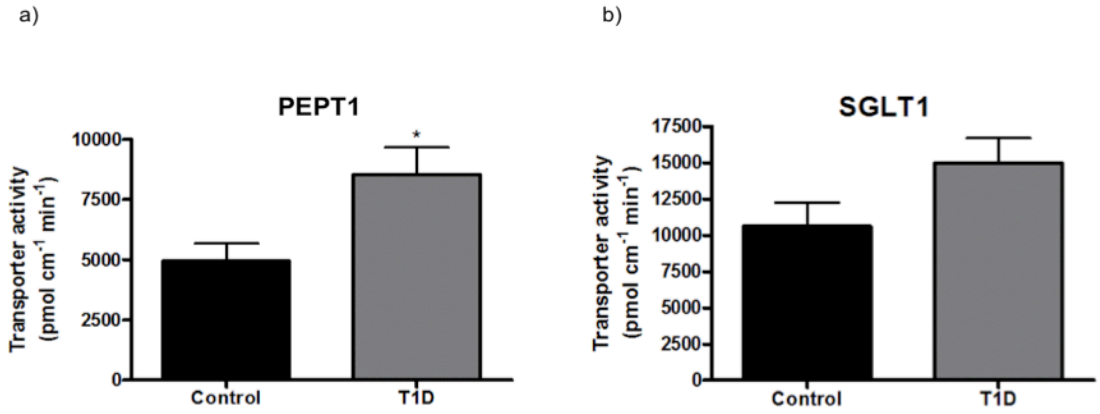

Figure 34 Transporter activities of PEPT1 and SGLT1 in control and diabetic mice

PEPT1 (a) and SGLT1 (b) activity was determined by specific uptake of radiolabeled substrates in control (black bar, n = 5) and diabetic mice (grey bar, n = 5). Data are presented as mean ± SEM.

As shown in Figure 34 (a), PEPT1 activity in control mice was 5290 ± 602 pmol cm^{-1} min^{-1} and increased significantly in the diabetic mice to 8166 ± 1435 pmol cm^{-1} min^{-1} but failed to reach significance. SGLT1 activity (Fig. 34 b) similarly increased in diabetic mice from 10620 ± 1630 pmol cm^{-1} min^{-1} (controls) to 14950 ± 1731 pmol cm^{-1} min^{-1} but also not significantly.

3.6.8 Ussing chamber based Isc measurements in control and diabetic mice

Jejunal tissue segments of non-fasted mice were used for resistance and Isc measurements that included PEPT1, SGLT1, B^0AT1 and SIT1. Recorded tissue resistance of the selected segments of control and diabetic mice revealed a significant increase in resistance in the diabetic state, as shown in Fig. 35

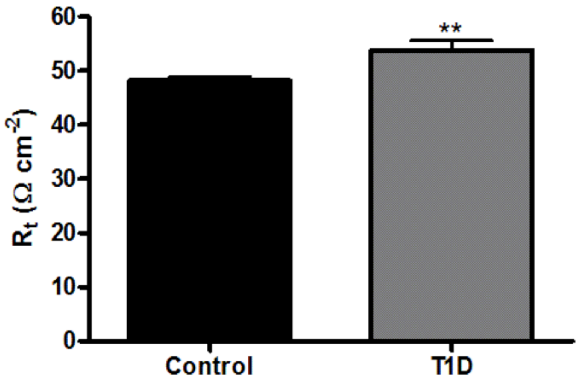

Figure 35 Tissue resistance measured in control and T1-diabetic mice

During Isc measurements the transepithelial conductance was measured and converted in tissue resistance by the use of Ohms` law.

Substrate-induced Isc levels in control mice were comparable to those reported in Tab. 12 and 15. Diabetic mice showed a significant decrease in electrogenic transport capacity for all transporters when compared to control mice. PEPT1 mediated transport for example was significant reduced from 29.4 ± 2.3 µA cm^{-2} in controls to 16.0 ± 2.2 µA cm^{-2} ($p < 0.01$).

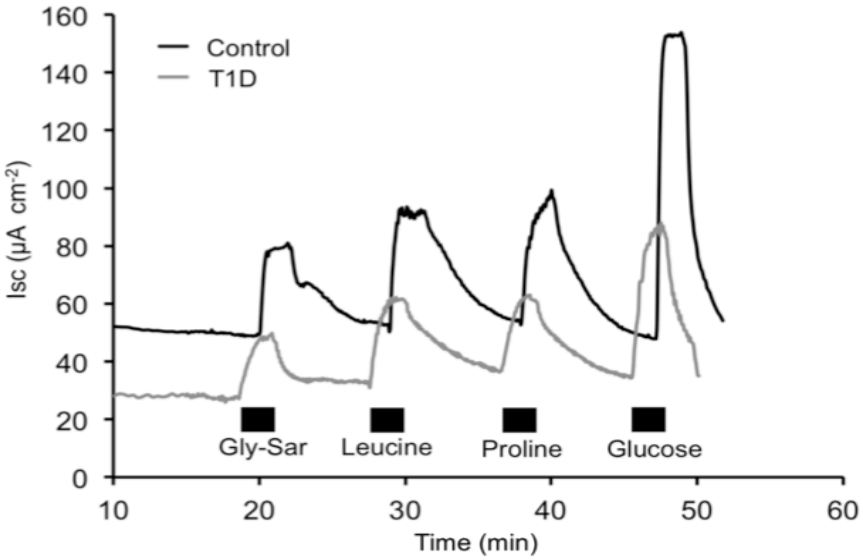

Figure 36 Representative current traces of Ussing chamber measurements in control and diabetic mice

Substrate induced short-circuit currents of PEPT1 with Gly-Sar, of B^0AT1 with L-leucine, of SIT1 with L-proline and of SGLT1 with D-glucose as substrates (black bars) were recorded in control (black line) and diabetic mice (grey line).

The B^0AT1 mediated transport of leucine was decreased from 46.4 ± 5.8 µA cm^{-2} to 29.6 ± 10.1 µA cm^{-2} but this reduction failed to be significant.

Table 15 Substrate-induced Isc (µA cm^{-2}) currents measured in control and diabetic mice

Data are presented as mean ± SEM (* $p < 0.05$; ** $p < 0.01$).

Treatment	PEPT1	B^0AT1	SIT1	SGLT1
Control	29.4 ± 2.3	46.4 ± 5.8	40.2 ± 4.8	87.0 ± 10.0
STZ	16.0 ± 2.2**	29.6 ± 10.1	16.4 ± 2.4*	43.6 ± 6.0**

SIT1 activity declined from 40.2 ± 4.8 µA cm^{-2} in control animals to 16.4 ± 2.4 µA cm^{-2} ($p < 0.05$) and for SGLT1 control currents accounting to 87.0 ± 10.0 µA cm^{-2} were reduced to 43.6 ± 6.0 µA cm^{-2} ($p < 0.01$) in STZ-treated mouse tissues.

4. Discussion

Until the 1970's it was believed that only monomers as the products of protein degradation were absorbed in the small intestine. However, as the main products of protein hydrolysis in the intestine, di-/ and tripeptides (80 %) were identified and it was shown that their concentration exceeds the levels of free amino acids (AA) around 3 to 4 times [149]. This observation stimulated studies aiming to assess whether short chain peptides can be absorbed in intact form. A novel proton-dependent transport system was finally identified and designated as PEPT1 [83, 84]. Transport of di-/tri-peptides derived from dietary intake in the small intestine is accordingly believed to be mediated by this proton-coupled peptide transporter in the apical membrane of the enterocytes. Whether transport of amino acids in peptide-bound form is quantitatively more important than transport of the free amino acids is still not known and the mouse model lacking PEPT1 was hoped to be able to define this question.

The *pept1*$^{-/-}$ mouse

Studies in the nematode *C. elegans* lacking the corresponding peptide transporter gene revealed a severe phenotype with an amino acid deficiency, retarded growth and development and reduced reproduction capacity [150]. Supplementation with free amino acids in the *pept1*$^{-/-}$ worm restored the number of progeny but had no effect on the postembryonic development or on body size. Yet, these experiments revealed for the first time that PEPT1 is needed and important for proper growth, development and reproduction. Different from the results obtained in *C. elegans*, the mouse lacking PEPT1 [151] showed no obvious phenotypic changes in development, body weight or fertility [152].

The aim of the present study was determine whether evidence can be found that in animals lacking the peptide transporter changes in expression and function of other intestinal nutrient (amino acid, sugar) transporters are compensating for the lack of a phenotype. For these experiments we focused on electrogenic transporters that can easily be determined in the transport capacity by currents generated in the transport cycle in Ussing chambers. In addition, tracer uptake studies were employed to determine for example differences in expression sites in the small intestine.

The present findings with Gly-Sar as a substrate confirmed that the deletion of PEPT1 leaves a residual transport of around 5 % , very similar to data reported by Hu *et al*. [151]

and Ma *et al.* [111]. An explanation for this residual activity may be some endocytosis [111, 153] or another (unknown) transporter capable of accepting Gly-Sar as a substrate.

For possible compensating mechanisms that could provide amino acids when PEPT1 is missing we selected amino acid transporters such as PAT1 and SIT1 and the glucose transporter SGLT1 for comparison. Our Ussing chamber studies did not reveal any indication for an adaptation in any of these transporters to the loss of PEPT1. Although we only studied a few transporters Hu *et al*., could also not find other amino acid transporters that showed changes in mRNA levels when PEPT1 was deleted [151] similar to our studies by Nässl *et al.* [152] that did not reveal changes in mRNA levels of any amino acid transporter in the gut nor changes in plasma amino acid levels. Interestingly, the heterozygous mice *pept1*$^{+/-}$ displayed in the present studies a decreased substrate-induced Isc's of PAT1, SIT1 and SGLT1 when compared to the *pept1*$^{-/-}$ mice but not when compared to wild type mice there was no difference and therefore these data were not considered as relevant to follow up. Taken together, the present findings argue against a compensation of the lack of PEPT1 in mice that could explain that animals show no impairments. A prominent role of PEPT1 in amino acid nutrition at least under normal dietary conditions is thus not assumed.

Since AA and glucose are the most important macronutrients absorbed in the intestine, PEPT1 and SGLT1 have been subjects of intensive studies. While PEPT1 is a low affinity high capacity transporter [92], SGLT1 shows the transport characteristics of a high affinity transporter [43]. Substrate affinities of the transporters and concentration dependent kinetics have been determined in numerous studies but mainly by using cell lines, especially Caco-2, and membrane vesicles of various species [45, 46, 48, 50, 105, 106, 108-110]. Kinetic constants as derived here in intact tissues via Ussing chamber studies are sparse and thus it is hard to compare our findings with those in literature.

We observed no major changes in K_m or V_{max} respectively maximal Isc (I_{max}) between mice lacking either PEPT1 or SGLT1T. The loss of PEPT1 increased the affinity of SGLT1 for its substrate modestly but did not change its maximal transporter capacity. What becomes obvious is that the apparent K_m values observed in our Ussing chamber studies are markedly higher that those determined in membrane vesicles or with the respective cloned transporters in heterologous expression systems. The apparent affinities determined in Ussing chambers are around 10-fold lower than those found in cell systems. The most plausible explanation for this deviation is the existence of an unstirred layer (UL) in intact tissues [154]. Unstirred layer effects on the absorptive capacity of enterocytes have been

investigated and discussed controversially. The glycocalyx of the villi entrap water and mucin adjacent to the BBM and therefore form a stagnant layer. The UL also has a lower pH than the bulk luminal fluid and this results in a hydrodynamic barrier [155]. However, the UL is not equally distributed across the epithelial cells, forming different diffusion limits and is described as vulnerable to stirring conditions [156]. This means in essence that a comparison of kinetic constants across models even for the same transporter protein is almost impossible as the experimental conditions overrule the affinity as defined by the protein structure.

Do high fat diets and obesity alter PEPT1 and SGLT1 transport?

A Western diet is characterized by intake of energy-dense food and usually contained a high-fat level. Paired with insufficient physical activity these key lifestyle parameters determine obesity and associated diseases such as type 2 diabetes and cardiovascular diseases. Indicators for the underlying metabolic impairments are hyperinsulinemia, hyperlipidemia, intra-abdominal obesity and hypertension.

Besides genetic models such as the *ob* / *ob* and *db* / *db* mice, the C57BL/6J (B6) mouse with feeding of a high fat (and high sugar) diet (HFD) represents the most frequently used model (diet-induced obesity, DIO) as it also reveals most alterations in human obesity syndromes [157]. In the present study we used this model with mice fed a diet providing 60 % of energy from fat. Such high fat diets change the morphology of the small intestine. We also found that the mean villus length in the proximal small intestine was significant increased in the HFD mice [158]. This finding confirmed data by Goda and Takase (1994) describing that a HFD (73 % energy from fat) in rats led in the jejunum to increased height of villi. Additionally, microvilli structure showed a reduced length and an increased diameter, leading to a reduced absorptive surface area of microvilli per enterocyte. They also reported a reduced total protein level in the BBM associated with decreased disaccharidase activities [159].

Our Ussing chamber measurements in DIO mice revealed a decrease in the Isc response of PEPT1, SIT1 and SGLT1, which may be caused by the changes in gut architecture. In a study by Hindlet *et al*., HFD (38 % energy from fat) in mice caused DIO and hyperleptinemia and the mRNA of PEPT1 was found to be reduced by 50 %, protein levels by 30 % and dipeptide transport in jejunal loops also was reduced [131]. In contrast to our Ussing chamber data, uptake studies employing the radiotracers failed to confirm a reduced PEPT1

activity in DIO mice but displayed a reduced SGLT1 activity. One reason for this discrepancy in the different outcomes of the Ussing chamber and uptake experiments might be the fact that we only used jejunal segments for the electrophysiological measurements, while mixed segments of the small intestine including duodenum, jejunum and ileum were used for the uptake experiments. Although changes in gut morphology in obese mice may cause these effects on the transporters, there is also evidence that leptin may be a key regulator in these obesity-associated changes. Leptin as the *ob* gene product is a multifunctional hormone produced and secreted by various tissues (placenta, brain, bone marrow) with many peripheral acting sides. Besides regulation of body weight and adiposity, leptin was shown to affect sugar and amino acid transport by either apical or basolateral receptor binding and signal transduction cascades [129, 133]. Fanjul *et al.* (2012) demonstrated a down-regulation of SGLT1 and B^0AT1 transporter activities in Caco-2 cells as a result of short-term apical administration of leptin and detected reduced transporter protein levels in BBM [133]. It has been suggested that luminal leptin produced by the gastric mucosa directly modulates SGLT1 in small intestinal BBM. In contrary, systemic leptin was found to lead to a less pronounced decrease in SGLT1 activity that in part is mediated by CCK [132]. Although we cannot assess whether leptin regulation is contributing to the effects observed, those need to be seen in light of the changes in intestinal morphology.

Is there a role of insulin in transporter regulation?

Insulin is a key regulator of metabolism that also exhibits important physiological actions on growth of the intestine and cell proliferation [120-122]. Whether insulin directly via its receptors also regulates intestinal transporter activity is a subject of controversy. Insulin receptors (IR's) were shown to be expressed on the vascular side of the intestinal epithelium of dogs [123] and rats [125]. Human Caco-2 were shown to possess IR's in the apical membranes [126, 127] and studies by Thamotharan *et al*. (1999) in these cells suggested insulin to act on PEPT1. Gly-Gln transport was determined in Caco-2 cells treated with 5 nM insulin over 90 min and was shown to increase dipeptide transport [106]. The increase was already detected after 30 min and was blocked by the addition of genistein, a tyrosine kinase inhibitor suggesting but not proving that the effects were mediated by the insulin receptor. Additional experiments in Caco-2 cells demonstrated also an elevation in cephalexin uptake by PEPT1 after insulin treatment [146]. Caco-2 as cancer cells suffer from the limitation that they are transformed and have a high expression level of IR's and

therefore are highly responsive to insulin which may not reflect the normal phenotype of enterocytes [126]. We therefore employed intestinal tissues for assessing putative insulin effects in *in vitro* and *in vivo* experiments.

In the *in vitro* studies, activities of the electrogenic transporters were measured in Ussing chambers while insulin was added to the basolateral site of the tissue. However, no changes in activity of the selected transporter systems were observed with the *in vitro* administration of insulin. It needs to be emphasized that in these experiments the tissue is disconnected from blood supply and from the hepatoenteral nerves which were postulated to be involved for example in the portal insulin stimulation of glucose absorption in the small intestine of rats [160]. To investigate insulin effects under more physiological conditions, we administered insulin in non-diabetic mice and determined transporter responses in isolated tissues. Although blood glucose was reduced after insulin injection (0.1U/kg body weight), similar to previous studies [161], insulin failed to significantly affect PEPT1 and SGLT1 mRNA and protein levels but resulted in a significantly decreased PEPT1 activity in uptake experiments while SGLT1 remained unaffected whereas Ussing chamber studies revealed no effect on transport currents.

Der-Boghossian *et al*. found when using a ten times higher insulin dose than used by us that mRNA levels of PEPT1 were significantly reduced whereas protein levels and transport activity of PEPT1 remained unchanged [154]. Pennington *et al*. described an increase in intestinal glucose uptake after insulin administration (1U / kg bodyweight) via SGLT1 [51] and Serhan *et al*. (2010) demonstrated *in situ* an increased SGLT1 activity following insulin treatment associated with alterations in Na^+ / K^+ ATPase in rat jejunum [162]. However, in our acute experiments with insulin lasting for only 30min, we did not find any evidence for a short-term regulation at any level of either PEPT1 or SGLT1 in intestine.

Is high luminal glucose modulating intestinal transport processes?

After a meal, intestinal luminal glucose increases to high levels. Despite the fact that SGLT1 is recognized as the most important glucose transporter in intestine, it was postulated that a second system that it phlorizin-insensitive (in contrast to SGLT1) contributes to overall glucose absorption when luminal concentrations exceed the capacity of SGLT1. Mace *et al.* proposed in 2009 based on their *in vivo* and *in vitro* studies in rats, that at luminal glucose concentrations of > 75 mM GLUT2 proteins are recruited into the apical membrane of enterocytes [79] to allow as an uniporter high glucose influx. They also demonstrated that

simultaneously to the insertion of GLUT2 into apical membranes PEPT1 was retrieved from the apical membrane at high luminal glucose. Mace *et al.* described the decrease of PEPT1 density as dependent on the PKC isoform βII, which in turn for activation depends on an increase in intracellular Ca^{2+}. The Ca^{2+} increase was accomplished by opening of apical voltage dependent calcium channels ($Ca_v1.3$) initiated by the membrane depolarizing action of SGLT1. Morgan *et al.* (2007) reported an influx of Ca^{2+} by membrane depolarization through SGLT1 activity as the initial intracellular signal for the PKC βII-dependent GLUT2 recruitment [78] and this was shown to depend on cytoskeleton rearrangements, like contractions of myosin II in the terminal web [77]. These studies collectively pointed to a prime role of cytosolic Ca^{2+} changes in a reciprocal regulation of PEPT1 and GLUT2.

That PEPT1 activity in epithelial cells is altered via changes in intracellular Calcium has been observed in other studies and models. Brandsch *et al*. already in 1994 showed PEPT1 expression and activity to be significantly decreased by the treatment of Caco-2 cells with different phorbol esters (PMA, Pbu) that activate PKC. Additionally they showed that the presence of staurosporine, a PKC inhibitor, increased PEPT1 mediated Gly-Sar uptake [163]. Besides PKC, changes in intracellular calcium (Ca^{2+}) regulating PEPT1 activity, was shown by Wenzel *et al.* (2002), in Caco-2 cells. The application of nifedipine, a Ca^{2+} channel blocker increased PEPT1-mediated transport, whereas ionomycin, a ionophore that increases intracellular Ca^{2+} concentration, induced a significant decrease in PEPT1 mediated uptake in Caco-2 cells [109].

We also observed that PEPT1 activity was decreased when the protein kinase C (PKC) activator Pbu (1 µM) was added for 30 min to the serosal side of the tissues in Ussing chambers (data not shown) suggesting that PKC activity may also regulate PEPT1 in mouse intestine. Similarly, ionomycin (data not shown) effects were observed in uptake studies with the radiotracers in everted gut rings.

When tissues in Ussing chambers were perfused with a high (75 mM) luminal glucose concentration under short-circuit and open voltage conditions a significantly reduced PEPT1 activity was observed while SIT1 and SGLT1 remained unaffected. In this respect we observed an effect according to the model by Mace *et al*. in which GLUT2 moves into the apical membrane while PEPT1 is retrieved [79]. If this would be the case also in mice, we should have observed a similar effect also in the radiotracer flux in the everted tissue showing a decline of Gly-Sar influx and an increase in glucose uptake attributed to GLUT2 but we could not find such effects. We therefore also conducted *in vivo* studies in which mice were submitted to an OGTT followed by uptake experiments in gut rings using a

GLUT2-specific substrate. However, all these studies failed to detect any GLUT2 activity in apical membranes. A possible explanation for the lack of an effect could be that the retention time of GLUT2 in the apical membrane was described as very short by a fast internalization ($t_{1/2}$ ~ 3.5 min) [164]. Thus, the time necessary for tissue preparation in our studies may have been too long to be able to observe GLUT2 activity and PEPT1 decrease. Even after changes in the experimental protocol (oral communication by Prof. Georg Kellet) by exposing the tissues to 75 mM glucose until incubation did not lead to any GLUT2 activity or an expected reciprocal decrease in PEPT1 activity. The observation by Stümpel *et al.* (2001) that the absorbed amount of glucose after an OGTT remained the same in mice lacking GLUT2 [165] raises the question, whether such a glucose-induced (high luminal glucose concentrations) GLUT2 insertion in the BBM might be species-dependent and only found in rats. The decreased electrogenic PEPT1 activity found in Ussing chambers when perfused with high glucose but not observed in gut rings in tracer studies or after an OGTT remains currently unexplained. Changes in membrane voltage or pH effects can essentially be ruled out as SGLT1 and PAT1 did not show any changes and both are dependent on these driving forces.

Are transporter activities altered in STZ-induced type 1 diabetes?

Type 1 diabetes (T1D) in laboratory animals is usually imposed by Streptozotocin (STZ) treatment via injections of various doses and variable frequencies [57-59, 108, 142-144, 148, 160, 166-172]. STZ is β-cell toxic and its uptake into ß-cells depends on GLUT2. It is a nitrosourea analogue linked to the carbon-2 of a hexose and acts via DNA alkylation in GLUT2 expressing cells in pancreas but also in liver and kidney [173].

We used a single high dose injection as described for BALB/c mice [148] leading to a dramatic increase in blood glucose within 5 days after STZ injection. However, initially, a dramatic drop in blood glucose was detected beginning three hours after STZ injection and lasting for 24 h before the hyperglycemia developed. This decline in blood glucose was most likely caused by a massive release of insulin into circulation as a result of ß-cell necrosis [174]. Our hematoxylin stainings of the Langerhans-islets, 5 days after STZ-injection, revealed atrophy, vacuolization and infiltrations with lymphocytes as described by others [166, 167, 175]. We also observed a glycosuria as a characteristic feature in the early phase of diabetes mellitus and accompanied by osmotic diuresis, glomerular hyperfiltration and polyuria [176]. Diabetic mice also showed a significant reduction in body weight over time with a major loss of pad fats or epididymal fat depots by excessive lipolysis [128] in

addition to a reduction in muscle mass [177]. These changes were associated with changes in plasma metabolites such as in branched-chain amino acids, intermediates of the urea cycle, ketogenic amino acids and gluconeogenic amino acids, such as threonine, proline and histidine (oral communication Pieter Giesbertz). These plasma metabolite changes are similar to those reported for humans and rabbits suffering from type 1 diabetes and in humans with type 2 diabetes [178, 179].

T1D effects on the gastrointestinal tract are described by delayed stomach to caecum transit time and slower propagation of myoelectric activity, as a result of changed glucagon and insulin concentrations and due to an increased intestinal length [142]. We were not able to detect any changes in the length of the small intestine, caecum or colon in the STZ-treated animals. However, villus morphology in jejunum changed and revealed that villus length was significantly increased in diabetic animals. Increased villus length was postulated to be a result of hyperplasia and/or hypertrophy of the intestinal epithelial cells [57, 58] and GLP-2 has been described as to affect primarily villus length [46, 180].

T1D was reported to markedly reduce intestinal transporter expression and impair regulation [59, 148, 170]. In the present study we examined PEPT1 and SGLT1 by profiling mRNA and protein expression levels and determined functional activity. In case of SGLT1 only the mRNA was increased but not protein level or function. In case of PEPT1, we observed an increase in mRNA and protein levels and increased tracer-based influx. This finding is in line with some reported that found PEPT1 mRNA and protein levels to increase while others show increased mRNA levels but a decrease in protein and transport activity [108, 144]. However, these studies are generally very difficult to compare with some groups carry out short-term experiments (analysis 96 h post injection) [108, 143] while other look at long-term effects (experiments up to 1 month post injection) [144] and moreover, all these studies were performed in rats.

Electrical measurements of transport activity of PEPT1, SIT1 and SGLT1 in Ussing chambers revealed for all proteins a significantly reduced activity. Initial transepithelial membrane potentials did not differ between tissues from control and T1D animals but tissue resistance was significant higher in diabetic mice indicating a reduced conductance. Only a few studies have been conducted with Ussing chamber measurements of tissues from STZ-treated animals - mostly from long-term treatment [169, 181, 182]. Perdue and Davidson (1988) found the mucosa of long-term STZ-treated rats to be thicker and the conductance of the tissue to be significantly lower [181]. The increase of thickness could account for an increased resistance as a consequence of the decreased conductance and is mirrored in

the increase in villus length for example that we observed here. The lower conductance however could also originate from a reduced density of ion-conducting proteins like channels or by effects on Na^+ / K^+ ATPase that changes in expression and catalytic activity in T1D [183, 184]. Since all electrogenic transporters – regardless of their function and specificity displayed a reduced Isc response, it is likely that changes in Na^+ / K^+ ATPase in T1D are causative. However, we can also not exclude that STZ that is transported via GLUT2 into cells enters epithelial cells in the intestine from the basolateral side causes cell dysfunctions. Findings on changes in Na^+/K^+-ATPase activity in the intestine of STZ-induced diabetic rodents mainly describe an increase in activity for the enzyme [184-186].

Since we did not determine Na^+ / K^+ ATPase activity nor expression levels in the intestine of STZ-treated mice, it remains speculative to propose that such changes may cause all electrogenic transporters to decrease in activity in type 1 diabetes.

Taken together, all studies described here that utilized primarily Ussing chambers to assess changes in electrogenic transporter expression in animals lacking PEPT1 or in animals treated with insulin or high fat diets did not reveal major alterations. Only in diabetic mice major reductions in transporter currents were observed and it is speculated that those arise by impairments in the driving forces and linked to Na^+ / K^+ ATPase.

References

1. Westheide, W.u.R., R., *Spezielle Zoologie Teil 1: Einzeller und Wirbellose Tiere*, ed. W.u.R. Westheide, R. Vol. 1. 2004, München: Spektrum Akademischer Verlag.
2. Müller, W.F., S., *Die Grundversorgung: Gehalt und Aufbereitung der Nahrung*, in *Tier- und Humanphysiologie*, W.u.F.S. Müller, Editor. 2007, Springer Verlag: Heidelberg. p. 1-657.
3. Hildebrand, M. and G.J. Gloslow, *Vergleichende und funktionelle Anantomie der Wirbeltiere*. 5 ed. 2004, Berlin, Heidelberg: Springer Berlin Heidelberg.
4. Levin, R.J., *Digestion and absorption of carbohydrates--from molecules and membranes to humans.* Am J Clin Nutr, 1994. **59**(3 Suppl): p. 690S-698S.
5. Eckert, R., Burggren, W., French, K., Randall, D., *Membranen: Barrieren und selektiver Transport*, in *Tierphysiologie*. 2002, Thieme Verlag, Stuttgart.
6. Clauss, W.C., C., *Tierphysiologie kompakt*. 1 ed. 2007, München: Spektrum Akademischer Verlag.
7. Lynch, A.M. and J.D. McGivan, *Evidence for a single common Na+-dependent transport system for alanine, glutamine, leucine and phenylalanine in brush-border membrane vesicles from bovine kidney.* Biochim Biophys Acta, 1987. **899**(2): p. 176-84.
8. Kleta, R., et al., *Mutations in SLC6A19, encoding B0AT1, cause Hartnup disorder.* Nat Genet, 2004. **36**(9): p. 999-1002.
9. Seow, H.F., et al., *Hartnup disorder is caused by mutations in the gene encoding the neutral amino acid transporter SLC6A19.* Nat Genet, 2004. **36**(9): p. 1003-7.
10. Kristensen, A.S., et al., *SLC6 neurotransmitter transporters: structure, function, and regulation.* Pharmacol Rev. **63**(3): p. 585-640.
11. Curran, P.F., et al., *Kinetic relations of the Na-amino acid interaction at the mucosal border of intestine.* J Gen Physiol, 1967. **50**(5): p. 1261-86.
12. Bohmer, C., et al., *Characterization of mouse amino acid transporter B0AT1 (slc6a19).* Biochem J, 2005. **389**(Pt 3): p. 745-51.
13. Broer, S., *The role of the neutral amino acid transporter B0AT1 (SLC6A19) in Hartnup disorder and protein nutrition.* IUBMB Life, 2009. **61**(6): p. 591-9.
14. Sepulveda, F.V. and M.W. Smith, *Discrimination between different entry mechanisms for neutral amino acids in rabbit ileal mucosa.* J Physiol, 1978. **282**: p. 73-90.
15. Wu, G., *Intestinal mucosal amino acid catabolism.* J Nutr, 1998. **128**(8): p. 1249-52.
16. Takanaga, H., et al., *Identification of mammalian proline transporter SIT1 (SLC6A20) with characteristics of classical system imino.* J Biol Chem, 2005. **280**(10): p. 8974-84.

17. Stevens, B.R. and E.M. Wright, *Kinetics of the intestinal brush border proline (Imino) carrier.* J Biol Chem, 1987. **262**(14): p. 6546-51.

18. Broer, A., et al., *Sodium translocation by the iminoglycinuria associated imino transporter (SLC6A20).* Mol Membr Biol, 2009. **26**(5): p. 333-46.

19. Kowalczuk, S., et al., *Molecular cloning of the mouse IMINO system: an Na+- and Cl- -dependent proline transporter.* Biochem J, 2005. **386**(Pt 3): p. 417-22.

20. Munck, B.G., *Transport of imino acids and non-alpha-amino acids across the brush-border membrane of the rabbit ileum.* J Membr Biol, 1985. **83**(1-2): p. 15-24.

21. Boll, M., H. Daniel, and B. Gasnier, *The SLC36 family: proton-coupled transporters for the absorption of selected amino acids from extracellular and intracellular proteolysis.* Pflugers Arch, 2004. **447**(5): p. 776-9.

22. Thwaites, D.T. and C.M. Anderson, *The SLC36 family of proton-coupled amino acid transporters and their potential role in drug transport.* Br J Pharmacol, 2011. **164**(7): p. 1802-16.

23. Frommer, W.B., S. Hummel, and J.W. Riesmeier, *Expression cloning in yeast of a cDNA encoding a broad specificity amino acid permease from Arabidopsis thaliana.* Proc Natl Acad Sci U S A, 1993. **90**(13): p. 5944-8.

24. Russnak, R., D. Konczal, and S.L. McIntire, *A family of yeast proteins mediating bidirectional vacuolar amino acid transport.* J Biol Chem, 2001. **276**(26): p. 23849-57.

25. Sagne, C., et al., *Identification and characterization of a lysosomal transporter for small neutral amino acids.* Proc Natl Acad Sci U S A, 2001. **98**(13): p. 7206-11.

26. Boll, M., et al., *Functional characterization of two novel mammalian electrogenic proton-dependent amino acid cotransporters.* J Biol Chem, 2002. **277**(25): p. 22966-73.

27. Anderson, C.M., et al., *H+/amino acid transporter 1 (PAT1) is the imino acid carrier: An intestinal nutrient/drug transporter in human and rat.* Gastroenterology, 2004. **127**(5): p. 1410-22.

28. Chen, Z., et al., *Structure, function and immunolocalization of a proton-coupled amino acid transporter (hPAT1) in the human intestinal cell line Caco-2.* J Physiol, 2003. **546**(Pt 2): p. 349-61.

29. Foltz, M., et al., *A novel bifunctionality: PAT1 and PAT2 mediate electrogenic proton/amino acid and electroneutral proton/fatty acid symport.* FASEB J, 2004. **18**(14): p. 1758-60.

30. Thwaites, D.T., et al., *Gamma-Aminobutyric acid (GABA) transport across human intestinal epithelial (Caco-2) cell monolayers.* Br J Pharmacol, 2000. **129**(3): p. 457-64.

31. Anderson, C.M., et al., *Taurine uptake across the human intestinal brush-border membrane is via two transporters: H+-coupled PAT1 (SLC36A1) and Na+- and Cl(-)-dependent TauT (SLC6A6).* J Physiol, 2009. **587**(Pt 4): p. 731-44.

32. Wright, E.M. and E. Turk, *The sodium/glucose cotransport family SLC5.* Pflugers Arch, 2004. **447**(5): p. 510-8.

33. Hediger, M.A., et al., *The ABCs of solute carriers: physiological, pathological and therapeutic implications of human membrane transport proteinsIntroduction.* Pflugers Arch, 2004. **447**(5): p. 465-8.

34. Hirayama, B.A., et al., *Kinetic and specificity differences between rat, human, and rabbit Na+-glucose cotransporters (SGLT-1).* Am J Physiol, 1996. **270**(6 Pt 1): p. G919-26.

35. Wright, E.M., et al., *Regulation of Na+/glucose cotransporters.* J Exp Biol, 1997. **200**(Pt 2): p. 287-93.

36. Hirsch, J.R., D.D. Loo, and E.M. Wright, *Regulation of Na+/glucose cotransporter expression by protein kinases in Xenopus laevis oocytes.* J Biol Chem, 1996. **271**(25): p. 14740-6.

37. Tyagi, N.K., et al., *A biophysical glance at the outer surface of the membrane transporter SGLT1.* Biochim Biophys Acta, 2011. **1808**(1): p. 1-18.

38. Crane, R.K., *Intestinal absorption of glucose.* Biomembranes, 1974. **4A**(0): p. 541-53.

39. Thorens, B., et al., *Cloning and functional expression in bacteria of a novel glucose transporter present in liver, intestine, kidney, and beta-pancreatic islet cells.* Cell, 1988. **55**(2): p. 281-90.

40. Thorens, B., *Molecular and cellular physiology of GLUT-2, a high-Km facilitated diffusion glucose transporter.* Int Rev Cytol, 1992. **137**: p. 209-38.

41. Fukumoto, H., et al., *Sequence, tissue distribution, and chromosomal localization of mRNA encoding a human glucose transporter-like protein.* Proc Natl Acad Sci U S A, 1988. **85**(15): p. 5434-8.

42. Hediger, M.A., et al., *Expression cloning and cDNA sequencing of the Na+/glucose co-transporter.* Nature, 1987. **330**(6146): p. 379-81.

43. Takata, K., *Glucose transporters in the transepithelial transport of glucose.* J Electron Microsc (Tokyo), 1996. **45**(4): p. 275-84.

44. Debnam, E.S. and R.J. Levin, *An experimental method of identifying and quantifying the active transfer electrogenic component from the diffusive component during sugar absorption measured in vivo.* J Physiol, 1975. **246**(1): p. 181-96.

45. Brot-Laroche, E., et al., *Temperature sensitivity and substrate specificity of two distinct Na+-activated D-glucose transport systems in guinea pig jejunal brush border membrane vesicles.* J Biol Chem, 1986. **261**(14): p. 6168-76.

46. Cheeseman, C.I., *Upregulation of SGLT-1 transport activity in rat jejunum induced by GLP-2 infusion in vivo.* Am J Physiol, 1997. **273**(6 Pt 2): p. R1965-71.

47. Kellett, G.L. and P.A. Helliwell, *The diffusive component of intestinal glucose absorption is mediated by the glucose-induced recruitment of GLUT2 to the brush-border membrane.* Biochem J, 2000. **350 Pt 1**: p. 155-62.

48. Mate, A., et al., *Regulation of sodium-glucose cotransporter SGLT1 in the intestine of hypertensive rats.* Am J Physiol Regul Integr Comp Physiol, 2006. **291**(3): p. R760-7.

49. Yang, C., et al., *Apical Na+-D-glucose cotransporter 1 (SGLT1) activity and protein abundance are expressed along the jejunal crypt-villus axis in the neonatal pig.* Am J Physiol Gastrointest Liver Physiol, 2011. **300**(1): p. G60-70.

50. Zheng, Y., et al., *Mechanisms of glucose uptake in intestinal cell lines: role of GLUT2.* Surgery, 2012. **151**(1): p. 13-25.

51. Pennington, A.M., C.P. Corpe, and G.L. Kellett, *Rapid regulation of rat jejunal glucose transport by insulin in a luminally and vascularly perfused preparation.* J Physiol, 1994. **478 (Pt 2)**: p. 187-93.

52. Cheeseman, C.I. and R. Tsang, *The effect of GIP and glucagon-like peptides on intestinal basolateral membrane hexose transport.* Am J Physiol, 1996. **271**(3 Pt 1): p. G477-82.

53. Hirsh, A.J. and C.I. Cheeseman, *Cholecystokinin decreases intestinal hexose absorption by a parallel reduction in SGLT1 abundance in the brush-border membrane.* J Biol Chem, 1998. **273**(23): p. 14545-9.

54. Banerjee, A.K., K. Raja, and T.J. Peters, *Effect of insulin induced hypoglycaemia on in vitro uptake of 3-O-methylglucose by rat jejunum.* Gut, 1989. **30**(10): p. 1348-53.

55. Osswald, C., et al., *Mice without the regulator gene Rsc1A1 exhibit increased Na+-D-glucose cotransport in small intestine and develop obesity.* Mol Cell Biol, 2005. **25**(1): p. 78-87.

56. Kellett, G.L., *The facilitated component of intestinal glucose absorption.* J Physiol, 2001. **531**(Pt 3): p. 585-95.

57. Fedorak, R.N., et al., *Altered glucose carrier expression: mechanism of intestinal adaptation during streptozocin-induced diabetes in rats.* Am J Physiol, 1991. **261**(4 Pt 1): p. G585-91.

58. Debnam, E.S., et al., *The effects of streptozotocin diabetes on sodium-glucose transporter (SGLT1) expression and function in rat jejunal and ileal villus-attached enterocytes.* Pflugers Arch, 1995. **430**(2): p. 151-9.

59. Wong, T.P., E.S. Debnam, and P.S. Leung, *Diabetes mellitus and expression of the enterocyte renin-angiotensin system: implications for control of glucose transport across the brush border membrane.* Am J Physiol Cell Physiol, 2009. **297**(3): p. C601-10.

60. Yoshikawa, T., et al., *Comparative expression of hexose transporters (SGLT1, GLUT1, GLUT2 and GLUT5) throughout the mouse gastrointestinal tract.* Histochem Cell Biol, 2011. **135**(2): p. 183-94.

61. Hwang, E.S., B.A. Hirayama, and E.M. Wright, *Distribution of the SGLT1 Na+/glucose cotransporter and mRNA along the crypt-villus axis of rabbit small intestine.* Biochem Biophys Res Commun, 1991. **181**(3): p. 1208-17.

62. Kanai, Y., et al., *The human kidney low affinity Na+/glucose cotransporter SGLT2. Delineation of the major renal reabsorptive mechanism for D-glucose.* J Clin Invest, 1994. **93**(1): p. 397-404.

63. Wright, E.M., *Renal Na(+)-glucose cotransporters.* Am J Physiol Renal Physiol, 2001. **280**(1): p. F10-8.

64. Gribble, F.M., et al., *A novel glucose-sensing mechanism contributing to glucagon-like peptide-1 secretion from the GLUTag cell line.* Diabetes, 2003. **52**(5): p. 1147-54.

65. Parker, H.E., et al., *Nutrient-dependent secretion of glucose-dependent insulinotropic polypeptide from primary murine K cells.* Diabetologia, 2009. **52**(2): p. 289-98.

66. Martin, M.G., et al., *Defects in Na+/glucose cotransporter (SGLT1) trafficking and function cause glucose-galactose malabsorption.* Nat Genet, 1996. **12**(2): p. 216-20.

67. Wright, E.M., et al., *Molecular genetics of intestinal glucose transport.* J Clin Invest, 1991. **88**(5): p. 1435-40.

68. Wu, X. and H.H. Freeze, *GLUT14, a duplicon of GLUT3, is specifically expressed in testis as alternative splice forms.* Genomics, 2002. **80**(6): p. 553-7.

69. Joost, H.G., et al., *Nomenclature of the GLUT/SLC2A family of sugar/polyol transport facilitators.* Am J Physiol Endocrinol Metab, 2002. **282**(4): p. E974-6.

70. Joost, H.G. and B. Thorens, *The extended GLUT-family of sugar/polyol transport facilitators: nomenclature, sequence characteristics, and potential function of its novel members (review).* Mol Membr Biol, 2001. **18**(4): p. 247-56.

71. Orci, L., et al., *Localization of the pancreatic beta cell glucose transporter to specific plasma membrane domains.* Science, 1989. **245**(4915): p. 295-7.

72. Johnson, J.H., et al., *The high Km glucose transporter of islets of Langerhans is functionally similar to the low affinity transporter of liver and has an identical primary sequence.* J Biol Chem, 1990. **265**(12): p. 6548-51.

73. Uldry, M., et al., *GLUT2 is a high affinity glucosamine transporter.* FEBS Lett, 2002. **524**(1-3): p. 199-203.

74. Jorns, A., M. Tiedge, and S. Lenzen, *Nutrient-dependent distribution of insulin and glucokinase immunoreactivities in rat pancreatic beta cells.* Virchows Arch, 1999. **434**(1): p. 75-82.

75. Kellett, G.L. and E. Brot-Laroche, *Apical GLUT2: a major pathway of intestinal sugar absorption.* Diabetes, 2005. **54**(10): p. 3056-62.

76. Zhao, F.Q. and A.F. Keating, *Functional properties and genomics of glucose transporters.* Curr Genomics, 2007. **8**(2): p. 113-28.

77. Mace, O.J., et al., *Calcium absorption by Cav1.3 induces terminal web myosin II phosphorylation and apical GLUT2 insertion in rat intestine.* J Physiol, 2007. **580**(Pt. 2): p. 605-16.

78. Morgan, E.L., et al., *Apical GLUT2 and Cav1.3: regulation of rat intestinal glucose and calcium absorption.* J Physiol, 2007. **580**(Pt. 2): p. 593-604.

79. Mace, O.J., et al., *An energy supply network of nutrient absorption coordinated by calcium and T1R taste receptors in rat small intestine.* J Physiol, 2009. **587**(Pt 1): p. 195-210.

80. Valera, A., et al., *Expression of GLUT-2 antisense RNA in beta cells of transgenic mice leads to diabetes.* J Biol Chem, 1994. **269**(46): p. 28543-6.

81. Guillam, M.T., et al., *Early diabetes and abnormal postnatal pancreatic islet development in mice lacking Glut-2.* Nat Genet, 1997. **17**(3): p. 327-30.

82. Thorens, B., et al., *Transgenic reexpression of GLUT1 or GLUT2 in pancreatic beta cells rescues GLUT2-null mice from early death and restores normal glucose-stimulated insulin secretion.* J Biol Chem, 2000. **275**(31): p. 23751-8.

83. Adibi, S.A., *Intestinal transport of dipeptides in man: relative importance of hydrolysis and intact absorption.* J Clin Invest, 1971. **50**(11): p. 2266-75.

84. Adibi, S.A. and M.R. Soleimanpour, *Functional characterization of dipeptide transport system in human jejunum.* J Clin Invest, 1974. **53**(5): p. 1368-74.

85. Adibi, S.A. and E.L. Morse, *The number of glycine residues which limits intact absorption of glycine oligopeptides in human jejunum.* J Clin Invest, 1977. **60**(5): p. 1008-16.

86. Adibi, S.A., et al., *Evidence for two different modes of tripeptide disappearance in human intestine. Uptake by peptide carrier systems and hydrolysis by peptide hydrolases.* J Clin Invest, 1975. **56**(6): p. 1355-63.

87. Ganapathy V. and Leibach F.H., *Is intestinal peptide transport energized by a proton gradient?* Am J Physiol, 1985. **249**: p. 153-60.

88. Ganapathy, V. and F.H. Leibach, *Role of pH gradient and membrane potential in dipeptide transport in intestinal and renal brush-border membrane vesicles from the rabbit. Studies with L-carnosine and glycyl-L-proline.* J Biol Chem, 1983. **258**(23): p. 14189-92.

89. Ganapathy, V., G. Burckhardt, and F.H. Leibach, *Characteristics of glycylsarcosine transport in rabbit intestinal brush-border membrane vesicles.* J Biol Chem, 1984. **259**(14): p. 8954-9.

90. Thwaites, D.T. and C.M. Anderson, *H+-coupled nutrient, micronutrient and drug transporters in the mammalian small intestine.* Exp Physiol, 2007. **92**(4): p. 603-19.

91. He, L., K. Vasiliou, and D.W. Nebert, *Analysis and update of the human solute carrier (SLC) gene superfamily.* Hum Genomics, 2009. **3**(2): p. 195-206.

92. Rubio-Aliaga, I. and H. Daniel, *Mammalian peptide transporters as targets for drug delivery.* Trends Pharmacol Sci, 2002. **23**(9): p. 434-40.

93. Daniel, H., et al., *From bacteria to man: archaic proton-dependent peptide transporters at work.* Physiology (Bethesda), 2006. **21**: p. 93-102.

94. Urtti, A., S.J. Johns, and W. Sadee, *Genomic structure of proton-coupled oligopeptide transporter hPEPT1 and pH-sensing regulatory splice variant.* AAPS PharmSci, 2001. **3**(1): p. E6.

95. Fei, Y.J., et al., *Identification of the histidyl residue obligatory for the catalytic activity of the human H+/peptide cotransporters PEPT1 and PEPT2.* Biochemistry, 1997. **36**(2): p. 452-60.

96. Bossi, E., et al., *Residues R282 and D341 act as electrostatic gates in the proton-dependent oligopeptide transporter PepT1.* J Physiol, 2008. **589**(Pt 3): p. 495-510.

97. Rubio-Aliaga, I. and H. Daniel, *Peptide transporters and their roles in physiological processes and drug disposition.* Xenobiotica, 2008. **38**(7-8): p. 1022-42.

98. Chen, X.Z., A. Steel, and M.A. Hediger, *Functional roles of histidine and tyrosine residues in the H(+)-peptide transporter PepT1.* Biochem Biophys Res Commun, 2000. **272**(3): p. 726-30.

99. Terada, T. and K. Inui, *Gene expression and regulation of drug transporters in the intestine and kidney.* Biochem Pharmacol, 2007. **73**(3): p. 440-9.

100. Kennedy, D.J., et al., *Optimal absorptive transport of the dipeptide glycylsarcosine is dependent on functional Na+/H+ exchange activity.* Pflugers Arch, 2002. **445**(1): p. 139-46.

101. Chen, M., et al., *Gene ablation for PEPT1 in mice abolishes the effects of dipeptides on small intestinal fluid absorption, short-circuit current, and intracellular pH.* Am J Physiol Gastrointest Liver Physiol, 2010. **299**(1): p. G265-74.

102. Lee, V.H., J.L. Sporty, and T.E. Fandy, *Pharmacogenomics of drug transporters: the next drug delivery challenge.* Adv Drug Deliv Rev, 2001. **50 Suppl 1**: p. S33-40.

103. Doring, F., et al., *Minimal molecular determinants of substrates for recognition by the intestinal peptide transporter.* J Biol Chem, 1998. **273**(36): p. 23211-8.

104. Liang, R., et al., *Human intestinal H+/peptide cotransporter. Cloning, functional expression, and chromosomal localization.* J Biol Chem, 1995. **270**(12): p. 6456-63.

105. Thamotharan, M., et al., *Functional and molecular expression of intestinal oligopeptide transporter (Pept-1) after a brief fast.* Metabolism, 1999. **48**(6): p. 681-4.

106. Thamotharan, M., et al., *Hormonal regulation of oligopeptide transporter pept-1 in a human intestinal cell line.* Am J Physiol, 1999. **276**(4 Pt 1): p. C821-6.

107. Winckler, C., et al., *Characteristics of dipeptide transport in pig jejunum in vitro.* J Comp Physiol B, 1999. **169**(7): p. 495-500.

108. Gangopadhyay, A., M. Thamotharan, and S.A. Adibi, *Regulation of oligopeptide transporter (Pept-1) in experimental diabetes.* Am J Physiol Gastrointest Liver Physiol, 2002. **283**(1): p. G133-8.

109. Wenzel, U., et al., *PEPT1-mediated cefixime uptake into human intestinal epithelial cells is increased by Ca2+ channel blockers.* Antimicrob Agents Chemother, 2002. **46**(5): p. 1375-80.

110. Knutter, I., et al., *High-affinity interaction of sartans with H+/peptide transporters.* Drug Metab Dispos, 2009. **37**(1): p. 143-9.

111. Ma K, H.Y., Smith DE., *Peptide transporter 1 is responsible for intestinal uptake of the dipeptide glycylsarcosine: studies in everted jejunal rings from wild-type and Pept1 null mice.* J Pharm Sci., 2011. **100(2)**: p. 767-774.

112. Jappar, D., et al., *Significance and regional dependency of peptide transporter (PEPT) 1 in the intestinal permeability of glycylsarcosine: in situ single-pass perfusion studies in wild-type and Pept1 knockout mice.* Drug Metab Dispos, 2010. **38**(10): p. 1740-6.

113. Lu, H. and C. Klaassen, *Tissue distribution and thyroid hormone regulation of Pept1 and Pept2 mRNA in rodents.* Peptides, 2006. **27**(4): p. 850-7.

114. Merlin, D., et al., *Colonic epithelial hPepT1 expression occurs in inflammatory bowel disease: transport of bacterial peptides influences expression of MHC class 1 molecules.* Gastroenterology, 2001. **120**(7): p. 1666-79.

115. Nguyen, H.T., et al., *Pathogenic bacteria induce colonic PepT1 expression: an implication in host defense response.* Gastroenterology, 2009. **137**(4): p. 1435-47 e1-2.

116. Dyer, J., et al., *Glycyl-L-proline transport in rabbit enterocyte basolateral-membrane vesicles.* Biochem J, 1990. **269**(3): p. 565-71.

117. Saito, H. and K. Inui, *Dipeptide transporters in apical and basolateral membranes of the human intestinal cell line Caco-2.* Am J Physiol, 1993. **265**(2 Pt 1): p. G289-94.

118. Terada, T., et al., *Functional characteristics of basolateral peptide transporter in the human intestinal cell line Caco-2.* Am J Physiol, 1999. **276**(6 Pt 1): p. G1435-41.

119. Irie, M., et al., *Efflux properties of basolateral peptide transporter in human intestinal cell line Caco-2.* Pflugers Arch, 2004. **449**(2): p. 186-94.

120. Westrom, B.R., et al., *Levels of immunoreactive insulin, neurotensin, and bombesin in porcine colostrum and milk.* J Pediatr Gastroenterol Nutr, 1987. **6**(3): p. 460-5.

121. Shulman, R.J., *Oral insulin increases small intestinal mass and disaccharidase activity in the newborn miniature pig.* Pediatr Res, 1990. **28**(2): p. 171-5.

122. Buts, J.P., et al., *Response of rat immature enterocytes to insulin: regulation by receptor binding and endoluminal polyamine uptake.* Gastroenterology, 1994. **106**(1): p. 49-59.

123. Gingerich, R.L., et al., *Identification and characterization of insulin receptors in basolateral membranes of dog intestinal mucosa.* Diabetes, 1987. **36**(10): p. 1124-9.

124. Pillion, D.J., V. Ganapathy, and F.H. Leibach, *Identification of insulin receptors on the mucosal surface of colon epithelial cells.* J Biol Chem, 1985. **260**(9): p. 5244-7.

125. Buts, J.P., et al., *Expression of insulin receptors and of 60-kDa receptor substrate in rat mature and immature enterocytes.* Am J Physiol, 1997. **273**(1 Pt 1): p. G217-26.

126. Baron-Delage, S., et al., *Reduced insulin receptor expression and function in human colonic Caco-2 cells by ras and polyoma middle T oncogenes.* J Biol Chem, 1994. **269**(28): p. 18686-93.

127. MacDonald, R.S., W.H. Thornton, Jr., and T.L. Bean, *Insulin and IGE-1 receptors in a human intestinal adenocarcinoma cell line (CACO-2): regulation of Na+ glucose transport across the brush border.* J Recept Res, 1993. **13**(7): p. 1093-113.

128. Nielsen, C.U., et al., *Epidermal growth factor and insulin short-term increase hPepT1-mediated glycylsarcosine uptake in Caco-2 cells.* Acta Physiol Scand, 2003. **178**(2): p. 139-48.

129. Zhang, Y., et al., *Positional cloning of the mouse obese gene and its human homologue.* Nature, 1994. **372**(6505): p. 425-32.

130. Kiess, W., et al., *Adipocytes and adipose tissue.* Best Pract Res Clin Endocrinol Metab, 2008. **22**(1): p. 135-53.

131. Hindlet, P., et al., *Reduced intestinal absorption of dipeptides via PepT1 in mice with diet-induced obesity is associated with leptin receptor down-regulation.* J Biol Chem, 2009. **284**(11): p. 6801-8.

132. Ducroc, R., et al., *Luminal leptin induces rapid inhibition of active intestinal absorption of glucose mediated by sodium-glucose cotransporter 1.* Diabetes, 2005. **54**(2): p. 348-54.

133. Fanjul, C., et al., *Leptin regulates sugar and amino acids transport in the human intestinal cell line Caco-2.* Acta Physiol (Oxf), 2012. **205**(1): p. 82-91.

134. Thamotharan, M., et al., *Mechanism of dipeptide stimulation of its own transport in a human intestinal cell line.* Proc Assoc Am Physicians, 1998. **110**(4): p. 361-8.

135. Shiraga, T., et al., *Cellular and molecular mechanisms of dietary regulation on rat intestinal H+/Peptide transporter PepT1.* Gastroenterology, 1999. **116**(2): p. 354-62.

136. Khanal, R.C. and I. Nemere, *Regulation of intestinal calcium transport.* Annu Rev Nutr, 2008. **28**: p. 179-96.

137. Furukawa, T., et al., *Selectivities of dihydropyridine derivatives in blocking Ca(2+) channel subtypes expressed in Xenopus oocytes.* J Pharmacol Exp Ther, 1999. **291**(2): p. 464-73.

138. Chandrashekar, J., et al., *The receptors and cells for mammalian taste.* Nature, 2006. **444**(7117): p. 288-94.

139. Steinert, R.E. and C. Beglinger, *Nutrient sensing in the gut: interactions between chemosensory cells, visceral afferents and the secretion of satiation peptides.* Physiol Behav, 2011. **105**(1): p. 62-70.

140. Hopfer, U., *Diabetes mellitus: changes in the transport properties of isolated intestinal microvillous membranes.* Proc Natl Acad Sci U S A, 1975. **72**(6): p. 2027-31.

141. Feldman, M. and L.R. Schiller, *Disorders of gastrointestinal motility associated with diabetes mellitus.* Ann Intern Med, 1983. **98**(3): p. 378-84.

142. Chesta, J., et al., *Delayed stomach to caecum transit time in the diabetic rat. Possible role of hyperglucagonaemia.* Gut, 1990. **31**(6): p. 660-2.

143. Bikhazi, A.B., et al., *Effect of diabetes mellitus and insulin on the regulation of the PepT 1 symporter in rat jejunum.* Mol Pharm, 2004. **1**(4): p. 300-8.

144. Der-Boghossian, A.H., et al., *Role of insulin on jejunal PepT1 expression and function regulation in diabetic male and female rats.* Can J Physiol Pharmacol, 2010. **88**(7): p. 753-9.

145. Daniel, H., *Molecular and integrative physiology of intestinal peptide transport.* Annu Rev Physiol, 2004. **66**: p. 361-84.

146. Watanabe, K., et al., *Effect of insulin on cephalexin uptake and transepithelial transport in the human intestinal cell line Caco-2.* Eur J Pharm Sci, 2004. **21**(1): p. 87-95.

147. Wong, T.P., E.S. Debnam, and P.S. Leung, *Involvement of an enterocyte renin-angiotensin system in the local control of SGLT1-dependent glucose uptake across the rat small intestinal brush border membrane.* J Physiol, 2007. **584**(Pt 2): p. 613-23.

148. Masumoto, S., et al., *Dietary phloridzin reduces blood glucose levels and reverses Sglt1 expression in the small intestine in streptozotocin-induced diabetic mice.* J Agric Food Chem, 2009. **57**(11): p. 4651-6.

149. Adibi, S.A. and D.W. Mercer, *Protein digestion in human intestine as reflected in luminal, mucosal, and plasma amino acid concentrations after meals.* J Clin Invest, 1973. **52**(7): p. 1586-94.

150. Meissner, B., et al., *Deletion of the intestinal peptide transporter affects insulin and TOR signaling in Caenorhabditis elegans.* J Biol Chem, 2004. **279**(35): p. 36739-45.

151. Hu, Y., et al., *Targeted disruption of peptide transporter Pept1 gene in mice significantly reduces dipeptide absorption in intestine.* Mol Pharm, 2008. **5**(6): p. 1122-30.

152. Nassl, A.M., et al., *Amino acid absorption and homeostasis in mice lacking the intestinal peptide transporter PEPT1.* Am J Physiol Gastrointest Liver Physiol, 2011. **301**(1): p. G128-37.

153. Ocheltree SM, K.R., Shen H, Yang D, Hughes BA, Smith DE., *Preliminary investigation into the expression of proton-coupled oligopeptide transporters in neural retina and retinal pigment epithelium (RPE): lack of functional activity in RPE plasma membranes.* Pharm Res. , 2003. **20**(9): p. 1364-1372.

154. Ferraris, R.P., et al., *Luminal glucose concentrations in the gut under normal conditions.* Am J Physiol, 1990. **259**(5 Pt 1): p. G822-37.

155. Doherty, M.M. and K.S. Pang, *First-pass effect: significance of the intestine for absorption and metabolism.* Drug Chem Toxicol, 1997. **20**(4): p. 329-44.

156. Pohl, P., S.M. Saparov, and Y.N. Antonenko, *The size of the unstirred layer as a function of the solute diffusion coefficient.* Biophys J, 1998. **75**(3): p. 1403-9.

157. Collins, S., et al., *Genetic vulnerability to diet-induced obesity in the C57BL/6J mouse: physiological and molecular characteristics.* Physiol Behav, 2004. **81**(2): p. 243-8.

158. Kolodziejczak, D., et al., *Mice lacking the intestinal peptide transporter display reduced energy intake and a subtle maldigestion/malabsorption that protects them from diet-induced obesity.* Am J Physiol Gastrointest Liver Physiol, 2013. **304**(10): p. G897-907.

159. Goda, T. and S. Takase, *Effect of dietary fat content on microvillus in rat jejunum.* J Nutr Sci Vitaminol (Tokyo), 1994. **40**(2): p. 127-36.

160. Stumpel, F., T. Kucera, and K. Jungermann, *Impaired stimulation of intestinal glucose absorption via hepatoenteral nerves in streptozotocin-diabetic rats.* Am J Physiol, 1999. **277**(2 Pt 1): p. G285-91.

161. Krauland, A.H., D. Guggi, and A. Bernkop-Schnurch, *Oral insulin delivery: the potential of thiolated chitosan-insulin tablets on non-diabetic rats.* J Control Release, 2004. **95**(3): p. 547-55.

162. Serhan, M.F. and S.I. Kreydiyyeh, *Insulin down-regulates the Na+/K+ ATPase in enterocytes but increases intestinal glucose absorption.* Gen Comp Endocrinol, 2010. **167**(2): p. 228-233.

163. Brandsch, M., et al., *Expression and protein kinase C-dependent regulation of peptide/H+ co-transport system in the Caco-2 human colon carcinoma cell line.* Biochem J, 1994. **299 (Pt 1)**: p. 253-60.

164. Kellett, G.L., et al., *Sugar absorption in the intestine: the role of GLUT2.* Annu Rev Nutr, 2008. **28**: p. 35-54.

165. Stumpel, F., et al., *Normal kinetics of intestinal glucose absorption in the absence of GLUT2: evidence for a transport pathway requiring glucose phosphorylation and transfer into the endoplasmic reticulum.* Proc Natl Acad Sci U S A, 2001. **98**(20): p. 11330-5.

166. Yu, R., et al., *Anti-hyperglycemic, antioxidant and anti-inflammatory effects of VIP and a VPAC1 agonist on streptozotocin-induced diabetic mice.* Peptides, 2011. **32**(2): p. 216-22.

167. Li, H.T., et al., *Antihyperglycemic effects of baicalin on streptozotocin - nicotinamide induced diabetic rats.* Phytother Res, 2010. **25**(2): p. 189-94.

168. Motyl, K.J., et al., *Bone inflammation and altered gene expression with type I diabetes early onset.* J Cell Physiol, 2009. **218**(3): p. 575-83.

169. Forrest, A., R. Makwana, and M. Parsons, *The short-circuit current of the ileum, but not the colon, is altered in the streptozotocin diabetic rat.* Can J Physiol Pharmacol, 2006. **84**(2): p. 173-9.

170. Burant, C.F., et al., *Small intestine hexose transport in experimental diabetes. Increased transporter mRNA and protein expression in enterocytes.* J Clin Invest, 1994. **93**(2): p. 578-85.

171. Debnam, E.S., W.H. Karasov, and C.S. Thompson, *Nutrient uptake by rat enterocytes during diabetes mellitus; evidence for an increased sodium electrochemical gradient.* J Physiol, 1988. **397**: p. 503-12.

172. Schmidt, R.E., J.S. Nelson, and E.M. Johnson, Jr., *Experimental diabetic autonomic neuropathy.* Am J Pathol, 1981. **103**(2): p. 210-25.

173. Lenzen, S., *The mechanisms of alloxan- and streptozotocin-induced diabetes.* Diabetologia, 2008. **51**(2): p. 216-26.

174. West, E.S., OR. Morrison, EY., *Streptozotocin alters pancreatic beta-cell responsiveness to glucose within six hours of injection into rats.* West Indian Med, 1996(45): p. 60-62.

175. Ravi, K., B. Ramachandran, and S. Subramanian, *Effect of Eugenia Jambolana seed kernel on antioxidant defense system in streptozotocin-induced diabetes in rats.* Life Sci, 2004. **75**(22): p. 2717-31.

176. Vidotti, D.B., et al., *Effect of long-term type 1 diabetes on renal sodium and water transporters in rats.* Am J Nephrol, 2008. **28**(1): p. 107-14.

177. Pighin, D., et al., *Role of lipids in the early developmental stages of experimental immune diabetes induced by multiple low-dose streptozotocin.* J Appl Physiol, 2005. **98**(3): p. 1064-9.

178. Vannini, P., et al., *Branched-chain amino acids and alanine as indices of the metabolic control in type 1 (insulin-dependent) and type 2 (non-insulin-dependent) diabetic patients.* Diabetologia, 1982. **22**(3): p. 217-9.

179. Mochida, T., et al., *Time-dependent changes in the plasma amino acid concentration in diabetes mellitus.* Mol Genet Metab. **103**(4): p. 406-9.

180. Ramsanahie, A.P., et al., *Effect of glucagon-like peptide-2 (GLP-2) on diurnal SGLT1 expression.* Dig Dis Sci, 2004. **49**(11-12): p. 1731-7.

181. Perdue, M.D., JS., *Altered regulation of intestinal ion transport by enteric nerves in diabetic rats.* Am J Physiol., 1988(254): p. 444-449.

182. Chang, E.B., R.M. Bergenstal, and M. Field, *Diarrhea in streptozocin-treated rats. Loss of adrenergic regulation of intestinal fluid and electrolyte transport.* J Clin Invest, 1985. **75**(5): p. 1666-70.

183. Krishnan, A.V., C.S. Lin, and M.C. Kiernan, *Activity-dependent excitability changes suggest Na+/K+ pump dysfunction in diabetic neuropathy.* Brain, 2008. **131**(Pt 5): p. 1209-16.

184. Vague, P., et al., *C-peptide, Na+,K(+)-ATPase, and diabetes.* Exp Diabesity Res, 2004. **5**(1): p. 37-50.

185. Luppa, D. and F. Muller, *Effect of diabetes and adrenocortical state on intestinal transport capacity and (Na+ + K+)-activated adenosine triphosphatase activity.* Diabete Metab, 1986. **12**(4): p. 191-6.

186. Gnanaprakasam, M.S. and L.M. Srivastava, *Effect of starvation, alloxan diabetes and adrenalectomy on Na+ K+-ATPase of the mucosa of the small intestine of rat.* Biochem Exp Biol, 1978. **14**(3): p. 257-62.

Appendix

Abbreviations

^{14}C	carbon 14
^{3}H	hydrogen 3, Tritium
AA	amino acids
Ag	silver
ATP	adenosine triphosphate
ATPase	sodium-potassium ATPase
B^0AT1	the sodium-dependent neutral amino acid transporter
BBM	brush border membrane
BBMV	brush border membrane vesicles
BLPT	basolateral peptide transporter
C	control
Ca^{2+}	calcium ion
Caco-2	human epithelial colorectal adenocarcinoma cells
Ca_v 1.3	voltage gated L-type Ca^{2+} channels
CCK-8	cholecystokinin 8
cDNA	complementary deoxyribonucleic acid
Cdx2	caudal-related homeobox protein 2
Cl^-	chloride ion
CP	crossing points
DAG	diacylglycerol
DIO	diet induced obesity
DPP-IV	dipeptidylpeptidase IV
ECL	extracellular loop
EEC	enteroendocrine cell
EGTA	ethylene glycol tetraacetic acid
ELISA	Enzyme Linked Immunosorbent Assay
EPEC	enteropathogenic *Escherichia coli*
ER	endoplasmic reticulum
GABA	γ-aminobutyric acid
GAPDH	glyceraldehyde-3-phosphate dehydrogenase
GGM	glucose-galactose malabsorption
GI	gastrointestinal tract

GIP	gastric inhibitory polypeptide
GLP-1	glucagon-like-peptide 1
GLP2	glucagon-like peptide 2
GLUT2	facilitative glucose transporter type 2
GLUT4	insulin-depended facilitative glucose transporter 4
GLUTag	differentiated murine enteroendocrine cells
Gly-Gln	glycylglutamine
Gly-Phe	glycyl phenylalanine
Gly-Sar	glycyl-sarcosine
GPCR	G-protein coupled receptor
GSIS	glucose-stimulated insulin secretion
H&E	Hemalum and Eosin
H^+	proton
H121	histidine residue 121
H_2O_2	hydrogen peroxide
H57	histidine residue 57
hcDNA	human complementary DNA
HCO_3	hydrogen carbogen
HeLa	cervical cancer derived cell line
HEPES	4-(2-hydroxyethyl)-1-piperazineethanesulfonic acid
HFD	high-fat diet
HMIT	myoinositol transporter
hSGLT1	human derived sodium/glucose cotransporter 1
HT29-Cl.19A	human colonic cell line
I	current
i.p	intraperitoneal
IEC	rat derived Intestinal Epithelial Cells
I_{oc}	open-circuit voltage
IP_3	inositol-1,4,5-triphosphat
IR	insulin receptor
Isc	short-circuit current
K^+	potassium ion
KCl	potassium chloride
L-DOPA	L-3,4-dihydroxyphenylalanine
MAPK	Mitogen-Activated Protein Kinase
MES	2-(N-morpholino) ethanesulfonic acid

$MgCl_2$	magnesium chloride
mKHB	modified Krebs-Henseleit Buffer
mRNA	messenger ribonucleic acid
mSGLT1	mouse derived sodium/glucose cotransporter 1
Na^+	sodium ion
NHE3	sodium proton exchanger 3
NTT's	neurotransmitter-sodium-symporter family
ob-R	leptin receptor
OGTT	oral glucose tolerance test
PAT1	proton-coupled amino acid transporter 1
PBS	phosphate buffered saline
PBS-T	phosphate buffered saline with Tween
Pbu	phorbol ester
RT PCR	real time polymerase chain reaction
PEPT1	proton-coupled peptide transporter 1
PEPT2	proton-coupled peptide transporter 2
PI-3K	phosphatidylinositol-3-Kinase
PKA	protein kinase A
PKC	protein kinase C
PKC β II	protein kinase C beta-II isoform
PLC βII	phospholipase C beta-II isoform
PMA	phorbol-12-myristate-13-acetate
R	resistance
RAS	Renin-Angiotensin System
RIE-1	intestinal epithelial cells
RIP1	rat insulin promoter 1
RS1	regulatory solute carrier protein, family 1, member 1
rSGLT1	rat derived sodium/glucose cotransporter 1
R_t, TER	tissue resistance
SAAT	single amino acid transporter
SGLT1	sodium/glucose cotransporter 1
SGLT2	sodium/glucose cotransporter 2
SIT1	sodium/imino-acid transporter 1
SKPT	rat renal cell line
Sp1	specificity protein 1, human transcription factor
SPF	specific pathogen free

STZ	Streptozotocin
System ASC	sodium-dependent neutral amino acid transporters
T1D	type 1 diabetes
T1R	sweet taste receptor family 1
T1R1/T1R3	heterodimers of TR1 (umami and savory amino acids)
T1R2/T1R3	heterodimers of TR1 (sweet taste)
T2D	type 2 diabetes
T2R	taste receptor family 2 (bitter taste)
TATA	Goldberg-Hogness-Box
TauT	Cl^- -dependent taurine transporter
TMD	transmembrane domain
TRC	taste receptor cell
U	voltage
UL	unstirred layer
U_t	transepithelial voltage
VCC	voltage current clamp
V_t	transepithelial potential
WHO	world health organization
Y56	tyrosine residue 56
α-MDG	alpha methyl-D-glucopyranoside
ΔV_t	tissue potential difference
ΔI	current difference
K_m	Michaelis-Menten constant
V_{max}/I_{max}	maximal transport velocity
rpm	rounds per minutes

Units of measurements

(°C)	degree Celsius
(Å)	Angstrom
(cm)	centimeter
(µm)	micrometer
(cm^2)	square centimeter
(M)	molar
(mM)	millimolar
(µM)	micromolar
(nM)	nanomolar
(kg)	kilogram
(g)	gram
(kDa)	kilo Dalton
(l)	liter
[81]	milliliter
(µl)	microliter
(rcf)	relative centrifugal force
(pmol)	picomole
(mosmol)	milliosmolarity
(µA)	microampere

Diets

Standard chow SPF Tierhaltung

(Gregor-Mendel-Strasse 2, 85350 Freising, Germany)

Standard Chow	**Einheit**	
Artikelnummer		V1534-3
Bezeichnung		R/M-H autoklavierbar
Kategorie		Alleinfutter
Hersteller		ssniff
Pelletgröße		10 mm
Haltung		SPF
Bestrahlung		25 kGy
Energie		
Bruttoenergie (GE)	MJ/Kg	16,3
Umsetzbare Energie (ME)	MJ/Kg	12,8
Umsetzbare Energie (ME)	MJ/Kg	
Zusammensetzung		
Protein	kJ%	33
Fettsäuren	kJ%	9
Kohlenhydrate	kJ%	58
Rohnährstoffe		
Trockensubstanz	%	87,8
Rohprotein (Nx6,25)	%	19,0
Rohfett	%	3,3
Rohfaser	%	4,9
Rohasche	%	6,4
N-freie Extrakt-stoffe (NfE)	%	54,2
Stärke	%	36,6
Zucker	%	4,7
Casein	%	
Maisstärke, mod./pre-gelat.	%	
Maltodextrin	%	
Saccharose	%	
Glukose/Dextrose	%	
Cellulose	%	
L-Cystin	%	

Vitamine	%	
Mineralstoffe& Spurenelement	%	
Cholin-Chlorid	%	
Butylhydroxy-toluol	%	
Sojaöl	%	
Palmöl	%	
Rindertalg	%	
Fettsäuren		
C4:0	%	
C12:0	%	
C14:0	%	0,01
C16:0	%	0,47
C16:1	%	0,01
C17:0	%	
C18:0	%	0,08
C18:1	%	0,62
C18:2	%	1,79
C18:3	%	0,23
C20:0	%	0,01
C20:1	%	0,02
C20:4	%	
Cholesterol	mg/kg	
Mineralstoffe	%	
Calcium	%	1,00
Phosphor	%	0,70
Natrium	%	0,24
Magnesium	%	0,23
Kalium	%	0,92
Vitamine	per kg	
Vitamin A	IE	25000
Vitamin D3	IE	1000
Vitamin E	mg	135
Vitamin K (als Menadion)	mg	20
Vitamin C	mg	
Vitamin B1	mg	86
Vitamin B2	mg	32
Vitamin B6	mg	32

Vitamin B12	µg	150
Nicotinsäure	mg	165
Pantothensäure	mg	62
Folsäure	mg	10
Biotin	µg	730
Cholin-Chlorid	mg	3000
Inositol	mg	100
Spurenelemente	per kg	
Eisen	mg	176,00
Mangan	mg	69,00
Zink	mg	94,00
Kupfer	mg	16,00
Iod	mg	2,20
Selen	mg	0,30
Cobalt	mg	2,10
Aminosäuren	%	
Lysin	%	1,10
Methionin	%	0,35
Met+Cys	%	0,70
Threonin	%	0,68
Tryptophan	%	0,25
Arginin	%	1,16
Histidin	%	0,45
Valin	%	0,90
Isoleucin	%	0,78
Leucin	%	1,33
Phenylalanin	%	0,87
Phe+Tyr	%	1,47
Glycin	%	0,82
Glutaminsäure	%	3,97
Asparaginsäure	%	1,66
Prolin	%	1,28
Alanin	%	0,81
Serin	%	0,92

Standard chow open mouse facility

(Liese-Beckmannstr.4, 85350 Freising, Germany)

Standard Chow	**Einheit**	
Artikelnummer		V 1534-0
Bezeichnung		R/M-H
Kategorie		Alleinfutter
Hersteller		ssniff
Pelletgröße		10 mm
Energie		
Bruttoenergie (GE)	MJ/Kg	16,3
Umsetzbare Energie (ME)	MJ/Kg	12,8
Umsetzbare Energie (ME)	MJ/Kg	
Zusammensetzung		
Protein	kJ%	33
Fettsäuren	kJ%	9
Kohlenhydrate	kJ%	58
Rohnährstoffe		
Trockensubstanz	%	87,7
Rohprotein (Nx6,25)	%	19,0
Rohfett	%	3,3
Rohfaser	%	4,9
Rohasche	%	6,4
N-freie Extrakt-stoffe (NfE)	%	54,1
Stärke	%	36,5
Zucker	%	4,7
Casein	%	
Maisstärke, mod./pre-gelat.	%	
Maltodextrin	%	
Saccharose	%	
Glukose/Dextrose	%	
Cellulose	%	
L-Cystin	%	
Vitamine	%	
Mineralstoffe& Spurenelement	%	
Cholin-Chlorid	%	

Butylhydroxy-toluol	%	
Sojaöl	%	
Palmöl	%	
Rindertalg	%	
Fettsäuren		
C4:0	%	
C12:0	%	
C14:0	%	0,01
C16:0	%	0,47
C16:1	%	0,01
C17:0	%	
C18:0	%	0,08
C18:1	%	0,62
C18:2	%	1,80
C18:3	%	0,23
C20:0	%	0,01
C20:1	%	0,02
C20:4	%	
Cholesterol	mg/kg	
Mineralstoffe	%	
Calcium	%	1,00
Phosphor	%	0,70
Natrium	%	0,24
Magnesium	%	0,22
Kalium	%	0,91
Vitamine	per kg	
Vitamin A	IE	15000
Vitamin D3	IE	1000
Vitamin E	mg	110
Vitamin K (als Menadion)	mg	5
Vitamin C	mg	
Vitamin B1	mg	18
Vitamin B2	mg	23
Vitamin B6	mg	21
Vitamin B12	µg	100
Nicotinsäure	mg	135

Pantothensäure	mg	43
Folsäure	mg	7
Biotin	µg	525
Cholin-Chlorid	mg	2990
Inositol	mg	100
Spurenelemente	per kg	
Eisen	mg	179,00
Mangan	mg	69,00
Zink	mg	94,00
Kupfer	mg	16,00
Iod	mg	2,20
Selen	mg	0,30
Cobalt	mg	2,10
Aminosäuren	%	
Lysin	%	1,00
Methionin	%	0,30
Met+Cys	%	0,65
Threonin	%	0,68
Tryptophan	%	0,25
Arginin	%	1,14
Histidin	%	0,44
Valin	%	0,88
Isoleucin	%	0,76
Leucin	%	1,30
Phenylalanin	%	0,85
Phe+Tyr	%	1,43
Glycin	%	0,80
Glutaminsäure	%	3,90
Asparaginsäure	%	1,61
Prolin	%	1,25
Alanin	%	0,79
Serin	%	0,89

Control diet (11% energy from fat) open mouse facility

(Liese-Beckmannstr.4, 85350 Freising, Germany)

Control Diet (11%)	**Einheit**	
Artikelnummer		E15000-04
Bezeichnung		EF R/M Kontrolle
Kategorie		Experimentalfutter
Hersteller		ssniff
Pelletgröße		10mm
Energie		
Bruttoenergie (GE)	MJ/Kg	18,0
Umsetzbare Energie (ME)	MJ/Kg	15,4
Umsetzbare Energie (ME)	MJ/Kg	15,0
Zusammensetzung		
Protein	kJ%	23
Fettsäuren	kJ%	11
Kohlenhydrate	kJ%	66
Rohnährstoffe		
Trockensubstanz	%	95,2
Rohprotein (Nx6,25)	%	20,8
Rohfett	%	4,2
Rohfaser	%	5,0
Rohasche	%	5,6
N-freie Extrakt-stoffe (NfE)	%	59,4
Stärke	%	46,8
Zucker	%	10,8
Casein	%	24,00
Maisstärke, mod./pre-gelat.	%	30,00
Maltodextrin	%	19,60
Saccharose	%	
Glukose/Dextrose	%	10,00
Cellulose	%	5,00
L-Cystein	%	0,20
Vitamine	%	1,00
Mineralstoffe& Spurenelement	%	6,00
Cholin-Chlorid	%	0,20

Butylhydroxy-toluol	%	
Sojaöl	%	4,00
Palmöl	%	
Rindertalg	%	
Fettsäuren		
C4:0	%	
C12:0	%	
C14:0	%	0,02
C16:0	%	0,45
C16:1	%	0,02
C17:0	%	
C18:0	%	0,19
C18:1	%	1,07
C18:2	%	2,12
C18:3	%	0,26
C20:0	%	0,02
C20:1	%	
C20:4	%	
Cholesterol	mg/kg	
Mineralstoffe	%	
Calcium	%	0,90
Phosphor	%	0,63
Natrium	%	0,19
Magnesium	%	0,21
Kalium	%	0,97
Vitamine	per kg	
Vitamin A	IE	15000
Vitamin D3	IE	1500
Vitamin E	mg	150
Vitamin K (als Menadion)	mg	20
Vitamin C	mg	30
Vitamin B1	mg	16
Vitamin B2	mg	16
Vitamin B6	mg	18
Vitamin B12	µg	30
Nicotinsäure	mg	49

Pantothensäure	mg	56
Folsäure	mg	19
Biotin	µg	310
Cholin-Chlorid	mg	1040
Inositol	mg	80
Spurenelemente	per kg	
Eisen	mg	166,00
Mangan	mg	98,00
Zink	mg	65,00
Kupfer	mg	14,00
Iod	mg	1,20
Selen	mg	0,14
Cobalt	mg	0,15
Aminosäuren	%	
Lysin	%	1,71
Methionin	%	0,73
Met+Cys	%	0,82
Threonin	%	0,93
Tryptophan	%	0,27
Arginin	%	0,76
Histidin	%	0,66
Valin	%	1,42
Isoleucin	%	1,09
Leucin	%	2,05
Phenylalanin	%	1,11
Phe+Tyr	%	2,22
Glycin	%	0,43
Glutaminsäure	%	4,69
Asparaginsäure	%	1,55
Prolin	%	2,39
Alanin	%	0,68
Serin	%	1,24

High-fat diet (60% energy from fat) open mouse facility

(Liese-Beckmannstr.4, 85350 Freising, Germany)

High-fat diet (60%)	**Einheit**	
Artikelnummer		E15741-34
Bezeichnung		EF R/M nach D12492 mod.
Kategorie		Experimentalfutter
Hersteller		ssniff
Pelletgröße		10mm
Energie		
Bruttoenergie (GE)	MJ/Kg	25,2
Umsetzbare Energie (ME)	MJ/Kg	20,6
Umsetzbare Energie (ME)	MJ/Kg	21,4
Zusammensetzung		
Protein	kJ%	19
Fettsäuren	kJ%	60
Kohlenhydrate	kJ%	21
Rohnährstoffe		
Trockensubstanz	%	97,1
Rohprotein (Nx6,25)	%	24,1
Rohfett	%	34,0
Rohfaser	%	6,0
Rohasche	%	6,1
N-freie Extrakt-stoffe (NfE)	%	27,0
Stärke	%	2,2
Zucker	%	22,4
Casein	%	27,69
Maisstärke, mod./pre-gelat.	%	
Maltodextrin	%	15,70
Saccharose	%	8,00
Glukose/Dextrose	%	
Cellulose	%	6,00
L-Cystin	%	0,35
Vitamine	%	1,00
Mineralstoffe& Spurenelement	%	6,40

Cholin-Chlorid	%	0,25
Butylhydroxy-toluol	%	0,01
Sojaöl	%	3,10
Palmöl	%	
Rindertalg	%	31,50
Fettsäuren		
C4:0	%	0,01
C12:0	%	0,03
C14:0	%	1,03
C16:0	%	8,06
C16:1	%	0,78
C17:0	%	0,38
C18:0	%	5,61
C18:1	%	12,13
C18:2	%	2,37
C18:3	%	0,33
C20:0	%	0,04
C20:1	%	0,01
C20:4	%	0,07
Cholesterol	mg/kg	290,00
Mineralstoffe	%	
Calcium	%	1,05
Phosphor	%	0,61
Natrium	%	0,20
Magnesium	%	0,17
Kalium	%	1,00
Vitamine	per kg	
Vitamin A	IE	15000
Vitamin D3	IE	1500
Vitamin E	mg	150
Vitamin K (als Menadion)	mg	20
Vitamin C	mg	30
Vitamin B1	mg	16
Vitamin B2	mg	16
Vitamin B6	mg	18
Vitamin B12	µg	30

Nicotinsäure	mg	45
Pantothensäure	mg	55
Folsäure	mg	19
Biotin	µg	310
Cholin-Chlorid	mg	2300
Inositol	mg	80
Spurenelemente	per kg	
Eisen	mg	139,00
Mangan	mg	82,00
Zink	mg	56,00
Kupfer	mg	12,00
Iod	mg	0,97
Selen	mg	0,13
Cobalt	mg	0,13
Aminosäuren	%	
Lysin	%	1,98
Methionin	%	0,83
Met+Cys	%	1,28
Threonin	%	1,07
Tryptophan	%	0,31
Arginin	%	0,88
Histidin	%	0,76
Valin	%	1,64
Isoleucin	%	1,25
Leucin	%	2,36
Phenylalanin	%	1,29
Phe+Tyr	%	2,57
Glycin	%	0,5
Glutaminsäure	%	5,41
Asparaginsäure	%	1,79
Prolin	%	2,76
Alanin	%	0,79
Serin	%	1,43

Danksagung

Eine Vielzahl von Menschen hat mich während der Entstehung dieser Arbeit begleitet, deshalb möchte ich mich hier und jetzt von Herzen für die Unterstützung, Zuspruch und Kritik bedanken:

Frau Daniel, ohne Sie und die Bereitstellung dieses Themas wäre diese Arbeit nie entstanden. Ich möchte mich bei Ihnen für die vielen konstruktiven, kritikreichen und sehr interessanten Gespräche während meiner Zeit in Ihrer Arbeitsgruppe bedanken. Auch wenn es nicht immer einfach war, ist es für mich eine sehr schöne und lehrreiche Zeit gewesen.

Herr Kottra, auch Ihnen möchte ich danken für Ihre geduldige Begleitung während dieser Zeit. Sie haben mir gezeigt, dass handwerkliches Geschick und eine Menge Geduld bei Messungen mit der Ussing-Kammer von Nöten sind und haben mich bei diversen Aufbau-, Umbau- und Neubauarbeiten immer tatkräftig unterstützt. Ich weiß nicht, wie viel Meterware Kunstoffschlauch durch unsere Hände gegangen ist?! Es war Einiges! Danke für Ihre Diskussionsbereitschaft, Ihr immer offenes Ohr für kleine oder auch große Probleme und all die zahlreichen guten und hilfreichen Ratschläge, die zum Entstehen dieser Arbeit beigetragen haben.

Liebe Helene, auch Dir gilt an dieser Stelle ein großes Dankeschön. Du hast mich bei allen Präparationen unglaublich unterstützt! Daher ist es nicht vermessen zu sagen, dass es nur ganz schwer ohne Dich gegangen wäre! Ich vermisse Deine Schleckerschublade und Deine aufbauenden Worte wenn es mal wieder nicht so lief wie es sollte!

Ich möchte mich auch bei Dagmar vom Lehrstuhl für Humanbiologie bedanken, die mich anfangs in die Kunst der Darmpräparation eingewiesen hat.

Im Institut habe ich viele liebe und hilfsbereite Menschen kennenlernen dürfen, ohne die die Arbeitszeit nur halb so schön gewesen wäre. Mein Dank gilt im Speziellen Pia, Kathrin, Chrissi, Anja und Vero für die vielen schönen und unvergesslichen Momente die ich mit Euch erleben durfte.

Liebe Tamara! Du hast mir immer mit der Arbeit weitergeholfen und Mut zugesprochen. Die inspirativen Balkongespräche, inklusive Kaffee und Kippchen werden mir fehlen. Danke.

Liebe Manu, ich danke Dir für die tolle Zeit die ich mit Dir am Lehrstuhl und vor allem darüber hinaus verbringen durfte. Ich denke so gerne an unsere Abende zurück, an denen doch das eine oder andere Gläschen getrunken und ausgesprochen lecker gekocht wurde. Du bist mir auch sehr ans Herz gewachsen.

Meine lieben Eltern haben mich mein ganzes Leben und besonders während der Promotion immer mit viel Zuversicht unterstützt. Ohne Euch wäre ich nicht der Mensch, der ich heute bin. Eure bedingungslose Liebe trägt mich und macht mich stark. Ich danke Euch aus tiefstem Herzen!

Zuletzt möchte ich meinem Mann Corvin danken. Du hast mein Leben unglaublich bereichert und ihm Sinn gegeben. Wenn ich mal den Weg aus den Augen verloren habe, oder der Verzweiflung nahe war, hast Du mich immer wieder ermutigt und mir gezeigt, dass es sich lohnt zu kämpfen. Spätestens mit der Geburt unseres Sohnes weiß ich, dass mir Eure Liebe so viel Kraft gibt, dass nichts unmöglich ist!

Ich liebe Euch. DANKE!

Eidesstattliche Erklärung

Hiermit versichere ich, dass die vorliegende Arbeit

Studies on dietary and hormonal regulation of selected nutrient transporters in mouse small intestine

selbständig verfasst und keine anderen als die angegebenen Quellen und Hilfsmittel benutzt habe. Die den benutzten Quellen wörtlich und inhaltlich entnommenen Stellen sind als solche kenntlich gemacht.

Diese Arbeit hat in gleicher oder ähnlicher Form noch keiner anderen Prüfungsbehörde vorgelegen.

Freising, den

Mena Katharina Eidens

Curriculum Vitae

Name:	Eidens (geb. Marth)
Vorname:	Mena Katharina
Geburtsdatum:	20. März. 1979
Geburtsort:	Halle (Westfalen)
Familienstand:	verheiratet (1 Kind)

Bildung

Seit 04/2008	**Technische Universität München** **Wissenschaftszentrum Weihenstephan** **Lehrstuhl für Ernährungsphysiologie** Promotion
10/1999-02/2008	**Justus-Liebig-Universität, Gießen** **Studium: Biologie** Abschluss: Diplom
08/1989-05/1999	**Ratsgymnasium, Rheda-Wiedenbrück** Abschluss: Hochschulreife

Freising, den

List of Publications

Amino acid absorption and homeostasis in mice lacking the intestinal peptide transporter PEPT1.

Nässl AM, Rubio-Aliaga I, Fenselau H, Marth MK, Kottra G, Daniel H. Am J Physiol Gastrointest Liver Physiol. 2011 Jul;301(1):G128-37

Increased plasma citrulline in mice marks diet-induced obesity and may predict the development of the metabolic syndrome.

Sailer M, Dahlhoff C, Giesbertz P, Eidens MK, deWit N, Rubio-Aliaga I, Boekschoten M, Müller M and Daniel H. PLoS One. 2013 May 14;8(5):e63950. doi: 10.1371